Optical properties of the human cornea

Sicam, V.A.

2007

Shape and wave aberration measurements
using the VU topographer and Scheimpflug photography

ISBN 90-9021406-2

Cover design: Superimposed images of VU topographer color reflection pattern on two different surfaces: the Rand surface (Right) and a post transplanted cornea (Left). Designed by: M.A. Collado, Hays, Kansas, USA.

VRIJE UNIVERSITEIT

Shape and wave aberration measurements using the VU topographer and Scheimpflug photography

ACADEMISCH PROEFSCHRIFT

ter verkrijging van de graad Doctor aan
de Vrije Universiteit Amsterdam,
op gezag van de rector magnificus
prof.dr. L.M. Bouter,
in het openbaar te verdedigen
ten overstaan van de promotiecommissie
van de faculteit der Geneeskunde
op woensdag 17 januari 2007 om 10.45 uur
in de aula van de universiteit,
De Boelelaan 1105

door

Victor Arni de Paz Sicam

geboren te Davao, Filipijnen

promotor:	prof.dr. R.M. Heethaar
copromotoren:	dr. G.L. van der Heijde
	dr. T.J.T.P. van den Berg

When you look into a mirror you do not see your reflection.
Your reflection sees you.

(AP, Internet, 2/25/99)

To Eloise, Beryl and Chrys

Leescommisie:
Prof.dr. S.Marcos (Instituto de Optica, Madrid)
Prof.dr. P.J. Ringens (VU University Medical Center, Amsterdam)
Prof.dr. F.J.A Groen (University of Amsterdam)
Prof.dr. A.C. Kooijman (University of Groningen)
Prof.dr. W.M.G. Ubachs (Vrije Universiteit Amsterdam)

This thesis is financially supported by
Advanced Medical Optics(AMO), Groningen and by the
Dutch Foundation for Technology (STW).

CONTENTS

1

INTRODUCTION

1.1 CLASSICAL APPROACH TO IMPROVE HUMAN VISION

Human vision is a complex process that involves various components of the eye and the human brain. The initial step in human vision is image formation on the retina. This is possible because the eye is able to refract light via the cornea and the lens to produce a focused retinal image that can stimulate neural responses which are processed by the brain to give information on what we see. Because the cornea and the lens can be modelled with spherical surfaces and the relevant light rays that form the retinal image make a small angle with the optical axis of the eye, *paraxial approximation* can be used in ray tracing of the light through the eye.[1] Use of the paraxial approximation in *geometrical optics* leads to the derivation of the refractive power (expressed in Diopter) of a spherical surface:

$$Power = \frac{n'-n}{r} \qquad (1)$$

Where n is the refractive index of the first medium, n' is the refractive index of the second medium and r is the radius of curvature of the surface expressed in meters. This classical description to describe refraction is often used in ophthalmic practice and is sufficient to deal with *defocus* and *astigmatism* of the eye. In *defocus* (Figure 1), the focus point in the image formation does not

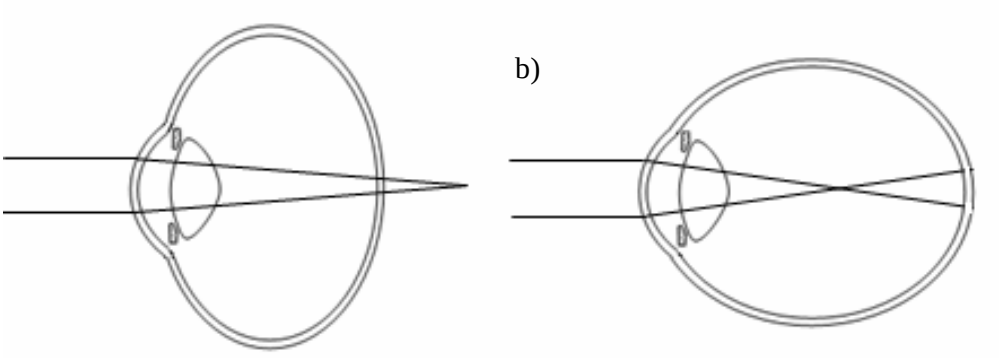

Figure1 *Schematic diagram of light refraction in a) a myopic and b) a hyperopic eye. The shape of the eye is exaggerated for illustration purposes*

exactly coincide with the retina. The focus can be located before the retina. In this case the eye is *myopic*. On the other hand, the focus is located behind the retina for a *hyperopic* eye. Astigmatism (Figure 2) happens when the focal point varies with meridian plane. The anterior corneal surface contributes to the astigmatism of the eye when the corneal shape is *toric*. Unlike a spherical surface, the radius of curvature for toric surfaces varies with meridian plane. It is known that the young human cornea usually has *with the rule* astigmatism. In this case, the corneal radius of curvature is maximum at the horizontal meridian and minimum at the vertical meridian. However, this trend reverses with an increase in age. Defocus and astigmatism, which can easily be corrected with appropriate spectacles or contact lenses, are called low order *monochromatic aberrations*. They are the dominant monochromatic aberrations of the human eye. *Chromatic aberration* is beyond the scope of this dissertation and therefore from this point onwards whenever aberration is mentioned it pertains to monochromatic aberration.

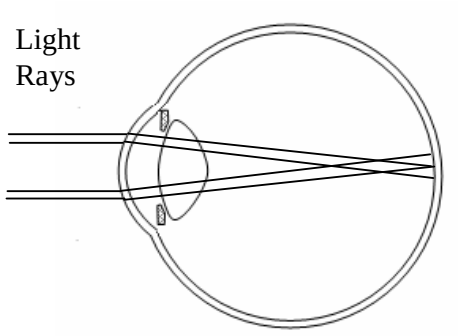

Vertical meridian bundle focused on the retina. Horizontal meridian bundle is out of focus.

Figure 2 *Schematic diagram of astigmatic refraction in an eye w/toric surface features.*

1.2 HIGHER ORDER ABERRATIONS OF THE EYE

There are higher order aberrations that exist for the human eye and their magnitude is usually less than in defocus or astigmatism. The two most relevant higher order aberrations are *spherical aberration* and *coma aberration*.[2] Spherical aberration (Figure 3) occurs when the focusing of peripheral

(marginal) rays deviate from that of the central rays (paraxial rays). The spherical aberration is positive/negative if the focusing of the marginal ray is before/after the paraxial focus. Coma (Latin for "comet") aberration is similar to spherical aberration; it applies to rays entering the lens at an angle. This aberration can be observed by tilting a lens under the sunlight. At the beginning the projected image of the sun is circular but as the lens is tilted with respect to the sun direction the resulting image takes an elongated shape, like a comet. This coma aberration is dependent upon lens shape. In the example illustrated in Figure 4, rays incoming from the periphery of the lens focus closer to the axis and produce a larger blurry spot than the paraxial rays.

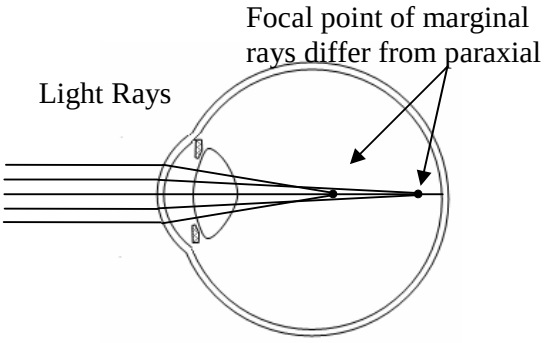

Figure 3 Schematic diagram of refraction in an eye with positive spherical aberration.

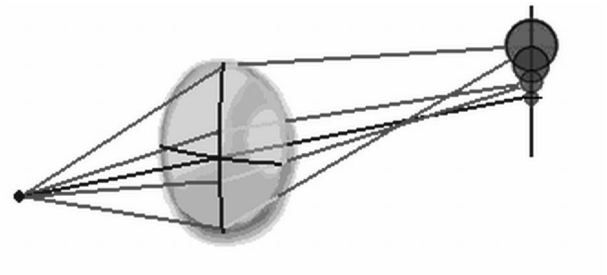

Figure 4 Coma Aberration.

A useful representation to describe the aberrations of the eye as well as the shape of corneal surfaces is the use of Zernike Polynomials which was formulated by the Dutch physicist Frits Zernike, recepient of the Nobel prize in 1953 for his discoveries in phase contrast microscopy. Shown in the Table 1 are the Zernike polynomials up to the 4^{th} order. Each Zernike term is specified by a radial order n and a frequency number m which corresponds to the highest exponent of the radial variable ρ and the coefficient of the angular variable θ respectively. An important property of the Zernike polynomials is that these polynomials constitute a complete basis and are orthonormal in a circle of unit radius.[3] Because of this property expanding to higher orders doesn't alter the

value of the lower order terms.[4] In terms of Zernike expansion the wave aberration function has the following form:

$$W(\rho,\theta)=\sum_{n=0}^{k}\sum_{\substack{m=-n\\ n-|m|=even}}^{n}C_n^m Z_n^m(\rho,\theta)$$

Where $W(\rho,\theta)$ being a polar representation of the wave aberration, Z_n^m a particular Zernike polynomial and C_n^m the coefficient belonging to the corresponding Zernike polynomial. Thus, each wave form or surface shape can be specified by a unique set of Zernike coefficients. It is important to note that the interpretation of each Zernike component depends on whether the expansion is done for a wave aberration or for describing corneal shape. For example, toricity describes shape while astigmatism describes refraction. The paraxial approximation approach is not sufficient to describe higher order aberrations and thus exact ray tracing is more appropriate. In this approach the wave aberration of an optical system is defined as the difference in optical path length of the marginal rays with respect to the principal ray.[5]

Table 1 *Zernike Polynomials*

Zernike Term(n,m)	Polar Representation	Wave Aberration Meaning	Corneal Shape Meaning
Z(0,0)	1	Bias	Piston
Z(1,-1)	$2\rho\sin(\theta)$	Prism y-direction	Tilt y-direction
Z(1,1)	$2\rho\cos(\theta)$	Prism x-direction	Tilt x-direction
Z(2,-2)	$\sqrt{6}\,\rho^2\sin(2\theta)$	Astigmatism 2nd ord. 45°	Toric 2nd ord. 45°
Z(2,0)	$\sqrt{3}\,(2\rho^2-1)$	Defocus	Rotation Symmetric 2nd ord.
Z(2,2)	$\sqrt{6}\,\rho^2\cos(2\theta)$	Astigmatism 2nd ord. 0°	Toric 2nd ord. 0°
Z(3,-3)	$\sqrt{8}\,\rho^3\sin(3\theta)$	Trefoil 30°	Trefoil 30°
Z(3,-1)	$\sqrt{8}\,(3\rho^3-2\rho)\sin(\theta)$	Coma y-direction	Coma y-direction
Z(3,1)	$\sqrt{8}\,(3\rho^3-2\rho)\cos(\theta)$	Coma x-direction	Coma x-direction
Z(3,3)	$\sqrt{8}\,\rho^3\cos(3\theta)$	Trefoil 0°	Trefoil 0°
Z(4,-4)	$\sqrt{10}\,\rho^4\sin(4\theta)$	Tetrafoil 22.5°	Tetrafoil 22.5°
Z(4,-2)	$\sqrt{10}\,(4\rho^4-3\rho^2)\sin(2\theta)$	Astigmatism 4th ord. 45°	Toric 4th ord. 45°
Z(4,0)	$\sqrt{5}\,(6\rho^4-6\rho^2+1)$	Spherical Aberration	Rotation Symmetric 4th ord.
Z(4,2)	$\sqrt{10}\,(4\rho^4-3\rho^2)\cos(2\theta)$	Astigmatism 4th ord. 0°	Toric 4th ord. 0°
Z(4,4)	$\sqrt{10}\,\rho^4\cos(4\theta)$	Tetrafoil 0°	Tetrafoil 0°

1.3 THE CORNEA AND CURRENT TECHNOLOGY TO OBTAIN OPTICAL PROPERTIES

1.3.1 Anterior Corneal Surface

The anterior corneal surface contributes to about 70% of the refractive power of the eye. Thus, measurement of the corneal shape is becoming a common procedure in ophthalmic practice. As early as the 19th century, images reflected off the anterior corneal surface have been studied (keratoscopy).[6] In 1880, A. Placido devised a keratoscopy target consisting of a disk with alternating black and white rings. The disk had a hole in its center through which the observer could visualize the subject's cornea. This target is still in use today for qualitative inspection. But now, the reflected image is captured by a camera and computer algorithms process this information to reconstruct the corneal shape. However, the accuracy of this procedure is not without problems. When reconstructing the corneal surface, numerical algorithms used in commercially available Placido disk topographers neglect skew ray reflections.[7,8,9] This leads to inaccuracy in reconstructing corneal surfaces that are not rotational symmetric.[10,11]

The corneal shape is reconstructed in Placido disk topography using

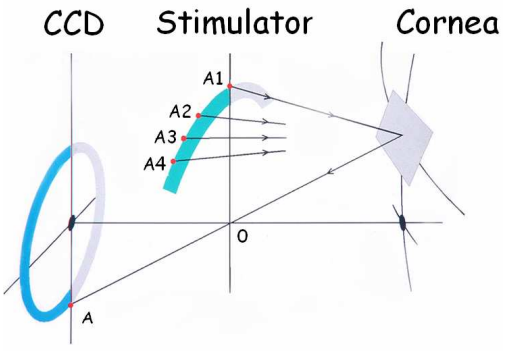

Figure 5 *Schematic diagram that shows the effect of skew ray ambiguity in determining source points in Placido disk topography.*

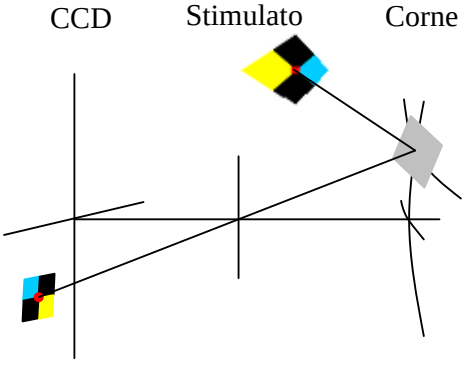

Figure 6 *Schematic diagram that shows one-to-one correspondence between image crossings and stimulator crossings of the VU topographer. There is no skew ray ambiguity in this system.*

reflection principles that relates an image point A, captured from a CCD or video camera, to its stimulator point A1 (see Figure 5). It is assumed that the reflection phenomenon occurs in a meridian plane. This assumption is valid if the corneal surface is rotation-symmetric. For non-rotation-symmetric surfaces skew-ray reflections can occur, rays coming from points A2, A3 and A4 in Figure 5 are skew rays. Thus, in ring topography, there is ambiguity in determining the stimulator point corresponding to an image point because the cornea is not a rotation-symmetric surface.

Vos, Van der Heijde, Spoelder, Van Stokkum, and Groen (1997) introduced a different topographer (the VU topographer) to deal with the skew ray problem.[12] In lieu of the ring stimulus, a color-coded pattern is used(see Figure 6). The stimulus pattern is designed so that the reflection pattern will appear as square objects if the corneal surface is spherical in form. In this system, the crossing points in the square pattern are chosen as starting information for the surface reconstruction algorithm. In principle, since the corresponding crossing points in the stimulator pattern is known, skew ray ambiguity is eliminated.

1.3.2 Posterior Corneal Surface

The posterior corneal surface also contributes to the refractive power of the cornea but for only about 10%. Direct measurement of the surfaces by means of reflection is difficult. However, there are other ways to do it. The shape of the posterior surface of the cornea can be measured using imaging techniques where the cornea is illuminated by a slit lamp and the illumination viewed at an oblique angle. One such technique is Scheimpflug photography which is applied in ophthalmology. In this technique the cross sectional plane illuminated by the slit beam can be sharply imaged. Thus, the captured image represents the sagittal cross section of the cornea and the lens of the eye if the slit illumination is vertical(see Figure 7). A drawback of this method is that the captured image is a deformed representation of the correct shape of the cornea and the lens. Two

factors contribute to this deformation. First, the image is viewed at an oblique angle causing distortion and second, light from the illuminated region is refracted as it passes through the lens and corneal interfaces causing changes in the form of the image. Nevertheless, correction for this is possible and is well described by Dubbelman, Van der Heijde and Weeber(2005).[13] Thus, with Scheimpflug photography, the shape of the posterior corneal surface can be accurately measured.

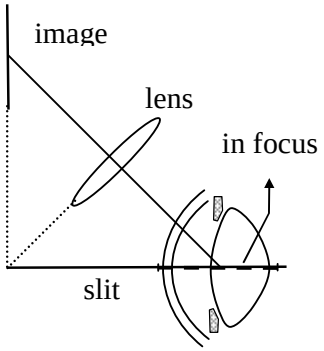

Figure 7 *Schematic diagram of a typical configuration of Scheimpflug photography applied to imaging of the eye.*

1.4 OVERVIEW AND AIMS OF THE STUDY

The current status regarding determination of the optical properties of the cornea is summarized as follows (note that since the refractive index of air, cornea and the aqueous humor is known, specifying corneal shape leads to the derivation of the refractive properties of the cornea):

1) Although Placido ring topography is a standard procedure to measure the shape of the anterior corneal surface, skew ray error problem remains an issue. The VU topographer was designed to eliminate skew ray error. However, prior to this study, experimental proof of this has not yet been shown.
2) Although there are several ways to measure the shape of the posterior corneal surface, little is known regarding the role of posterior surface with respect to the wave aberrations of the eye.

This study aims to answer the following questions:

1) Can the surface of the cornea be accurately reconstructed using images coming from a colored pattern (The VU topographer)?

2) What is the contribution of the corneal posterior surface to the corneal wave aberration?

To answer the first question, two approaches were employed. The theoretical and numerical approach is discussed in Chapter 2 and the experimental approach is discussed in Chapter 3. Chapter 2 describes an algorithm that was developed for the VU topographer. This algorithm reconstructs the corneal surface using photos of reflection patterns on the cornea and information of the location of the reflection source (stimulator). Numerical simulation was done to assess the performance of this algorithm in reconstructing various surfaces. For this algorithm to be useful, it is important that the error coming from this algorithm should be smaller than errors coming from other sources in actual eye measurements. An example of a source for errors in actual eye measurements would be the depth of focus of the imaging system. Another example would be eye movements. With knowledge of these sources of errors it will be shown with actual eye measurements in addition to tests done on artificial surfaces that the VU topographer reconstructs the shape of the anterior corneal surface with reasonable accuracy. This is the main discussion of Chapter 3. A comparison was done with measurements coming from a ring topographer to show the improvement of surface reconstruction of the anterior corneal surface due to elimination of the skew ray error.

Three chapters address the second question. Using Scheimpflug photography the contribution of the corneal posterior surface to corneal wave aberration was determined. The contribution to astigmatism, spherical aberration and coma aberration is discussed in chapters 4, 5 and 6 respectively. Since the Scheimpflug images are 2D images, combining information from measurements of varied meridian orientation is necessary to reconstruct the essential 3D shape property of the posterior surface. In this manner the contribution of the wave aberration of the posterior surface can be determined. Usually, the design of intraocular lenses is dependent on information of the optical properties of the

anterior corneal surface. The contribution of the posterior corneal surface is neglected. In applications, it will be interesting to know with certainty when neglecting the contribution of the posterior surface is valid and when it is not.

REFERENCES

1. Hecht E, **Optics 2nd edition** (1987). Reading, Massachusets: Addison-Wesley Publishing Company, Inc. pp.134-210.
2. Rabbetts RB, **Bennet and Rabbetts' Clinical Visual Optics 3rd edition** (1998). Oxford: Butterworth-Heinemann pp. 281-285.
3. Born M, Wolf E. **Principles of Optics 7th edition** (1999) Cambridge: Cambridge University Press p. 523.
4. Atchison DA. Recent advances in representation of monochromatic aberrations of human eyes. Clin Exp Optom 2004; 87:137-148.
5. Hopkins HH. **Wave Theory of Aberrations** (1950). Oxford: Clarendon Press p. 12
6. Reynolds AE. Introduction: History of Corneal Measurement. In **Corneal Topography: Measuring and Modifying the Cornea.** (Schanzlin, DJ & Robin JB eds.) (1992) Springer-Verlag vii-x.
7. Van Saarloos PP, Constable IJ. Improved Method for Calculation of Corneal Topography for any Photokeratoscope Geometry. Optom Vis Sci 1991; 68:960-965.
8. Massig JH, Lingelbach E, Lingelbach B. Videokeratoscope for accurate and detailed measurement of the cornea surface. App Opt 2005; 44: 2281-2287.
9. Klein SA. Axial curvature and the skew ray error in corneal topography. Optom Vis Sci 1997;74: 931-944.
10. Greivenkamp JE, Mellinger MD, Snyder RW, Schwiegerling JT, Lowman AE, Miller JM. Comparison of Three Videokeratoscopes in Measurement of Toric Test Surfaces. J Ref Surg 1996; 12: 229-239.
11. Rand RH, Howland HC, Applegate RA. Mathematical model of a Placido disk keratometer and its implications for recovery of corneal topography. Optom Vis Sci 1997; 74: 926-930.
12. Vos FM, Van der Heijde GL, Spoelder HJW, Van Stokkum IHM, Groen FCA. A new PRBA-based instrument to measure the shape of the cornea. IEEE Trans Instrum Meas 1997; 46:794-797.
13. Dubbelman M, Van der Heijde GL, Weeber HA. Change in shape of the aging human crystalline lens with accommodation. Vision Research 2005; 45: 117-132.

2

CORNEAL SURFACE RECONSTRUCTION ALGORITHM THAT USES ZERNIKE POLYNOMIAL REPRESENTATION

VADP Sicam, J Coppens, TJTP van den Berg, RGL van der Heijde

Journal of the Optical Society of America A 21, 1300-1306, 2004.

ABSTRACT

We developed an algorithm that directly determines Zernike coefficients describing corneal anterior surface derived from the reflection image of a stimulus with pseudo random encoding. This algorithm does not need to include calculation of corneal height maps. The numerical performance of the algorithm is good. It has the potential of determining corneal shape with submicron accuracy in obtaining Zernike coefficients. When applied to real eye measurements the accuracy of the procedure will be limited to the topographer that is used.

2.1 INTRODUCTION

The cornea and the lens play a major role in shaping the aberrations of the human eye.[1] In principle, it has been shown that the corneal wave aberration of the eye can be obtained from a corneal surface data represented as a Zernike polynomial expansion.[2] In performing this procedure, the usual available information given by corneal topographers is the corneal height map derived from various surface reconstruction algorithms.[3, 4,5] The process can be described by the following flow: corneal reflection measurements → corneal height data → Zernike representation (corneal shape) → Zernike representation (wave-front). We developed a method where the first part of the described flow, corneal reflection measurements → corneal height data, is bypassed and instead do a direct conversion, corneal reflection measurements → Zernike representation (corneal shape).

We applied this algorithm to a topographer that, unlike ring topographers that employ a Placido disk system, uses a color-coded stimulus pattern. By using this topographer it is easy to uniquely determine one-to-one correspondence between points on the recorded Purkinje image and points on the source pattern using a pseudo random array.[3] This property makes it possible to develop a corneal surface reconstruction algorithm that does not have to be dependent on axial symmetry, thus avoiding skew-ray ambiguity and errors caused by this dependence when Placido rings are used as targets. The skew-ray error issue with topographers that use Placido rings is discussed thoroughly by Klein[6]. Nevertheless, in a separate paper, Klein introduces an algorithm applicable to Placido rings that avoids this problem[7].

The surface reconstruction we used includes tracing rays from image points to stimulus points and fitting of surface normals to calculate the Zernike coefficients representing the surface. This procedure is similar to that of Halstead et al, but in our case the surface representation is made as a Zernike

expansion instead of using splines.[4] One of the advantages of Halstead's algorithm is its stability in the presence of noise. This is due to the fact that this algorithm uses a least squares fitting routine. However, the disadvantage of the algorithm compared to that of Klein's is its relatively slow processing speed. In our case, instead of using a non-linear minimization scheme, we introduce an approximation (eqn. 10) used in the least squares fitting routine. This linearization scheme improves the calculation time. The performance of this algorithm is evaluated using numerical and experimental data.

2.2 CONIC SURFACES AND ZERNIKE POLYNOMIAL REPRESENTATION

To help in the analysis of the performance of the surface reconstruction method, a discussion on symmetric conic surfaces and Zernike polynomial representation will be useful.

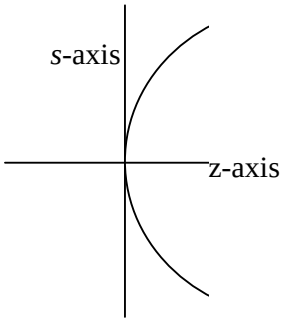

Figure 1 *Diagram showing reference axis used in describing conic surface.*

By using the reference axis illustrated in Figure 1, a symmetric conic surface can be expressed by the following equation[8]:

$$s^2 - 2rz + kz^2 = 0. \qquad (1)$$

This reference axis selection differs from that recommended by the OSA task force only in that the z-axis points in the opposite direction.[9] In Equation (1), r is the radius of curvature measured at the apex of the surface and k is the parameter describing what type of conic the surface is. For example: $k = 0$ for a parabola, $k = 1$ for a sphere, any other positive value of k describes an ellipse and $k < 0$ describes a hyperbola.[10] The apex of the surface is located at $(s,z) = (0,0)$. The variable, s, is actually the combination of both x-axis and y-axis:

$$s^2 = x^2 + y^2. \qquad (2)$$

This means that the surface described by Equation (1) is symmetric about the *z* axis. Equation (1) is a quadratic equation with respect to the sagitta *z*, and the solution expanded in Mclaurin series is given by

$$z = \frac{s^2}{2r} + \frac{ks^4}{8r^3} + \frac{k^2 s^6}{16r^5} + \frac{5k^3 s^8}{128r^7} + \ldots \quad (3)$$

The sagitta *z* can also be represented in standard Zernike notation[9]:

$$z = \sum C_n^m Z_n^m(\rho,\theta). \quad (4)$$

where $Z_n^m(\rho,\theta)$ are Zernike polynomials and the C_n^m's are the corresponding Zernike coefficients which can be expressed in μm. The indices *n* and *m* describe radial order and azimuthal frequency of the sinusoidal component respectively. The variable, ρ, is related to *s* by the following equation:

$$s = r_p \rho. \quad (5)$$

Where, r_p is the pupil radius chosen to represent the surface. A good discussion of Zernike polynomials is done by Malacara[11]. Comparing Equation (3) with Equation (4), we have the following approximation for the apical radius of curvature *r* and the *k* parameter with respect to the Zernike coefficients (consider expanding up to radial order = 6):

$$r = \frac{r_p}{2(2\sqrt{3}C_2^0 - 6\sqrt{5}C_4^0 + 12\sqrt{7}C_6^0)}. \quad (6)$$

$$k = \frac{8r^3}{r_p^3}(6\sqrt{5}C_4^0 - 30\sqrt{7}C_6^0). \quad (7)$$

Equations (6) & (7) show that one of the benefits of describing corneal shape using Zernike polynomials is that information about the apex radius of curvature *r* and the conic parameter *k* is readily available. The approximation becomes better when the radial order used in the expansion is increased. In addition, the use of the conic parameter *k* helps in determining whether the reconstruction is good not only on the corneal apex but also on the periphery.

2.3 RECONSTRUCTION ALGORITHM

Figure 2 shows a schematic diagram of the Vrije University topographer. What are available from the measurements are stimulator points (examples s_i and s_j in the figure) and their matching image points (examples, c_i and c_j in the figure). There are two reference planes used in the reconstruction method. The first one is an *x-y* plane (described by points A & D in Figure 3) that includes the apex of the corneal surface to be reconstructed. The second plane is a modified CCD *u-v* plane (described by points B & C in Fig. 3). The plane is not the actual CCD plane because the CCD image's pixel coordinates are converted to millimetres by means of calibration such that line segment *AD* is now equal in distance to line segment *BC* in Figure 3. This is done to make the representation of the surface to be reconstructed in *u-v* coordinates. The calibration has two conversions: The first converts pixel counts into millimetres, the second relates the Purkinje image plane to the *AD* plane.

The ray SP corresponds to the incident light ray coming from the stimulator point. This ray is reflected by

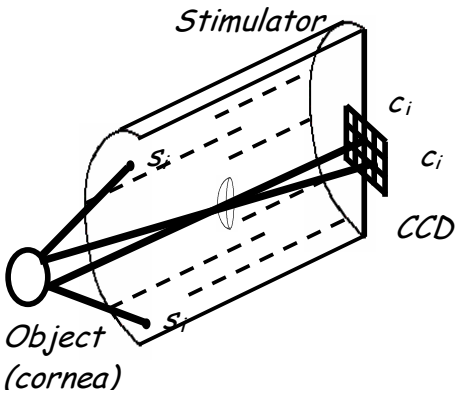

Figure 2 *Schematic diagram of the VU*

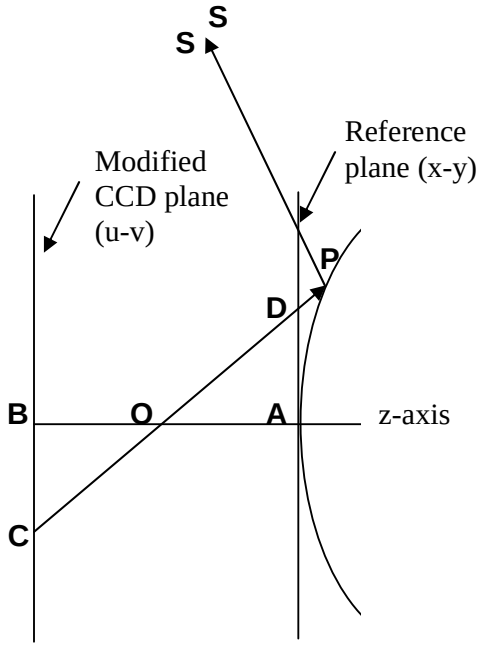

Figure 3 *Schematic diagram showing backward ray tracing principle used in the surface reconstruction algorithm.*

the surface and proceeds in the direction of ray *PO*. Following the law of reflection the angle bisector of $\angle SPO$ should correspond to the normal of the surface at point P. Using this criterion, a least squares fitting routine was set up so that the correct set of Zernike coefficients describing the surface (denoted by curve AP in Figure 3) is obtained. Backward ray tracing was done in the implementation of this routine since this is more straightforward compared to the forward ray tracing. For forward ray tracing the direction of ray *SP* is not readily available.

The implementation of the least squares routine is initiated by considering an arbitrary surface. This surface can be represented as a sum of Zernike polynomials, and therefore has its own unique set of Zernike coefficients C_n^m. Since we are using Zernike polynomials the coordinate system we use (origin at point A of Figure 3) is scaled to make the pupil area (with pupil radius r_p) of the corneal surface a unit circle. Point C in the CCD plane has coordinates (u, v, -*OB*), where *OB* is the distance between the nodal point O and point B. Line *CO* is traced to point D, which has the coordinates (x, y, *OA*), where $x = -u$, $y = -v$ and $OA = OB$. Point C is used as a reference point to determine the intersection point of ray *OD* with the surface, denoted by P in Figure 3.

P(x_p,y_p, z_p) has the following coordinates:

$$x_p = -u - \frac{u}{OA} z_p . \tag{8}$$

$$y_p = -v - \frac{v}{OA} z_p . \tag{9}$$

$$z_p = \sum_i^K C_i [Z_i(-u,-v) - Z_i(0,0)] * (1 + \frac{u^2 + v^2}{OA * AR}) . \tag{10}$$

Where, Z_i's are Zernike polynomials and C_i's are the Zernike coefficients. The single index i is used here to simplify the mathematical representation. Subtraction of the evaluation at (0,0) keeps the apex of the surface in the origin. Equations (8) and (9) are obvious from the geometry of the system and equation (10) is derived using geometrical principles as shown in Figure 4.

The length, $z_{p,}$ in Equation (10) is the sum of the length of line segments *DF* and *FG*. We can relate these lengths to easily derivable quantities, angles α and β.

$$\tan\alpha = \frac{\sqrt{u^2 + v^2}}{OA}. \qquad (11)$$

$$\tan\beta = \frac{\sqrt{u^2 + v^2}}{AR}. \qquad (12)$$

Where *AR* is related to $r_{p,}$ the pupil radius chosen to represent the surface and *r*, the apex radius of curvature of the surface to be reconstructed:

$$AR = \frac{r}{r_p}. \qquad (13)$$

Note that *AR* is a dimensionless quantity instead of length dimension because when the surface representation is done in Zernike expansion everything is converted using the scaling factor $1/r_p$ to make the area considered for the expansion a unit circle.

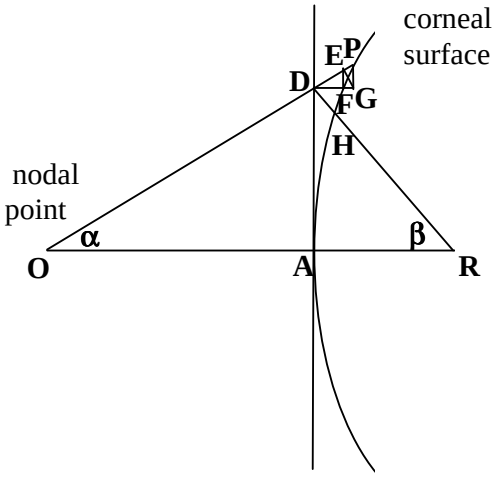

Figure 4 *Diagram used to derive Equation (10)*

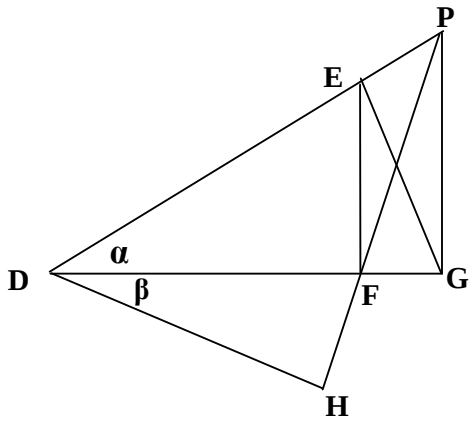

Figure 5 *Blow-up of a section in Figure 4*

In Figure 5 a blow-up of a part Figure 4 is shown. The segment *HFP* is strictly speaking not a line but a curve. The triangle *DFH* and *FPG* are almost similar triangles so

$$\angle FPG \cong \beta \qquad (14)$$

Hence,

$$\tan\beta \cong \frac{FG}{PG} \qquad (15)$$

The angle α is a small angle since the corneal surface apex is at a considerable distance to the nodal point (307.6 mm). Thus the line segment PG and EF is approximately equal. Thus,

$$\tan\beta \cong \frac{FG}{EF} \qquad (16)$$

Also,

$$\tan\alpha = \frac{EF}{DF} \qquad (17)$$

By multiplying Equations (16) and (17) and rearranging we arrive at:

$$FG \cong DF \tan\alpha \tan\beta \ . \qquad (18)$$

By using Equations (11), (12) & (18) we arrive at Equation (10). Although we used more than one approximation in arriving at relation (18) it will be shown later that the performance of this approximation is good. However, as also will be shown later, the error of the approximation gets worse when evaluating the peripheral sections of the cornea.

Once the intersection point is defined, other relevant vectors can be obtained. Let point O and point S in Fig. 3 be denoted by coordinates (0,0,0) and (x_s,y_s,z_s) respectively, then the following vectors are obtained through backward ray tracing.

$$\overrightarrow{OP} = < x_p, y_p, z_p > - < 0,0,0 > . \qquad (19)$$

$$\overrightarrow{PS} = < x_s, y_s, z_s > - < x_p, y_p, z_p > . \qquad (20)$$

The angle bisector of $\angle SPO$ is just

$$\vec{n} = \frac{\overrightarrow{PS}}{\left\|\overrightarrow{PS}\right\|} - \frac{\overrightarrow{OP}}{\left\|\overrightarrow{OP}\right\|} . \qquad (21)$$

Tangent vectors of the surface at point P can be evaluated using differentiation:

$$\vec{t}_u = \frac{\partial x_p}{\partial u}\hat{x} + \frac{\partial y_p}{\partial u}\hat{y} + \frac{\partial z_p}{\partial u}\hat{z} . \qquad (22)$$

$$\vec{t_v} = \frac{\partial x_p}{\partial v}\hat{x} + \frac{\partial y_p}{\partial v}\hat{y} + \frac{\partial z_p}{\partial v}\hat{z}\,. \tag{23}$$

Substituting Equations (8) and (9) to Equations (25) and (26) we arrive at:

$$\vec{t_u} = \left[-1 + \frac{\partial}{\partial u}\left(\frac{-uz_p}{OA}\right)\right]\hat{x} + \frac{\partial}{\partial u}\left(\frac{-vz_p}{OA}\right)\hat{y} + \frac{\partial z_p}{\partial u}\hat{z}\,. \tag{24}$$

$$\vec{t_v} = \frac{\partial}{\partial v}\left(\frac{-uz_p}{OA}\right)\hat{x} + \left[-1 - \frac{\partial}{\partial v}\left(\frac{-vz_p}{OA}\right)\right]\hat{y} + \frac{\partial z_p}{\partial v}\hat{z} \tag{25}$$

The angle bisector of $\angle$SPO is not yet normal to $\vec{t_u}$ and $\vec{t_v}$ with the initial set of Zernike coefficients, therefore the inner product of $\vec{n}$ with $\vec{t_u}$ and $\vec{t_v}$ will be non-zero. The goal is to minimize this inner product and this would serve as the error function in the general least squares method used in the reconstruction procedure. These inner products can be written as:

$$\vec{n} \bullet \vec{t_u} = -n_x + n_x \frac{\partial}{\partial u}\left(\frac{-uz_p}{OA}\right) + n_y \frac{\partial}{\partial u}\left(\frac{-vz_p}{OA}\right) + n_z \frac{\partial z_p}{\partial u} \tag{26}$$

$$\vec{n} \bullet \vec{t_u} = -n_y + n_x \frac{\partial}{\partial v}\left(\frac{-uz_p}{OA}\right) + n_y \frac{\partial}{\partial v}\left(\frac{-vz_p}{OA}\right) + n_z \frac{\partial z_p}{\partial v} \tag{27}$$

Note that z_p is a function of u and v, thus Equations (26) and (27) can be written in compact form:

$$\vec{n} \bullet \vec{t_u} = -n_x + \sum_i^K M_i(u,v)C_i \tag{28}$$

$$\vec{n} \bullet \vec{t_v} = -n_y + \sum_i^K N_i(u,v)C_i \tag{29}$$

where the C_i 's are Zernike coefficients and the functions M_i and N_i can be derived using equations (26),(27), and (10).

By applying Equation (28) and (29) to the N image points we create a matrix equation in the form $\vec{e} = \vec{y} - B\vec{c}$ where $\vec{e}$ is the error to be minimized,

$$\vec{y}=\begin{pmatrix} n_{x1} \\ \vdots \\ n_{xN} \\ n_{y1} \\ \vdots \\ n_{yN} \end{pmatrix},\quad B=\begin{bmatrix} M_{11} & \cdots & M_{1K} \\ \vdots & \vdots & \vdots \\ M_{N1} & \cdots & M_{NK} \\ N_{11} & \cdots & N_{1K} \\ \vdots & \vdots & \vdots \\ N_{N1} & \cdots & N_{NK} \end{bmatrix},\quad \mathbf{C}=\begin{pmatrix} C_1 \\ C_2 \\ \vdots \\ C_K \end{pmatrix} \tag{30}$$

The solution for this minimization is given by:

$$\vec{C}=[B^T B]^{-1}[B^T \vec{y}]. \tag{31}$$

With the new set of Zernike coefficients, **C** obtained from Equation (31), the process is repeated going back to Equations (8) to (10) and when applied to numerical simulations, the convergence is fast. By starting from a flat surface, even with only 3 repetitions, the solution given is already close to actual values. This reveals that an input that is close to the correct corneal shape is not necessary.

2.4 NUMERICAL TESTING

The reconstruction algorithm can be tested numerically by the following procedure. First, given a set of image points on a camera and a known surface (i.e. *k* and *r* are known values for a given conic surface), the stimulator points are calculated. Next, the pairing of image points and stimulator points is used as input and the reconstruction algorithm is applied. The output of this procedure is a set of Zernike coefficients describing the surface.

Table 1 *Numerical Performance of the Algorithm on a Small Sphere* [a]

Pupil Diameter (mm)	Reconstructed *r* (mm)	Reconstructed *k*
7	6.9999	1.00
8	6.9997	1.00
9	6.9988	0.99
10	6.9947	0.95
11	6.9776	0.82

[a] r = 7.8700 mm, k = 0.82, radial order = 10.

Table 1 shows results of using this procedure. The reference surface used is a sphere (k = 1.0) of 7 mm radius to simulate a small cornea. The typical corneal size is larger[10]. The Zernike expansion order used is 10. The pupil diameter $2r_p$ was varied from 7 mm to 11 mm to simulate reconstructing a full corneal width. The reconstruction is still good up to a pupil diameter of 9 mm. The reconstructed radius of curvature deviates from the theoretical value by no greater than 1.2 μm. For a pupil diameter of 10 mm the error in the reconstructed radius of curvature is about 5.3 μm. The corresponding reconstructed shape factor *k* is 0.95. The deviation in the reconstructed shape factor when 10 mm pupil diameter was chosen for the reconstruction indicates that the error is mainly caused by the breakdown of Equation (18) when reconstructing the peripheral section of the cornea. Nevertheless, this breakdown in the approximation does not happen for reconstructing corneal surface with larger sizes. Table 2 shows results of simulating a typical corneal surface with apex radius of curvature, r = 7.8700 mm and shape factor k = 0.82[10]. The reconstruction works well even for a large pupil diameter of 11 mm. The error in the reconstructed apex radius of curvature is submicrometer for a pupil diameter as high as 10 mm and for a pupil diameter of 11 mm the error is 1.2 μm. For all cases in Table 2 the surface reconstruction gave accurate values of the shape factor *k*.

Table 2 *Numerical Performance of the Algorithm on a Typical Cornea*[a]

Pupil Diameter (mm)	Reconstructed *r* (mm)	Reconstructed *k*
7	7.8700	0.82
8	7.8700	0.82
9	7.8699	0.82
10	7.8696	0.82
11	7.8688	0.81

[a] r = 7.8700 mm, k = 0.82, radial order = 10.

We can verify how the algorithm reconstructs a surface that is a combination of a parabolic term and an astigmatic term:

$$z = \frac{s^2}{2r} + qs^2 \sin 2\theta \,. \quad (32)$$

Where q is the degree of astigmatism. We choose this surface to include the simple nonsymmetric Zernike term Z_2^{-2} in the analysis.

Table 3 shows results of applying the algorithm to a numerical simulation of an astigmatic surface. The radial order used in the Zernike expansion for this case is order 10. Surfaces with corneal astigmatism from 0.5 D to 2.0 D were considered. For this type of surface the non-zero Zernike coefficients would be the symmetric power coefficient C_2^0 and the non-symmetric astigmatic coefficient C_2^{-2}. The algorithm produces better accuracy in reconstructing the symmetric coefficient compared to the non-symmetric coefficient. Nevertheless the algorithm reconstructs both symmetric and non-symmetric Zernike coefficients with a good accuracy of better than 0.1 μm.

Table 3 *Numerical Performance of the Algorithm Applied to an Astigmatic Surface*[a]

Corneal Astigmatism (D)	Reconstructed $C_2^{0(b)}$ (μm)	Theoretical C_2^{-2} (μm)	Reconstructed C_2^{-2} (μm)
0.5	288.6889	2.43	2.44
1.0	288.6890	4.86	4.88
1.5	288.6892	7.29	7.32
2.0	288.6894	9.72	9.77

[a] r = 8.00 mm, pupil diameter =7.0 mm, radial order =10.
[b] Theoretical value of C_2^0 is 288.6751

Table 4 *Numerical Performance of the Algorithm Applied to a Surface described by Higher-Order Zernike Polynomial* Z_8^{-8} [a]

Reconstructed $C_2^{0(b)}$ (μm)	Theoretical C_8^{-8} (μm)	Reconstructed C_8^{-8} (μm)
288.6891	2.43	2.49
288.6894	4.86	4.97
288.6901	7.29	7.46
288.6910	9.72	9.94

[a] r = 8.00 mm, pupil diameter =7.0 mm, radial order =10.
[b] Theoretical value of C_2^0 is 288.6751

Simulation was also made for a surface that is a combination of a parabolic term and a surface described by the higher order Zernike polynomial Z_8^{-8} for which

$$z = \frac{s^2}{2r} + qs^8 \sin 8\theta \quad (33)$$

Most of the parameters used for this simulation are the same as the ones used for the astigmatic surface. The theoretical values for the coefficient C_8^{-8} were chosen such that it has the same values as the ones used for C_2^{-2} in the simulation of an astigmatic surface. As shown in Table 4 the accuracy in reconstructing C_2^{0} for this simulation is practically the same as that made for the astigmatic surface. The accuracy in reconstructing C_8^{-8} is slightly worse than that of C_2^{-2}. This may be attributed to the fact that the shape of the Zernike polynomial Z_8^{-8} has dominant features in the periphery and from the simulation of a small cornea (results shown in Table 1), the algorithm has difficulties when evaluating the peripheral region. Nevertheless, the accuracy in reconstructing the coefficient C_8^{-8} is still submicrometer (< 0.3 μm).

Further numerical tests were made for a surface that is a combination of a parabolic surface and a shape function proposed by Rand *et. al.*[12](see Figure 6):

$$z = \frac{s^2}{2r} + g(s,\theta) \tag{34}$$

$$g(s,\theta) = \begin{cases} \varepsilon \sin 8\theta & for \quad s \geq 2mm \\ 2(s-1.5)\varepsilon \sin 8\theta & for \; 1.5 < s < 2mm \\ 0 & for \quad s \leq 1.5mm \end{cases} \tag{35}$$

The shape function $g(s,\theta)$ is meant to maximize the meridional ambiguity which makes this type of surface difficult to reconstruct using Placido ring topographers. We used ε=0.01 mm for this simulation and a pupil diameter of 8 mm.

As shown in Fig. 7, because of the nature of the surface, quite a number of polynomials is needed to capture the surface topography. For a radial order of 8 (Figure 7b), only the outer edges of the peripheral

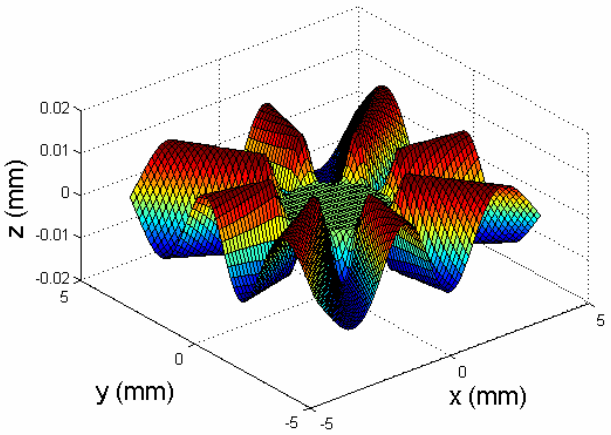

Figure 6 *Theoretical shape function.*

corrugations of the shape function is reconstructed. Increase of the radial order used in the reconstruction slowly reveals the actual feature of the shape function. Using a radial order of 20 (Figure 7e), the reconstructed surface already has all the distinguishing features of the original shape function, with the amplitude of the peripheral corrugations obtained as 10.2 μm compared to 10.0 μm of the original shape function. This means that for the peripheral section of the surface the accuracy in reconstructing height values is submicron. This result is comparable to the accuracy in determining height values of the algorithm reported by Klein.[7]

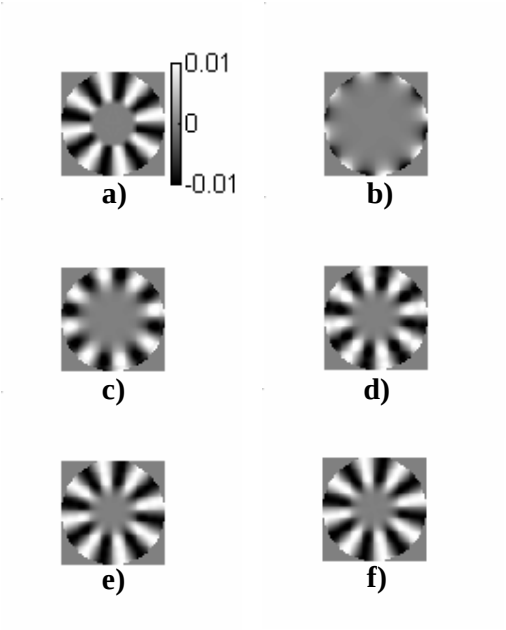

Figure 7 *Grey-scale contour map (in mm) of a) the theoretical shape function and its reconstruction using varying radial orders b) order 8, c) order 12, d) order 16, e) order 20 and f) order 24.*

2.5 EXPERIMENTAL PERFORMANCE

For numerical simulations, the accuracy of the corneal representation becomes better with increasing Zernike radial order used in representing the surface. However, this principle cannot be applied to real eye measurements because of noise. Many factors contribute to this noise, e.g., instrument noise, eye movements, variation in tear film and measurement variation caused by the operator of the topographer.

Measurements were taken on five human eyes taking five trials for each eye and the variation due to noise were noted for different radial order used in the Zernike expansion. The signal to noise ratio in shown in Fig. 8 indicates that when using higher radial orders the higher order signal becomes comparable to noise (S/N ≅ 1). We show this to caution future users of this algorithm that

increasing indefinitely the radial order used in the Zernike expansion does not necessarily improve the surface reconstruction.

We applied the algorithm to reconstruct surfaces of spherical balls (Table 5). The measurements have a repeatability of better than 15 μm in determining the radius of curvature of the balls, and the variation in the calculated k-value of the surface is less than 0.1.

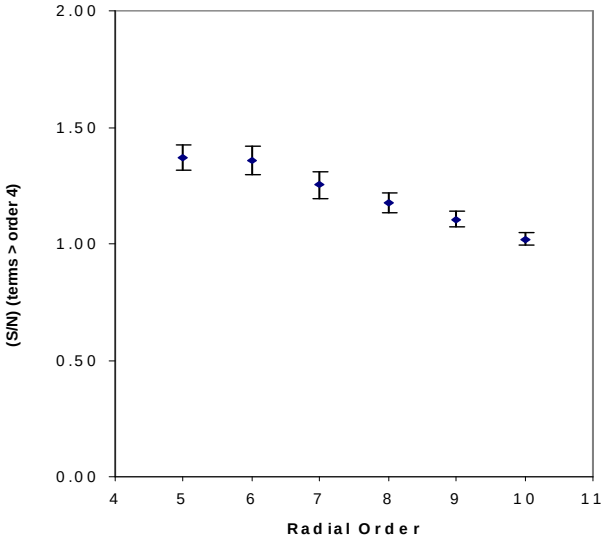

Figure 8 *Signal to Noise Ratio vs. Radial Order*

When the position of the surface apex is aligned with respect to the topographer optical axis, the measured Zernike coefficients C_1^{-1} and C_1^{1} have very small absolute values (Figure 9). This is useful as a guide to locate a reference position for the corneal surface. On the other hand, the Zernike power terms C_2^{0} have small variations (< 2 μm) when the same surface is placed at different locations within 0.5 mm from the reference position (Figures 9 and 10).

Table 5 *Measurements on Spherical Balls with Varying Radii*

Measured *r* (mm)	Theoretical *k*	Reconstructed *r* (mm)	Reconstructed *k*
5.999	1.00	6.004 ± 0.008	1.14 ± 0.05
6.998	1.00	6.999 ± 0.003	0.99 ± 0.02
8.000	1.00	7.993 ± 0.006	0.93 ± 0.05
9.000	1.00	8.998 ± 0.006	0.99 ± 0.05
9.976	1.00	9.982 ± 0.008	1.14 ± 0.05

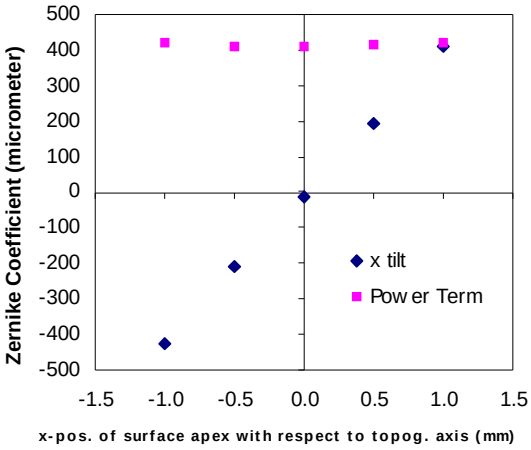

Figure 9 *Effect of alignment on Zernike tilt and power term.*

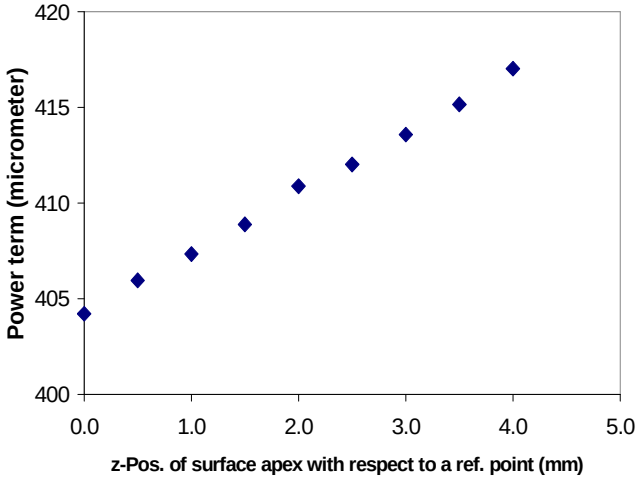

Figure 10 *Effect of z-position of surface on Zernike power term.*

2.6 CONCLUSIONS

We have demonstrated a method of calculating Zernike coefficients that describe corneal shape without the intermediate step of determining corneal height maps. This creates new possibilities for calculating the contribution of the cornea to wave aberrations of the eye. Our surface reconstruction technique may be employed by using other surface representation as well, e.g., splines and Taylor series polynomials. The advantage of using Zernike coefficients is that familiar clinical parameters such as corneal apex radius of curvature *r*, shape parameter *k*, and astigmatism are readily available.

We have shown that the developed algorithm has the numerical potential of determining apex radius of curvature of corneal surface, surface height values and Zernike coefficients (for corneal shape) with submicrometer accuracy.

Using a color-coded stimulus pattern instead of the traditional placido rings is helpful because it provides one-to-one correspondence between source and image points. Therefore, no meridional assumption on the orientation of the corneal normal is necessary, which makes the algorithm we used free from skew

ray error. The use of a linearization scheme in the least squares fitting routine of the algorithm improves the calculation time compared with other existing algorithms that use least squares fitting.

We note also that the numerical error of the algorithm is small compared to noise when measuring real eyes. If there is a need for improvement, then it should be more on minimizing measurement variability than in improving the numerical accuracy of the algorithm.

REFERENCES

1. P. Artal and A. Guirao. "Contributions of the cornea and the lens to the aberrations of the human eye," Opt. Let. **23**(21), 1713-1715, (1998).
2. A. Guirao and P. Artal. "Corneal wave aberration from videokeratography: accuracy and limitations of the procedure," J. Opt. Soc. Am. A, **17(**6), 955-965, **(**2000).
3. F.M Vos, G.L. van der Heijde, H.J.W Spoelder I.H.M. van Stokkum and F.C.A. Groen. "A new PRBA-based instrument to measure the shape of the cornea," IEEE Trans. Instrum. Meas. **46**(4), 794-797, (1997).
4. M.A. Halstead, B.A. Barsky, S.A. Klein and R.B. Mandell. "A spline surface algorithm for reconstruction of corneal topography from a videokeratographic reflection pattern," Optom. Vis. Sci., **72**, 821-827, 1995.
5. R. Mattioli and N.K. Tripoli. "Corneal Geometry Reconstruction with the Keratron Videokeratographer." Optom. and Vis. Sci., **74**(11), 881-894 (1997).
6. S.A. Klein. "Axial curvature and the Skew Ray Error in Corneal Topography," Optom. and Vis. Sci. **74**(11), 931-944, (1997).
7. S.A. Klein. "Corneal Topography Reconstruction Algorithm that Avoids the Skew Ray Ambiguity and the Skew Ray Error," Optom. and Vis. Sci. **74**(11), 945-962 (1997).
8. A.W. Greynolds. "Superconic and subconic surfaces in optical design," in 2002 International Optical Design Conference (Tucson, AZ, USA, June 3-7, 2002) Technical Digest, p.2, Tucson, AZ, USA, June 3-7, Copyright 2002, Optical Society of America.
9. L .N. Thibos, R.A. Applegate, J.T. Schwiegerling and R. Webb. Standards for reporting the optical aberrations of eyes. J. of Ref. Surg., **18,** 652-660, (2002).

10. M. Dubbelman, H.A. Weeber, G.L. van der Heijde and H.J. Völker-Dieben. "Radius and asphericity of the posterior corneal surface determined by corrected Scheimpflug photography." Acta Ophth. Scand., **80**, 379-383, (2002).
11. D. Malacara. Optical Shop Testing 2nd Ed. (John Wiley & Sons, New York, 1992).
12. R. H. Rand, H. C. Howland and R. A. Applegate. "Mathematical Model of a Placido Disk Keratometer and Its Implications for Recovery of Corneal Topography." Optom. And Vis. Sci. 74(11), 926-930 (1997).

3

TOPOGRAPHER RECONSTRUCTION OF THE NON-ROTATION-SYMMETRIC ANTERIOR CORNEAL SURFACE FEATURES

VADP Sicam and RGL van der Heijde

Optometry and Vision Science 83, 2006.

ABSTRACT

Purpose: To demonstrate the performance of a topographer (the VU topographer) that uses a color-coded stimulus pattern to reconstruct both the rotation-symmetric and non-rotation-symmetric shape features of the anterior corneal surface.

Methods: Spherical surfaces, toric surfaces, the Rand surface (surface with peripheral corrugations) and sample eyes were measured. A ring topographer (Keratron) and the Haag-Streit Ophthalmometer were used for comparison.

Results: All three instruments produced similar values for the radii of curvature of spherical surfaces with a tolerance of 0.02 mm. The Keratron gave under-estimated values for the astigmatic power of toric surfaces (> 0.25 D for toric surfaces with astigmatism > 9 D). Because it eliminates skew ray error, only the VU topographer was able to reconstruct the correct shape of the Rand surface in contrast with ring topographers. The effect of skew ray error was also observed in the surface reconstruction of a radially keratotomized (RK) eye. There was height difference of 2.75 ± 1.25 μm between the output of the VU topographer and the output of the Keratron.

Conclusion: The VU topographer is just as accurate in reconstructing the rotation-symmetric features of the anterior corneal surface as the ring topographers, but is superior in recovering the non-rotation-symmetric shape features.

3.1 INTRODUCTION

Computer-assisted videokeratographs (CAVK) are used in standard ophthalmic practice to reconstruct the geometric shape of the anterior corneal surface. A technique that is widely used in CAVK devices is Placido disk imaging.[1,2] In this type of imaging system, a series of rings is reflected onto the cornea, and the reflected images are recorded in a video camera. Based on the information generated from the recorded images, the shape of the anterior surface of the cornea is reconstructed using mathematical algorithms. It is known that commercially available Placido ring topographers use algorithms that assume that the light rays coming from one meridian of the ring pattern is reflected onto the same meridian in the virtual image.[3,4] This assumption excludes skew ray reflections. Consequently, errors (the skew ray error) will occur in the surface reconstruction, because the corneal surface is not a rotation-symmetric object.[5] Thus, with a Placido ring topographer it will be difficult to reconstruct corneal shapes that are not rotation-symmetric.[6,7] Efforts have been made to produce cornea topographers that can perform better than Placido ring topographers.[4,8,9,10] However, these instruments have not yet been validated with test surfaces that are not rotation-symmetric.

In this study, measurements of different types of surfaces were made with a special cornea topographer (the VU topographer) based on a color-coded stimulus pattern.[8] The advantage of using such an instrument is that it facilitates the development of surface reconstruction algorithms that are free from skew ray errors, because there is one-to-one correspondence between stimulator points and image points.[11] Eliminating the skew ray errors makes it possible to accurately reconstruct non-rotation-symmetric surfaces.

3.2 THE SKEW RAY ERROR AND NON-ROTATION-SYMMETRIC SURFACES

The toric surface is the simplest non-rotation-symmetric surface that is relevant in ophthalmic practice. The skew ray error introduces height errors in the reconstruction of toric surfaces when a Placido ring topographer is used. Tripoli, Cohen, Obla, Coggins and Holmgren (1996) observed that the height error in the reconstructed surface can be as much as 6.5 μm for a toric surface with 4 diopter astigmatic power.[7] This amount of height error can be substantial and its effect on the calculation for the radius of curvature can be derived from the equation of a conic curve[11]:

$$s^2 - 2rz + kz^2 = 0 \qquad (1)$$

where s is the radial axis in the x-y plane and z is the height (or sag) axis. Consider a corneal surface with average values for the shape parameters r and k (radius of curvature and asphericity): r = 7.87 mm and k = 0.82.[12] When a 7 mm corneal zone is taken as an example: a 6.5 μm height error on the edge of this corneal zone will produce an uncertainty of 58 μm (0.3 diopter) in the calculation for the radius of curvature. This uncertainty is greater than the generally accepted tolerance of 0.25 diopter in standard clinical practice.

Skew ray errors also occur in the reconstruction of another type of non-rotation-symmetric surface. Rand, Howland and Applegate (1997) proposed a surface that could not be reconstructed with Placido ring topography.[6] The mathematical representation of this surface is a combination of a sphere and a surface with corrugations on the periphery (shown in the Figure 1):

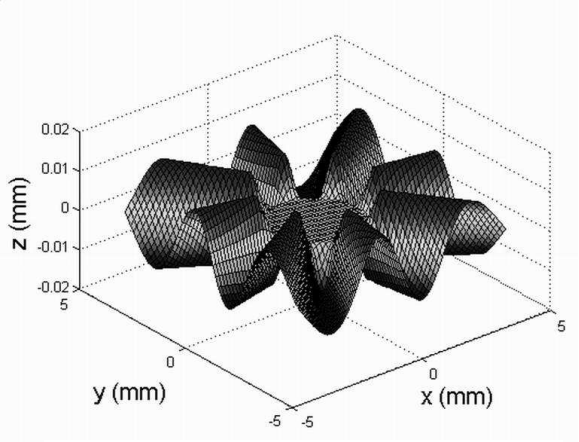

Figure 1 *3D plot of the Rand function*

$$z = r - \sqrt{r^2 - s^2} + \begin{cases} \varepsilon \sin 8\theta & for \quad s \geq 2mm \\ 2(s-1.5)\varepsilon \sin 8\theta & for \quad 1.5 < s < 2mm \\ 0 & for \quad s \leq 1.5mm \end{cases} \qquad (2)$$

where ε is a parameter representing the amplitude of the peripheral corrugations. Rand made numerical simulations of this surface with an amplitude of $\varepsilon = 0.01$ mm, demonstrating that smooth ring images will be produced both in the central and the peripheral region. It is only in the transition region ($1.5 < s < 2.0$) that the reflected pattern reveals that the surface deviates from that of a sphere. Klein(1997) developed an algorithm that avoids the skew ray ambiguity and skew ray error and applied it to a numerical simulation of a surface that is a modified version of that proposed by Rand et. al.[13] This version has similar corrugations in the peripheral region, but with a wider transition period (between 1.5 and 3.0 mm corneal zone). The algorithm was applied to a simulation of a Placido system with 16 rings. Because the transition zone is wider than that of the Rand surface, 5 out of the 16 rings in the image pattern correspond to reflections within this transition zone. Information about these five rings was sufficient to reconstruct the peripheral corrugations of this modified Rand surface. Klein's algorithm is expected to fail when the width of the transition period is reduced in such a way that information about this reduced region is insufficient to make an acceptable reconstruction of the corneal surface. Because of this limitation, Rand proposed that radial lines should be included in the stimulus pattern to overcome the problem of skew ray ambiguity. Theoretically, the addition of radial lines will provide valuable information, especially in the peripheral region of the Rand surface. However, it is anticipated that it will interfere with the ring edge detection.

Another approach (shown in Figures 2A-C) in dealing with skew ray reflection was presented by Vos, Van der Heijde, Spoelder, Van Stokkum and Groen (1997).[8] In this approach, a color-coded stimulus pattern is used instead of Placido rings, and a one-to-one correspondence between stimulator points and image points can be achieved. Thus, this system overcomes the skew ray ambiguity problem. Furthermore, the task of ring edge detection is replaced by

the task of detecting crossings in the colored pattern. Therefore, this system does not have the drawback of the radial lines interfering with edge detection as in ring topography.

In this paper we aim to demonstrate the performance of the VU topographer in reconstructing both the rotation-symmetric and the non-rotation-symmetric surface features of the corneal surface. Spherical test surfaces, toric test surfaces, the Rand surface and sample eyes were used to assess this performance.

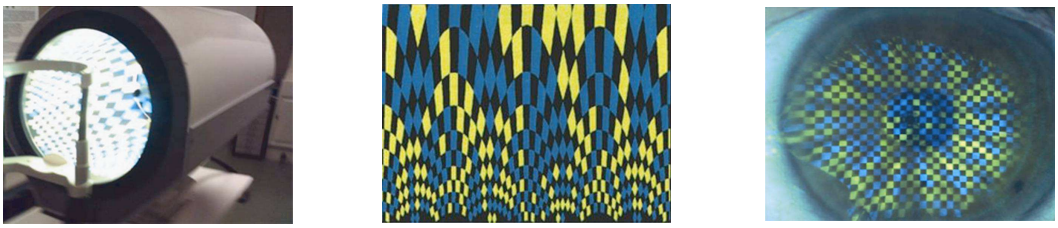

(A) (B) (C)

Figure 2 *(A) The VU topographer (B) Topographer colored pattern flattened from a cylindrical orientation and (C) Reflection of the colored pattern in the human eye.*

3.3 METHODS

3.3.1 Instruments

Radii of curvature of the test surfaces were measured with three different instruments:

1) The Haag-Streit Ophthalmometer (*accuracy* = 0.02 mm)[14],
2) The Keratron Cornea Topographer: Software Release 4.3 (*precision* < 0.1 D)[15],
3) The VU topographer (*precision* = 0.01 mm).[8]

Accuracy refers to how close the measured value is to the real value, while *precision* refers to how close repeated measurements are to each other. A *precision* of 0.1D is equivalent to a *precision* of 0.02 mm for a sphere with 8.00

mm radius. The Haag-Streit Ophthalmometer (variant of the Javal-Schiotz Ophthalmometer) measurements were used as a gold standard, an accuracy of 0.02 mm for the radius of curvature measurements is sufficient to demonstrate the measurement error originating from skew ray ambiguity.

The simulated K option was chosen for the Keratron to measure the radii of curvature of the test surfaces. In this process the meridian axis with the minimum radius of curvature (axial radius of curvature[16] at the edge of the 3 mm corneal zone) is first identified and then the axial radius is determined 90 degrees from this meridian. For the VU topographer the surface was reconstructed with Zernike polynomials as a surface model.[11] For many corneal measurements, order 10 is sufficient to produce accurate surface reconstruction, but for some surfaces, especially those with a complex shape, higher orders (up to order 20) were included to determine the actual shape of the surfaces.[11,17] After the surface had been reconstructed, the corneal shape at the edge of the 3 mm corneal zone was evaluated to determine the minimum and maximum axial radius of curvature, similar to the simulated K procedure for the Keratron.

Although the instantaneous curvature map is a standard output of the Keratron, an additional procedure was included in the analysis to compare this output with the output of the VU topographer. This procedure starts with the height map. An 8 mm corneal zone was chosen as a reference area for comparison. Beyond this zone, height data from the Keratron are incomplete or unreliable mainly due to shadows from eyelashes.

A Zernike fitting of the height map derived from the Keratron was performed. Because the data from both the Keratron and the VU topographer are now expressed in Zernike expansion, the instantaneous curvature is readily available for both instruments, using the derivative definition of radius of curvature:[16]

$$r_i = \frac{[1+(dz/ds)^2]^{3/2}}{\pm(d^2z/ds^2)} \qquad (3)$$

Equation (3) is applied in a circular cylindrical coordinate system, with *z* as the corneal height axis and *s* as the radial axis. Therefore, the instantaneous radius of curvature is the meridian instantaneous radius of curvature, in other words the local curvature when looking at a two- dimensional meridian slice of the anterior corneal surface.

In viewing height maps, the Zernike parabolic term Z_2^0 is removed to make it possible to see the higher order features of the surfaces.

3.3.2 Surfaces

3.3.2.1 Spheres

The performance of the VU topographer in reconstructing spherical surfaces is first demonstrated. Grade 100 metal ball-bearings manufactured for automobile sub-assemblies were used as test surfaces. According to the standards of the AFBMA (Anti-Friction Bearing Manufacturers Association), grade 100 refers to a tolerance of 1.3 μm in the diameter.

3.3.2.2 Toric surfaces

To assess the performance of the VU topographer in measuring astigmatism, we used toric surfaces of PMMA material manufactured by Procornea BV Netherlands. To characterize astigmatism of the surfaces, the difference in axial power between the meridians with maximum and minimum radius of curvature can be used to define astigmatic power:

$$Astigmatic \quad Power = (n-1)\left[\frac{1}{r_{\min}} - \frac{1}{r_{\max}}\right] \qquad (4)$$

In this formulation the effective index of refraction of the cornea (*n*) is taken to be 1.3375.[18] Table 1 lists the shape parameters of the surfaces, as measured with the Haag-Streit Ophthalmometer.

Table 1 *Shape parameter specifications of toric surfaces*

Min Radius (mm)	Max Radius (mm)	Astigmatic Power (D)
7.50	8.01	2.87
7.05	8.02	5.79
6.56	8.00	9.26
6.06	7.99	13.45

Each toric surface, which is a disk of 12.8 mm in diameter, is placed in a mount with a manual rotation stage. Thus, the orientation of the surface with respect to the topographer can be changed. Repeated measurements reveal that both the Keratron and the VU topographer produce radii measurements of the toric surfaces that are independent of the surface orientation as long the apex normal of the toric surface is aligned to the optical axis of the topographer. For the measurements described in this study the toric surfaces were positioned in such a way that the axis with minimum axial radius of curvature was in the vertical direction.

3.3.2.3 Rand surface

Based on the specification described in equation (2) with amplitude $\varepsilon = 0.01$ mm and r = 8.00 mm, SUMIPRO BV Netherlands produced a Rand surface made from PMMA material. This surface also has the same disk diameter (12.8 mm) as the toric surfaces and can therefore be mounted on the same rotation stage that is used for the toric surfaces. Measurements to reconstruct the map of this surface were made for both the Keratron and the VU topographer.

A Zernike expansion of equation (2) was used to analyze the measurements.

3.3.2.4 Human eye samples

Measurements were also made of two human eye samples (42 year-old male eye that had undergone radial keratotomy (RK) 10 years earlier and a 27 year-old male eye with no corneal abnormalities) were also done. Written informed

consent was obtained from both men after they had been informed about the nature and possible consequences of the study, in accordance with the tenets of the Helsinki declaration. Because measurements for the VU topographer were made with the line of sight as a reference axis (objective method alignment principle recommended by OSA working group)[19], the pupil center option for viewing corneal maps in the Keratron was used. The pupil center option allows the surface reconstruction process of the Keratron to be aligned with the line of sight. This axis is different from the pupillary axis.[20]

3.4 RESULTS AND DISCUSSION

Radius of curvature measurements for spheres and toric surfaces made by the Haag-Streit Ophthalmometer, Keratron and the VU topographer are shown in Table 2. All three instruments give practically the same values for the radius of curvature of the spheres and the maximum radius of curvature of the toric surfaces. However, the Keratron gives slightly higher values for the minimum radius of curvature of all toric surfaces, compared to both the VU topographer

Table 2 *Radius of curvature measurements for spheres and toric surfaces*

Surface Type	Surface Parameter	Haag-Streit Ophthalmometer	Keratron Release 4.3	VU Topographer
Sphere #1	Radius	7.00 ± 0.02	7.02 ± 0.01	6.98 ± 0.02
Sphere #2	Radius	8.00 ± 0.02	8.01 ± 0.01	8.00 ± 0.02
Sphere #3	Radius	9.00 ± 0.02	9.00 ± 0.03	9.00 ± 0.02
Toric #1	**Min Radius**	**7.50 ± 0.02**	***7.54 ± 0.01***	**7.51 ± 0.01**
Toric #1	Max Radius	8.01 ± 0.02	8.03 ± 0.02	8.00 ± 0.01
Toric #2	**Min Radius**	**7.05 ± 0.02**	***7.09 ± 0.01***	**7.03 ± 0.01**
Toric #2	Max Radius	8.02 ± 0.02	8.04 ± 0.01	7.99 ± 0.01
Toric #3	**Min Radius**	**6.56 ± 0.02**	***6.62 ± 0.01***	**6.54 ± 0.01**
Toric #3	Max Radius	8.00 ± 0.02	8.01 ± 0.01	7.98 ± 0.01
Toric #4	**Min Radius**	**6.06 ± 0.02**	***6.11 ± 0.01***	**6.08 ± 0.01**
Toric #4	Max Radius	7.99 ± 0.02	8.00 ± 0.01	8.00 ± 0.01

Note: The error values are based on literature accuracy value for the Haag-Streit Ophthalmometer (HSO) and on the standard deviation of five trial measurements for the Keratron and the VU topographer.

and the Haag-Streit Ophthalmometer. Consequently, the Keratron gives under-estimated values for the astigmatic power of the toric surfaces as can be seen in Figure 3. The under-estimation is more than a quarter of diopter for those toric surfaces with higher astigmatic power i.e. 0.41 D error for the 9.26 D toric surface. This observation is consistent with the results of other investigators showing that ring topographers give under-estimated values for the corneal astigmatic power.[21,22] On the other hand, no systematic difference was found between the output of the measurements coming from the VU topographer and the Haag-Streit Ophthalmometer.

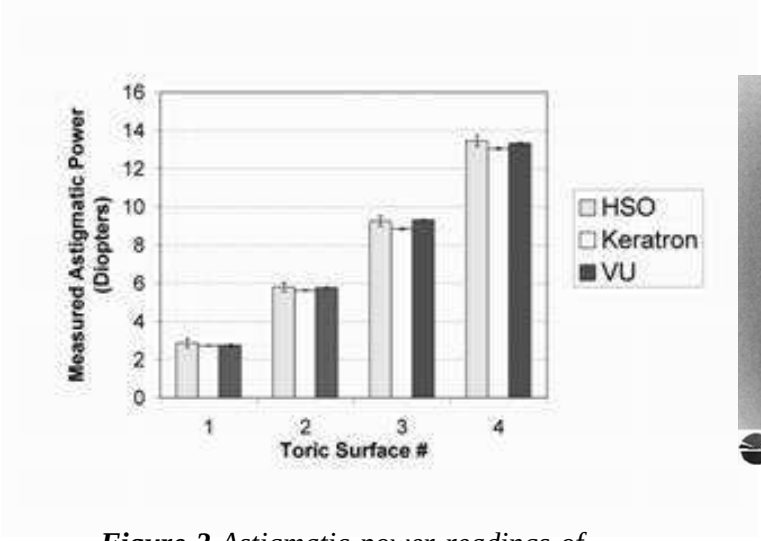

Figure 3 *Astigmatic power readings of toric surfaces as measured with the Haag-Streit Ophthalmometer (HSO), the Keratron and the VU topographer, respectively.*

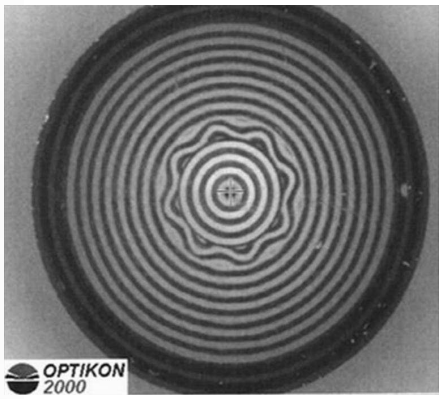

Figure 4 *Captured photo of reflection from the Rand surface taken with the Keratron*

Photos of the reflection coming from the Rand surface are shown in Figures 4 and 5A, which correspond to measurements from the Keratron and the VU topographer, respectively. As Rand had predicted for ring topographers, the ring reflection in the peripheral section shows smooth rings, giving the impression that the corrugation does not exist. On the other hand, the photo of colored pattern reflection taken with the VU topographer immediately indicates the irregularity of the Rand surface. Figure 5B shows the crossing points detected

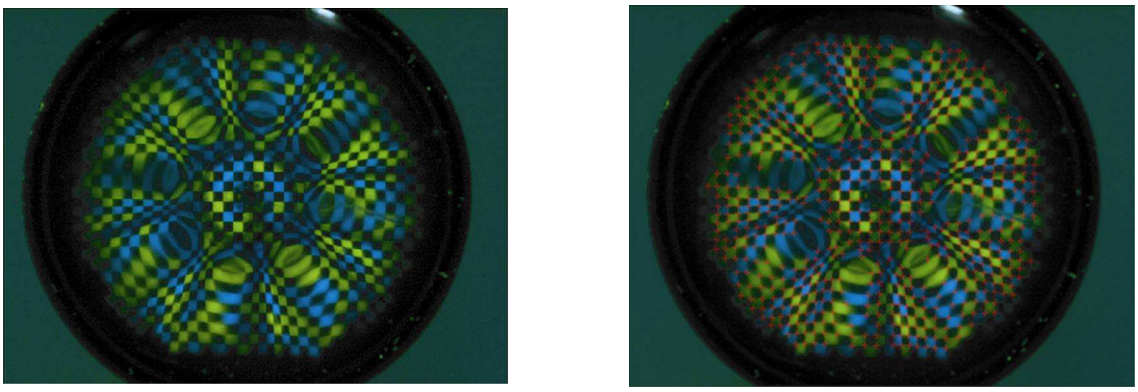

(A) (B)

Figure 5 *(A) Captured photo of reflection from the Rand surface taken with the VU topographer. Photo (B) includes the detected crossings on the colored reflection pattern.*

for the photo taken from the VU topographer. Image processing techniques involving application of filter functions and pseudorandom encoding were used to detect these crossings.[8,23] It can be observed that some crossing points were not detected, particularly those regions where the cross pattern is blurred. However, the detected crossings were sufficient to make a good reconstruction of the Rand surface as will be discussed further.

The curvature map produced by the Keratron (Figure 6A) was not able to show the curvature changes in the peripheral region of the Rand surface. Instead it shows a substantial region in the periphery where the curvature value is constant. However, the height map data from the Keratron (Figure 6B) does reveal corrugations in the peripheral region but the actual shape of the corrugations was not reconstructed correctly. The onset of the corrugations should appear in the region of the 3-4 mm corneal zone. Instead, it appears near the edge of the 6 mm corneal zone. Moreover, the amplitude of the reconstructed corrugations is not uniform, contrary to what should be expected. It appears that this is due to difficulties in processing information in the transition zone (with winding ring pattern) in the Rand surface reflection pattern (see Figure 4). This problem is not encountered when processing colored pattern

photos made by the VU topographer (Figure 5A & 5B), since it is possible to find crossings in this region with reasonable accuracy.

The curvature map (Figure 6D) derived from the Keratron height map also revealed this corrugation feature, but with similar shortcomings as in the height map. Some of the mounds which are indicated by the high diopter regions (48-50 Diopter) are located in the vicinity of the 5-6 mm corneal zone, instead of in the area starting from the 3-4 mm corneal zone. These mounds are also not uniformly distributed over the surface. The derived curvature map (Figure 6D), revealing the corrugation feature of the Rand surface, in contrast with the absence of this feature in the Keratron curvature map (Figure 6A), shows the potential importance of the height map. It shows that an appropriate algorithm can be applied to the Keratron height map to produce a better curvature map than what is obtained from software release 4.3.

The VU topographer surface reconstruction of the Rand surface reveals a

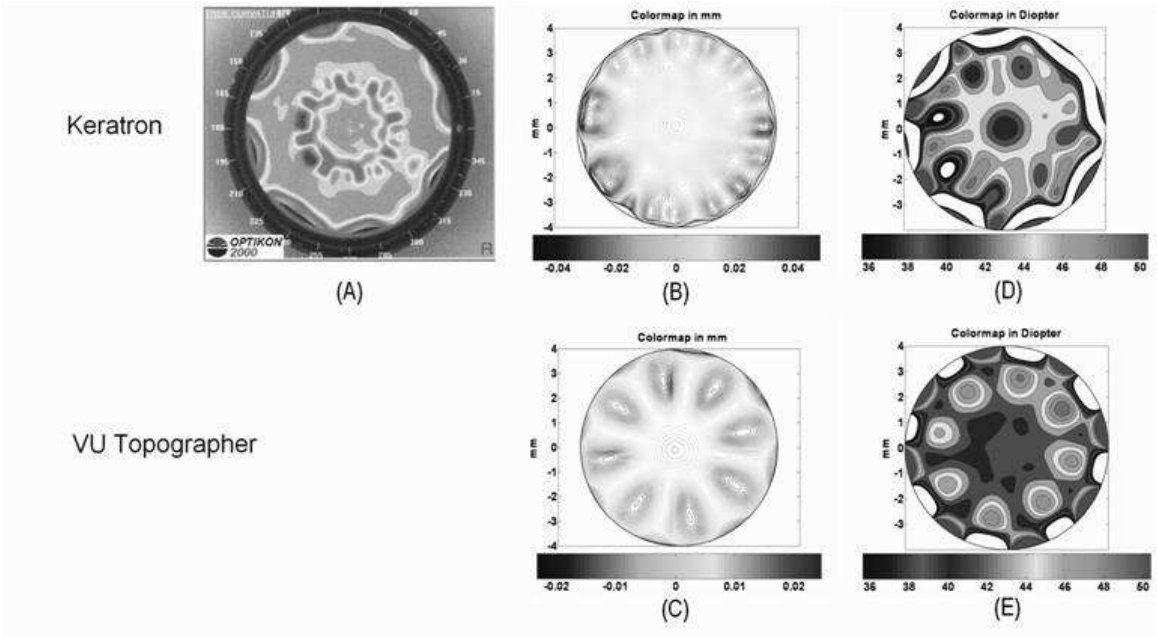

Figure 6. Curvature map (A),(D) & (E) and height map (B) & (C) measurements of the Rand surface. (A),(B) & (D) are derived from the Keratron and (C) & (E) from the VU topographer.

shape which agrees with the specification of the Rand shape function (Equation 2). The height map (Figure 6C) reveals the correct corrugation feature of the Rand surface, and the onset of this feature starts in the region of the 3-4 mm corneal zone. The amplitude of peripheral corrugation is quite uniform, and measured 10.7 ± 0.5 μm (mean and standard deviation of the 8 mounds), which is close to the manufacturer's specification of 10 μm. Furthermore, the corresponding curvature map reveals the mounds of the corrugation in the correct surface region. A closer look to the Zernike coefficients describing the surface shows that the VU topographer reconstructed the Rand shape with reasonable accuracy.

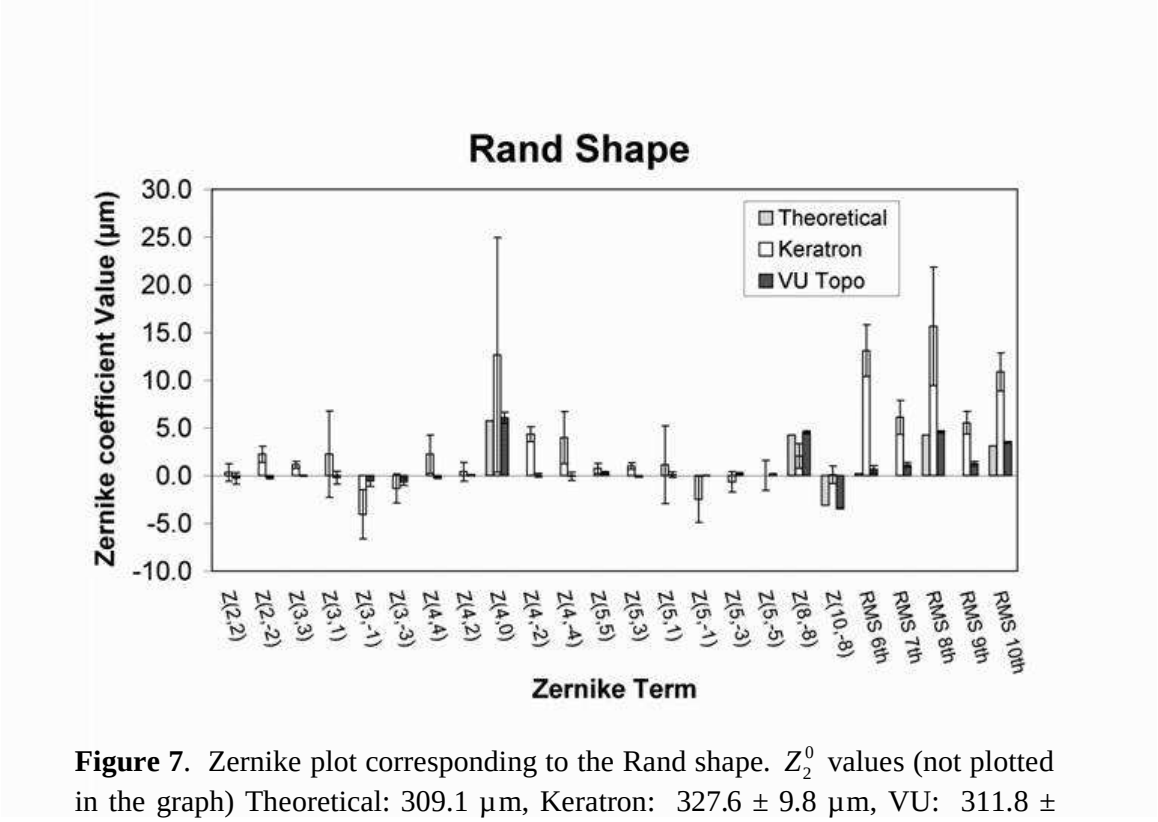

Figure 7. Zernike plot corresponding to the Rand shape. Z_2^0 values (not plotted in the graph) Theoretical: 309.1 μm, Keratron: 327.6 ± 9.8 μm, VU: 311.8 ± 0.4 μm.

Figure 7 shows a graph of the Zernike coefficients (2nd to 5th order) which corresponds to the height map of Figures 6B and 6C for the Rand shape. The Zernike terms Z_8^{-8} and Z_{10}^{-8} are also included in the graph since these terms contain the function $\sin(8\theta)$:

$$Z_8^{-8} = \rho^8 \sin(8\theta) \quad (5)$$

$$Z_{10}^{-8} = (10\rho^{10} - 9\rho^9)\sin(8\theta) \quad (6)$$

When the Rand shape is expanded into Zernike polynomials, the coefficients of Z_8^{-8} and Z_{10}^{-8} will have non-zero values. For orders 6th to 10th the RMS values per order are shown instead of the individual components. Except for Z(2,0), the differences between VU topographer values for the Zernike coefficients compared to the theoretical values are sub-micrometer. The manufacturing of the Rand shape and the accuracy of the surface reconstruction method contribute to these differences. The precision of the VU topographer, indicated by error bars in the graph, is small enough such that the higher order surface features of the Rand shape were still recovered accurately. On the other hand, the measurement for the Keratron shows large deviation compared to the theoretical values. This is mainly due to the problem of edge detection of the rings encountered in the transition region of the Rand surface, thus creating a large

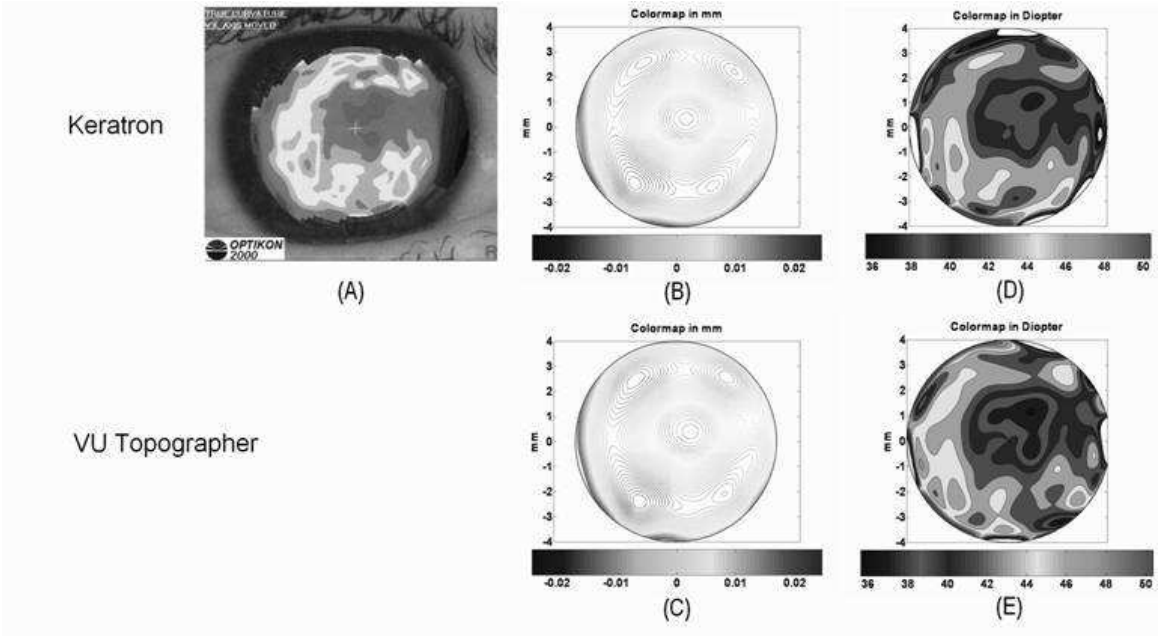

Figure 8. Curvature map (A),(D) & (E) and height map (B) & (C) measurements of a post-RK eye. (A),(B) & (D) are derived from the Keratron and (C) & (E) from the VU topographer.

value for the precision of the measured Zernike coefficients. Nevertheless, the effect of the skew ray error could still be observed in these measurements. The amplitudes of Z_8^{-8} and Z_{10}^{-8} for the Keratron are 2.1 ± 1.3 μm (mean and standard deviation for three trials) and 0.1 ± 0.9 μm respectively. These are lower than that of the VU topographer (4.5 ± 0.2 μm and -3.5 ± 0.1 μm) and the theoretical value (4.2 μm and -3.1 μm). Figures 8B and 8C shows corneal height maps, from the Keratron and the VU topographer respectively, for a 42 year-old eye 10 years post RK. The height map shows four hills in the peripheral region of the cornea, a feature which can be expected in a post-RK eye, and these hills are separated by valleys, as seen in the height map. The curvature maps for both instruments (Figures 8A and 8D for the Keratron and Figure 8E for the VU topographer) were able to "see" these hills as manifested by the higher dioptric values in these regions compared to that of the central curvature of the cornea. However, the large white region on the left hand side of the curvature map produced by the Keratron (Figure 8A) does not reveal the valley that is present in the height map. On the other hand, the corresponding curvature map from the VU topographer (Figure 8E) shows this feature as a dark grey interval between two light grey regions. The failure of the ring topographer to identify this feature is an indication of the effect of skew ray ambiguity, which makes it difficult for ring topographers to detect curvature changes along the angular direction, as was clearly demonstrated in the Rand shape example. Although, both instruments reveal similar qualitative features in the height maps, the hills in the Keratron height map are lower than the hills in the VU topographer height map. Taking the lowest point of the height map as a reference point, the four hills in the Keratron height map are 2.75 ± 1.25 μm lower than the hills in the VU topographer.

Figure 9 shows a graph of the Zernike coefficients (2^{nd} to 5^{th} order) which corresponds to the height map of Figures 8B and 8C for the post-RK eye. For orders 6^{th} to 10^{th} the RMS values per order are shown instead of the individual

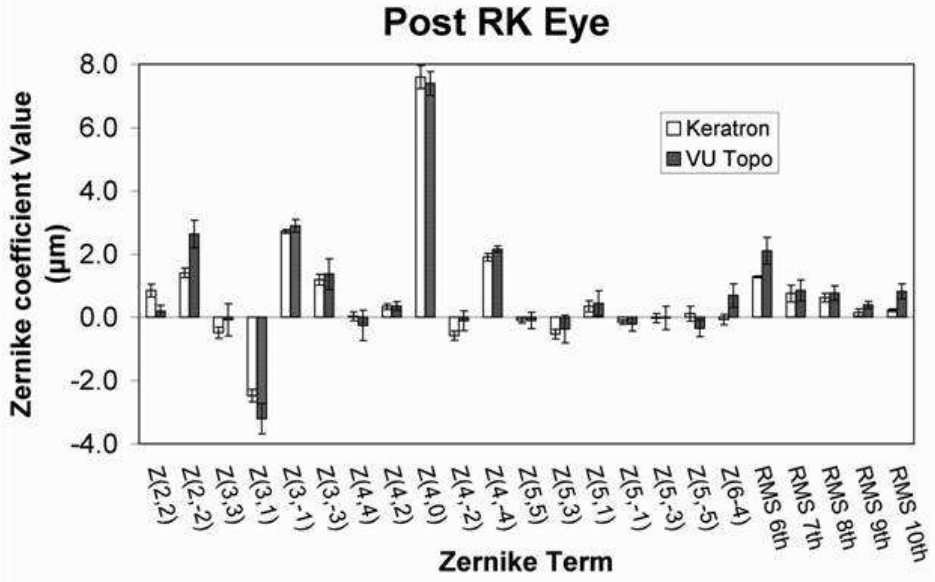

Figure 9. Zernike plot corresponding to the shape of the cornea of a post-RK eye. Z_2^0 values (not plotted in the graph) Keratron: 300.6 ± 2.5 µm, VU: 299.7 ± 0.4 µm

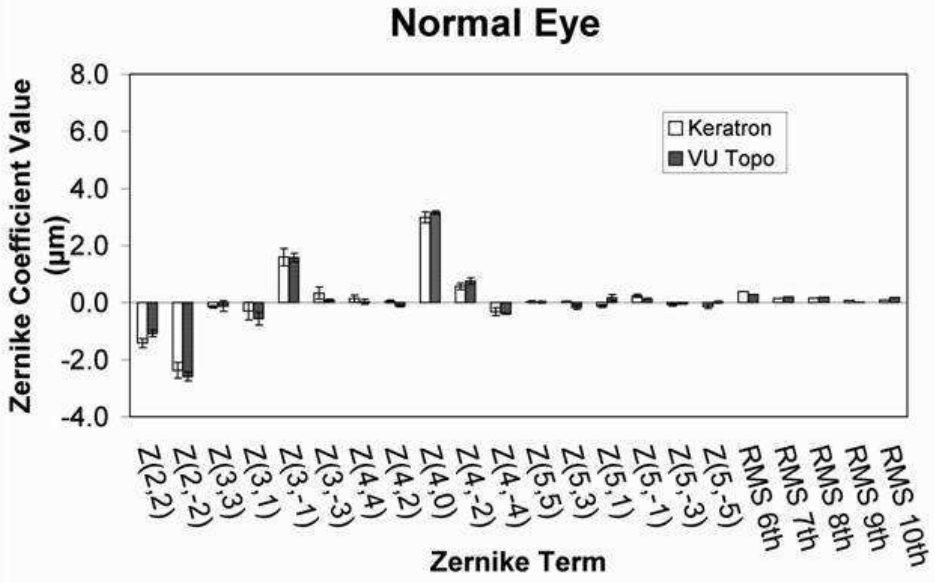

Figure 10. Zernike plot corresponding to the shape of a typical normal cornea. Z_2^0 values (not plotted in the graph) Keratron: 303.5 ± 1.2 µm, VU: 303.0 ± 0.3 µm.

components. Because the shape feature of this corneal surface is analogous to the shape of the function: $\sin(4\theta)$, the Zernike term Z_6^{-4} is also included:

$$Z_4^{-4} = 10\rho^4 \sin(4\theta) \qquad (7)$$

$$Z_6^{-4} = (6\rho^6 - 5\rho^4)\sin(4\theta) \qquad (8)$$

Because this corneal surface is irregular, the reconstruction was made up to the 14th order of Zernike expansion. Both the Keratron and the VU topographer produced similar values for the rotation-symmetric Zernike terms Z_2^0 & Z_4^0 (the difference in the mean values is within the range of the precision of both instruments). On the other hand, the values of the non-rotation-symmetric Zernike terms Z_2^2, Z_2^{-2}, Z_3^1 and Z_6^{-4} differed between the two instruments in the order of 1 μm. Z_2^2 and Z_2^{-2} are Zernike components describing astigmatism. The Keratron gave lower magnitude (38% lower) for the combined magnitudes of these Zernike components compared with that of the VU topographer. This difference is quite large compared to the underestimation observed for the toric surfaces (4%). It should be noted that the total astigmatism is described by Z_2^2 and Z_2^{-2} plus higher order Zernike components. The Keratron measured 1.49 ± 0.21 Diopter for the astigmatism at an axis of 173 ± 1 degrees while the VU measured 1.71 ± 0.20 Diopter at an axis of 172 ± 3. The close match of the measured axis of astigmatism (axis of the meridian with least radius of curvature) indicates that the difference in the measured astigmatism could not be due to alignment errors but to two factors: 1) the effect of skew ray ambiguity in the reconstruction of the non-rotation-symmetric surface properties of the cornea when a ring pattern is used and 2) the effect of uncertainties in the edge detection of the rings. Although uncertainties in the edge detection of the rings contribute to the error, the results suggest that the effect of the skew ray error increases with the complexity of the surface. The error is less for the toric surfaces compared to the post RK eye and the Rand surface.

The same analysis was applied to a typical eye with no abnormalities (see Figure 10). It is notable that, in general, the non-rotation-symmetric surface components of this cornea are smaller than those of the irregular cornea (Figure 9). Therefore for this eye, both the Keratron and the VU topographer produced Zernike coefficients with differences that are negligible. This also shows that the

axis alignment to reconstruct the corneal surface is the same for both instruments. Otherwise, substantial differences in the amplitudes of the surface components would have been observed.

3.5 CONCLUSIONS

This study has demonstrated the superior results obtained by using colored pattern (the VU topographer) in corneal topography, especially in the reconstruction of non-rotation-symmetric surfaces such as the artificial Rand surface and irregular corneas. This is because the VU topographer eliminates the skew ray problem encountered in ring topography. The VU topographer also measures the correct astigmatic power of toric surfaces, while ring topographers under-estimate these values. Consequently, because accurate surface reconstruction of the cornea is important in refractive surgery, contact lens fitting and research on wave aberration of the eye, the VU topographer is far superior to the Placido ring technique for corneal topography.

ACKNOWLEDGMENT

We thank Yevgeni Markine for improving the crossing detection and color identification procedure in the VU topographer image-processing software.

REFERENCES

1. Koch DD, Haft EA. Introduction to Corneal Topography. In: Gills JP, Sanders DR, Thornton SP, Martin RG, Gayton JL, Holladay JT, eds. *Corneal Topography: The State of the Art.* New Jersey: SLACK Incorporated; 1995:1-15.

2. Mejia-Barbosa Y, Malacara-Hernandez D. A review of methods for measuring corneal topography, Optom Vis Sci 2001; 78:240-253.
3. Van Saarloos PP, Constable IJ, Improved Method for Calculation of Corneal Topography for any Photokeratoscope Geometry. Optom Vis Sci 1991; 68:960-965.
4. Massig JH, Lingelbach E, Lingelbach B. Videokeratoscope for accurate and detailed measurement of the cornea surface. App Opt 2005; 44: 2281-2287.
5. Klein SA. Axial curvature and the skew ray error in corneal topography. Optom Vis Sci 1997;74: 931-944.
6. Rand RH, Howland HC, Applegate RA. Mathematical model of a Placido disk keratometer and its implications for recovery of corneal topography. Optom Vis Sci 1997; 74: 926-930.
7. Tripoli NK, Cohen KL, Obla P, Coggins JM, Holmgren DE. Height Measurement of Astigmatic Test Surfaces by a Keratoscope that uses plane geometry surface reconstruction. Am Jour Ophth 1996;121: 668-676.
8. Vos FM, Van der Heijde GL, Spoelder HJW, Van Stokkum IHM, Groen FCA. A new PRBA-based instrument to measure the shape of the cornea. IEEE Trans Instrum Meas 1997; 46:794-797.
9. Zhou F, Hong X, Miller DT, Thibos LN, Bradley A. Validation of a combined corneal topographer and aberrometery based on Shack-Hartmann wave-front sensing. J Opt Soc Am A Opt Image Sci Vis 2004; 21:683-696.
10.Jongsma FHM, De Brabander J, Hendrikse F, Stultiens BAT. Development of a Wide Field Height Eye Topographer: Validation on Models of Anterior Eye Surface. Optom Vis Sci 1998; 75:69-77.
11.Sicam VADP, Coppens J, Van den Berg TJTP, Van der Heijde RGL. Corneal surface reconstruction algorithm that uses Zernike polynomial representation. J Opt Soc Am A Opt Image Sci Vis 2004; 21:1300-1305.
12.Dubbelman M, Weeber HA, Van der Heijde RGL, Völker-Dieben HJ. Radius and asphericity of the posterior corneal surface determined by corrected Scheimpflug photography. Acta Ophth Scand 2002; 80: 379-383.
13.Klein SA. Corneal topography reconstruction algorithm that avoids the skew ray ambiguity and the skew ray error. Optom Vis Sci 1997; 74: 945-962.
14.Eskridge JB, Amos JF, Bartlett JD. *Clinical Procedures in Optometry*. Philadelphia: J.B. Lippincott Company; 1991:137.
15.Mattioli R, Tripoli NK. Corneal Geometry Reconstruction with the Keratron Videokeratographer. Optom Vis Sci. 1997; 74: 881-894.
16.Salmon TO, Horner DG. Comparison of Elevation, Curvature, and Power Descriptors for Corneal Topographic Mapping. Optom Vis Sci 1995; 72:800-808.
17.Carvalho LA. Accuracy of Zernike Polynomials in Characterizing Optical Aberrations and the Corneal Surface of the Eye. Inv Ophth Vis Sci 2005; 46:1915-1926.

18.Borish IM. *Clinical Refraction*. Chicago: The Professional Press, Inc.; 1975:622.
19.Applegate RA, Thibos LN, Bradley A, Marcos S, Roorda A, Salmon TO, Atchison DA. Reference Axis Selection: Subcommittee Report of the OSA Working Group to Establish Standards for measurement and Reporting of Optical Aberrations of the Eye. J Ref Surg 2000; 16: S656-S658.
20.Mandell RB, Chiang CS, Klein S. Location of the Major Corneal Reference Points. Optom Vis Sci. 1995; 72: 776-784.
21.Greivenkamp JE, Mellinger MD, Snyder RW, Schwiegerling JT, Lowman AE, Miller JM. Comparison of Three Videokeratoscopes in Measurement of Toric Test Surfaces. J Ref Surg 1996; 12: 229-239.
22.Ventura L, Riul C, Sousa SJF, De Groote J-J, Filho ABR, Oliveira GCD. Corneal astigmatism measuring module for slit lamps. Phys Med Bio 2006; 51: 3085-3098.
23. Spoelder HJW, Vos FM, Petriu EM, Groen FCA. Some Aspects of Pseudo Random Binary Array-Based Surface Characterization. IEEE Trans Instrum Meas 2000; 49:1331-1336.

4

THE SHAPE OF THE ANTERIOR AND POSTERIOR SURFACE OF THE AGING HUMAN CORNEA

M Dubbelman, VADP Sicam and GL Van der Heijde

Vision Research 46, 993-1001, 2006.

ABSTRACT

Purpose: To determine the shape and astigmatism of the posterior corneal surface in a healthy population with age, using Scheimpflug photography corrected for distortion due to the geometry of the Scheimpflug imaging system and the refraction of the anterior corneal surface.

Methods: Scheimpflug imaging was used to measure in 6 meridians the cornea of the right eye of 114 subjects, ranging in age from 18 to 65 years.

Results: The average radius of the anterior corneal surface was 7.79 ± 0.27 (sd) mm and the average radius of the posterior corneal surface was 6.53 ± 0.25 (sd) mm. Both surfaces were found to be flatter horizontally than vertically. The cylindrical component of the posterior surface of 0.33 mm is twice that of the anterior surface (0.16 mm).

The asphericity of both the anterior and the posterior surface was independent of the radius of curvature at the vertex, refractive error and gender. In contrast with that of the anterior corneal surface, the asphericity of the posterior corneal surface varied significantly between meridians. With age, the asphericity of both the anterior and the posterior corneal surface changes significantly, which results in a slight peripheral thinning of the cornea.

Conclusion: On average, the astigmatism of the posterior corneal surface (-0.305 D) compensates the astigmatism of the anterior corneal surface (0.99 D) with 31%. The results show that the effective refractive index is 1.329, which is lower than values commonly used. There is no correlation between the asphericity of the anterior and the posterior corneal surface. As a result, the shape of the anterior corneal surface provides no definitive basis for knowing the asphericity of the posterior surface.

4.1 INTRODUCTION

Although the anterior corneal surface has been frequently described in the literature, accurate data on the shape of the posterior surface of the cornea is scarce. This is mainly because imaging of this surface must always be performed through the anterior surface of the cornea, which acts as a magnifying glass and distorts the perceived shape of the posterior cornea. During the past two decades, interest in the exact shape of the corneal surface has increased, especially due to new developments such as refractive surgery, for which a complete description of the whole cornea is required. More accurate data on the shape of the posterior surface could improve the optical modeling of the eye. The radius of the posterior corneal surface in the schematic eye of Gullstrand is 6.8 mm (Atchison & Smith, 2000), while in the schematic eye of Le Grand & El Hage (1980) and Liou & Brennan (1997), it is 6.5 mm and 6.4 mm, respectively. The asphericity of the posterior corneal surface is needed in order to model the higher order aberrations, but different values have been used due to the lack of accurate data. Kooijman (1983) used the same asphericity as that of the anterior corneal surface, while Lotmar (1971) and Navarro, Santamaria & Bescos (1985) assumed the posterior corneal surface to be spherical. Liou & Brennan (1997) entered the asphericity of the posterior corneal surface as a variable in the modeling of their schematic eye, which resulted in a shape factor 'p' of 0.4 (Q-value of -0.6). Furthermore, post-surgical refractive power after cataract surgery could be predicted more accurately if more was known about the posterior surface. In IOL calculations, the cornea is regarded as a single refractive surface with an effective refractive, which varies from 1.332 to 1.3375, because there is usually no knowledge of corneal thickness and radius of the posterior corneal surface (Bennet & Rabbets, 1998). For this effective refractive index, it is assumed that there consists a fixed ratio between the radius of the anterior and posterior corneal surface. This is also the reason that the calculation of corneal

power sometimes fails after previous refractive surgery of the cornea, because this ratio has been changed (Gimbel, Sun & Kaye, 2000). Finally, it is important to know whether the shape of the cornea changes with age, because this could influence the stability of the corneal shape after refraction surgery.

The radius of curvature of the posterior cornea has most frequently been measured on the basis of the size and location of Purkinje images (Royston, Dunne & Barnes, 1990; Dunne, Royston & Barnes, 1992; Garner, Owens, Yap, Frith & Kinnear, 1997; Lam & Douthwaite, 2000). Dunne et al. (1992) found that the posterior surface exhibited more toricity than the anterior surface. The asphericity of the posterior corneal surface cannot be measured using Purkinje imaging, so it was measured by combining videokeratoscopy with pachymetric thickness measurements (Patel, Marshall & Fitzke, 1993; Lam & Douthwaite, 1997). Lam & Douthwaite (1997) found a significant relationship between anterior and posterior asphericity in the vertical meridian. Patel et al. (1993) measured the asphericity in the vertical and horizontal meridian and found some difference in asphericity. Nevertheless, this combination of videokeratoscopy with subsequent thickness measurements is quite sensitive to misalignment, and is rather time-consuming.

Scheimpflug photography has the advantage of being a non-contact technique whereby the anterior surface, the thickness profile, and the posterior surface are determined in one step (Brown, 1973). This eliminates alignment errors that may occur when combining videokeratoscopy and pachymetry, and accelerates the measurement procedure. However, standard Scheimpflug photography suffers from distortion of the images due to the geometry of the Scheimpflug imaging system and the refraction of the anterior corneal surface. To obtain an accurate measurement of the anterior and posterior corneal surfaces, we developed a method to correct for these two types of distortion (Dubbelman & Van der Heijde, 2001; Dubbelman, Van der Heijde & Weeber, 2005). In an earlier study (Dubbelman, Weeber, Van der Heijde & Völker-Dieben, 2002),

this method was used to measure the age-dependency of the shape of the posterior corneal surface in the vertical meridian. In contrast with the radius, the asphericity appeared to be age-dependent. Nevertheless, only the vertical meridian was measured, and because of the reflections of the iris, especially in the older subjects, the Scheimpflug image was occasionally saturated in the periphery of the cornea.

In the present study, a CCD camera with a higher dynamic range and a higher resolution (25% higher than the camera used in our earlier study). Furthermore, a larger group of subjects was measured, and the shape of the corneal surface was investigated in six meridians instead of only the vertical meridian. This makes it possible to measure the change in radius, asphericity and thickness of the whole cornea as a function of age.

4.2 METHODS

Scheimpflug images of the anterior eye segment were made of the right eye of 114 subjects, ranging from 18 to 65 years of age (average age ± sd: 39 ± 14 years). The group consisted of 57 females (average age: 38 ± 14 years) and 57 males (average age: 39.5 ± 15). The measurements were performed with the full understanding of the subjects and written consent was obtained from each subject. None of the subjects had suffered from diabetes mellitus, had undergone ocular surgery, or had worn contact lenses in the previous 2 years.

The radius and astigmatism of the anterior corneal surface and the ocular refractive error of the right eye were measured with a Topcon KR-3500 auto kerato-refractometer. The equivalent refractive error (ERE) varied between –6.88D and +3.5D (average ± sd: -1.33 ± 2.18). No difference in refractive error was found between males and females, and there was no correlation between ERE and age.

Two series of Scheimpflug images were made in six meridians (90°, 60°, 30°, 0°, 150°,120°) and the time interval between each series varied from 1 to 3 minutes (2 x 6 images in total). Images were obtained with the Topcon SL-45 Scheimpflug camera, the film of which was replaced by a CCD-camera (St-9XE, SBIG astronomical instruments) with a dynamic range of 16 bits of grey values (512 x 512 pixels, pixel size 20 x 20 micrometer, magnification: 1x). All measurements were performed between 10 a.m. and 4 p.m.

The Topcon SL-45 Scheimpflug camera is equipped with a fixation target (a green blinking LED). The intensity of the LED can be increased, which makes fixation less difficult for the subject and increases the reproducibility of the measurements. In order to correct for the angle between the optical and the visual axis (Dragomirescu, Hockwin, & Koch, 1980), the fixation target is displaced 5° nasally from the slitbeam, which is in accordance with the average value for the angle alpha. The visual axis is also downwards relative to the optical axis by 2-3° (Atchison, & Smith, 2000). Because of the variation in the angle between subjects (3°- 8°), the Scheimpflug camera was adapted to make it possible to change the position of the fixation target between 1° and 8° in both the horizontal and the vertical direction. As a result, all Scheimpflug images were taken along the optical axis, which has the advantage that the shape of the cornea is maximally symmetric in all six meridians. The procedure for aligning the slit along the optical axis was as follows. First of all, the subject was asked to fixate on the target, which was in average position (H:5°, V:2.5°). The slit (low intensity) was positioned in a horizontal position, while the anterior eye segment was observed through the eye-piece. Using the crosshairs in the eye-piece, the cornea, the iris plane and the pupil center, the position of the fixation target was fine-tuned in order to align the slit along the optical axis. The same procedure was followed with the slit in the vertical position. After the adjustment of the fixation target, which had to be done only once at the beginning of the measurements, the slit was positioned perpendicularly to the

apex of the cornea using an electronic-acoustical device, which uses the slit light reflected by the cornea to give an audible signal (Dragomirescu et al. 1980). Finally, an image was obtained with a Xenon flash-light and the Scheimpflug imaging system was rotated 30°, after which, if necessary, the slit was adjusted again in order to position it perpendicular to the apex of the cornea.

Ray tracing was used to correct each image for distortion due to the geometry of the Scheimpflug camera and the magnifying effect of the anterior surface. This method has been described extensively in an appendix of Dubbelman, Van der Heijde & Weeber, 2005, and was validated by measuring an artificial eye with known dimensions (Dubbelman & Van der Heijde, 2001). A patterned grid of known geometry was used to calibrate the camera.

To describe the anterior and posterior corneal shape, it was assumed that the cornea was meridionally symmetric and could be described by the following conic of revolution (Malacara, 1988), which is used in various forms (Kiely, Smith & Carney, 1984; Atchison & Smith, 2000):

$$y = \frac{c(x - x_o)^2}{1 + \sqrt{1 - kc^2(x - x_o)^2}} + y_o,$$

where c is the curvature (inverse radius) at the vertex (x0, y0). The y-axis is the axis of revolution of both the conic and the optical axis of the cornea. The conic constant (k) indicates how rapidly a surface flattens (k<1) or steepens (k>1) with distance from the apex, and thus indicates the degree to which an aspherical surface differs from the equivalent spherical form.

$$R(\theta) = R_1 - \Delta R \cos^2(\theta - axis)$$

To determine the radius of both corneal surfaces as a function of meridian, a $\cos^2$ function was fitted to the radii of the six meridians in order to find either the maximal radius (R_1), the cylinder (ΔR) and the axis where the radius is minimal (Kiely, Smith & Carney, 1982). The sign convention of the angle θ is

shown in Figure 1. In the first instance, it was assumed that the k-value would exhibit similar periodic behaviour as the radius. Therefore, the $\cos^2$ function was also used to model the meridional variation of the k-value. According to the value of k, the surface is a hyperboloid when k<0, a paraboloid when k=0, a prolate ellipsoid when 0<k<1, a circle when k=1 and an oblate spheroid when k>1. Three other parameters that are commonly used to describe a conic are the Q-value (where k=Q+1), the shape factor 'p' (where k=p) and the eccentricity e (where $k=-e^2+1$). The conic of revolution was fitted to both corneal surfaces at an aperture of 7.5mm, and for each meridian the radius at the vertex and the k-value were determined.

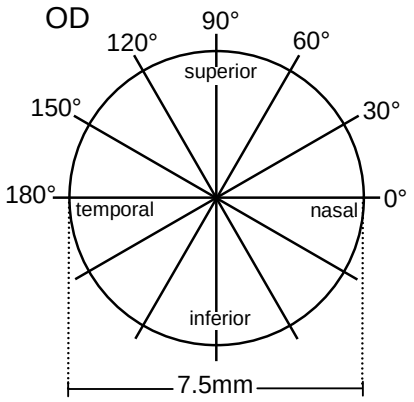

Figure 1 *Scheimpflug images were made at the indicated six meridians and analyzed at an aperture of 7.5mm.*

4.3 RESULTS

Figure 2 shows the effect of correction of a Scheimpflug image. Note the change in the corneal thickness and the shape of the posterior surface.

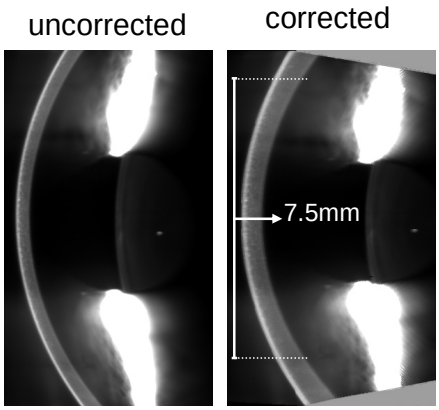

Figure 2 *Effect of correction of a Scheimpflug image. The aperture of 7.5 mm has been indicated in the corrected image.*

4.3.1 Radius and astigmatism

Figure 3 shows an example of the radius of curvature at the vertex (R) of the anterior and the posterior corneal surface as a function of meridian, and Figure 4 shows the variation in the k-value in the same subject. The radius of

Table 1

Mean and standard error values for the results of the fit of the cos^2 function that was used to investigate the variation of the radius as a function of meridian.

Subjects:	Males (n=57)	Females (n=57)	Total
Age-range	18-65 years		
	Mean ± standard error (se)		
Anterior cornea	**Radius at the vertex**		
Mean Radius (mm)	7.87±0.04	7.72±0.03	7.79±0.025
R1 (mm)	7.95±0.03	7.80±0.03	7.87±0.025
ΔR (mm)	-0.16±0.01	-0.16±0.01	-0.16±0.01
Axis (º)	93±3	96.5±4	95±3
Goodnes of fit (r^2)	0.84±0.03	0.83±0.03	0.84±0.02
Posterior cornea			
Mean Radius (mm)	6.60 ± 0.03	6.456 ± 0.03	6.53 ± 0.2
R1 (mm)	6.77±0.03	6.61±0.03	6.69±0.02
ΔR (mm)	-0.33±0.02	-0.32±0.02	-0.325±0.01
Axis (º)	93±6	100.5±5	97±4
Goodnes of fit (r^2)	0.82±0.02	0.83±0.02	0.825±0.01
Central thickness (mm)	0.581±0.004	0.578±0.005	0.579±0.003
Ratio mean posterior/anterior radius	0.84±0.02	0.84±0.02	0.84±0.01

*Results are given for males (n=57), females (n=57) and the whole group (n=114). R1 refers to the flatter meridian, ΔR is the cylindrical component and the axis indicates the axis of the steepest meridian. Also shown are the corneal thickness and the ratio of the mean value of the radius of the posterior and the anterior corneal surface. The mean radius was calculated as: R1+0.5*ΔR (mm).*

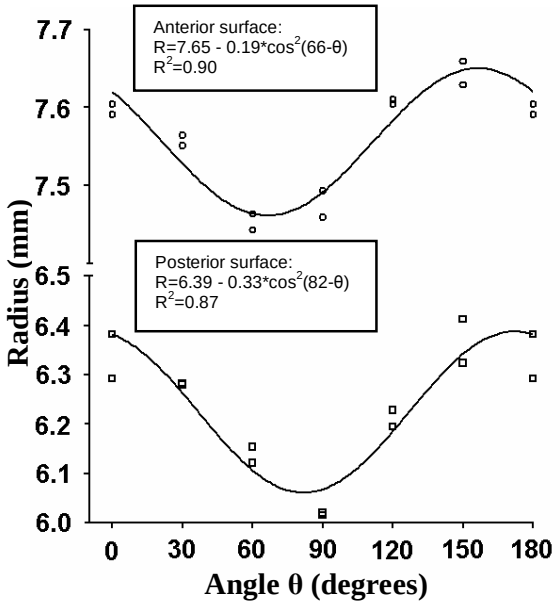

Figure 3 *Typical example for a 47 year-old female of the radius at the vertex of the anterior and the posterior corneal surface as a function of meridian. The solid line represents the cos^2 function fitted through the 12 data points.*

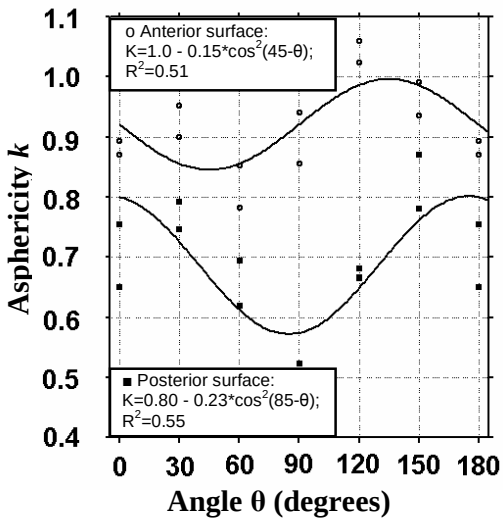

Figure 4 *Typical example of the variation of the k-value as a function of meridian for the same subject as in Figure 3. It can be seen that the cos^2 function (solid line) is not an adequate model to describe the variation.*

curvature for both corneal surfaces could be well fitted using the $\cos^2$ function. To indicate that the function is periodic, the data points of zero degrees have also been plotted at 180 degrees but were included only once in the fit. The goodness of fit is less good for subjects with a small astigmatism. The average R-squared (r^2 ±sd) for all subjects for the anterior and the posterior corneal surface was 0.84 ± 0.2 and 0.82 ± 0.15, respectively, but excluding subjects with astigmatism of the anterior corneal surface smaller than 0.5 diopter gave even better fits (0.91 ± 0.09 and 0.84 ± 0.15). The results of the radius for all subjects have been summarized in Table 1, in which the whole group has also been sub-divided into males and females. The only statistical difference (unpaired t-test) between genders was found for the radius of both the anterior and the posterior corneal surface (both $p<0.01$). For all other parameters, including asphericity and trends with age, no gender difference could be observed.

The mean central corneal thickness (±sd) was 0.579 ± 0.033 mm, which was not age-dependent ($r=0.004$, $p=0.97$). There was also no significant change with age in the mean radius of the anterior or the posterior corneal surface ($p=0.97$ and $p=0.26$, respectively). Both corneal surfaces were found to be flatter horizontally than vertically, and there was no significant difference between the axis of the two surfaces. Because the dioptric power of the anterior surface is positive while that of the posterior surface is negative, the astigmatism arising from the anterior surface is reduced by the astigmatism of the posterior surface. Furthermore, the cylindrical component in mm of the posterior surface was almost twice that of the anterior surface. The difference between the maximal and minimal radius of curvature of the posterior surface was thus significantly greater than that of the anterior surface.

There was a significant correlation between the mean radius ($R1+0.5*\Delta R$) of both corneal surfaces and the equivalent refractive error (ERE). The radius of curvature of both corneal surfaces tends to be smaller in myopic subjects than in

hypermetropic subjects. This linear regression was more pronounced for the anterior surface (7.84 (±0.03) + 0.04 (±0.01) x ERE; n=114; r=0.29; p=0.002) than for the posterior surface (6.56 (±0.03) + 0.02 (±0.01) x ERE; n=114; r=0.19; p=0.05).

For the anterior corneal surface, there was good agreement between the results obtained with the Scheimpflug camera and the kerato-refractometer. The mean radius at the vertex ± sd of the anterior corneal surface measured with the kerato-refractometer was 7.768 ± 0.27 mm. The mean of the paired difference ± sd in the average radius of the anterior corneal surface obtained with the two methods was 0.025 mm ± 0.046 mm. The mean of the paired difference in cylinder (ΔR ± sd) was 0.004 ± 0.065 mm, and the mean of the paired difference in axis ± sd was 2º ± 18º. If the difference in axis was calculated for only those subjects with a cylinder larger than 0.5 diopter, the difference ± sd decreased to 1º ± 11º.

4.3.2 Asphericity

The asphericity as a function of meridian could be fitted less well with the $\cos^2$ function than the radius (Figure 3&4). The average r^2 ± sd of the fit for all subjects for the anterior and the posterior surface was 0.59 ± 0.26 and 0.48 ± 0.26, respectively. Figure 5 shows the r^2 as a function of the subjects with at least the amount of astigmatism of the

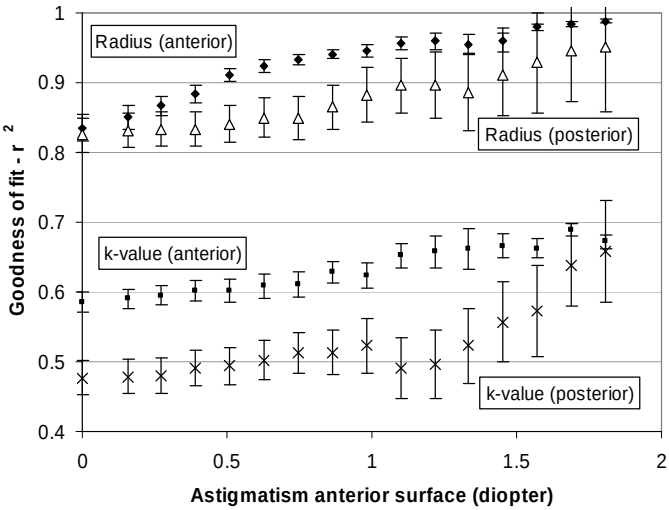

Figure 5 *The goodness of fit (r^2) of the cos2 function through the radius at the vertex and the asphericity of the anterior and the posterior corneal surface (see Fig. 3&4) as a function of the astigmatism of the anterior corneal surface. In contrast with the radius, the fit for the k-value does not improve when the astigmatism increases.*

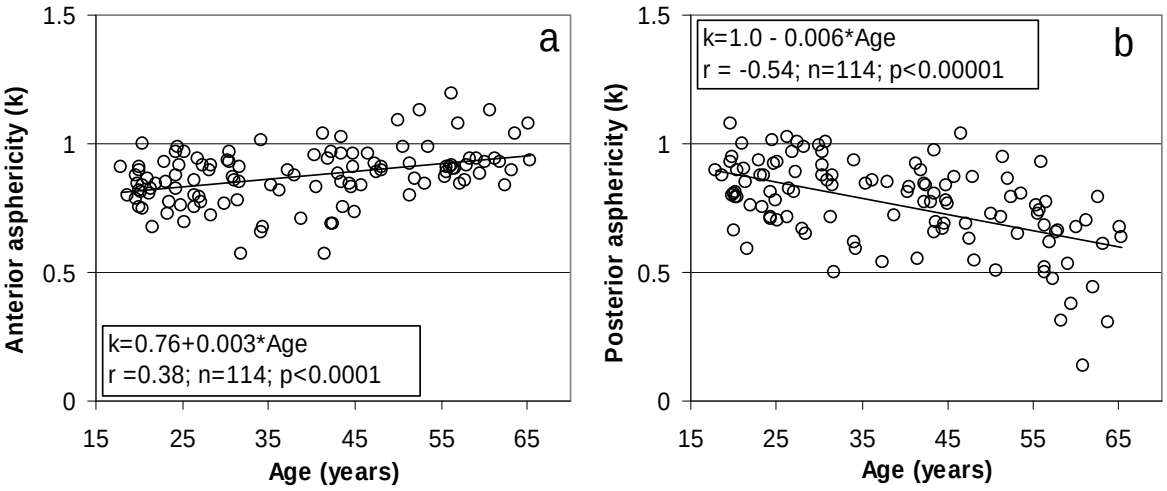

Figure 6 *The change in the mean asphericity of the anterior (a) and the posterior (b) surface of the cornea with age.*

anterior corneal surface indicated at the x-axis. In contrast with the radius, excluding subjects with a small astigmatism of the anterior corneal surface does not improve the goodness of fit for the asphericity. This indicates that the asphericity does not exhibit the same meridional variation as the radius. It appeared that the asphericity of both the anterior and the posterior surface was independent of the radius of curvature at the vertex and the refractive error. Figure 6 shows the average k-value of the 12 measurements (two series of 6 meridians) of the anterior and posterior asphericity as a function of age. The asphericity of both the anterior and the posterior surface show a significant change with age. On average, the k-value for both surfaces is between 1 and 0, which indicates that the surfaces can be described by a flattened ellipse. The age-dependent increase and decrease in the k-value of the anterior and the posterior surface respectively, result in a peripheral thinning of the cornea. Figure 7 shows the average shape of the cornea of an 18 year-old and a 65 year-old subject. Calculation shows that there was an average

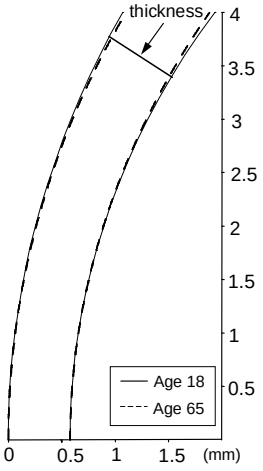

Figure 7 *Illustration of the peripheral thinning of the cornea with age. Indicated is the average shape for an 18 year-old subject (solid line) and a 65 year-old subject (dashed line).*

difference of 19 micrometer in peripheral thickness along the perpendicular line at 3.75 mm from the apex between the young and the old subject. Figure 8 shows the variation in asphericity of both corneal surfaces for the six meridians in two age-groups (18 to 41.5 years and 41.5 to 65 years). For each subject, the two measurements for each meridian were averaged and the mean value (± standard error) for the age-group is given in the graph. It can be seen that there is no significant variation in the k-value for each corneal meridian of the anterior corneal surface. The standard deviation (±sd) of the 12 measurements was 0.068 ± 0.029 (range 0.02-0.165), which was not age-dependent. Nevertheless, the posterior surface showed greater variation in the 6 meridians, with an average standard deviation (±sd) of 0.12 ± 0.042 (range 0.05-0.236). With age, this standard deviation increased significantly (linear regression: 0.09 (±0.27)+ 0.0007 (±0.0003)*age; r=0.25; p=0.007). This greater variation with age can also be seen in Figure 8. In the younger age-group, the maximal difference between the k-values of the meridians of the posterior surface was 0.21, while it increased to 0.33 in the older age-group. For both groups the k-value of the posterior surface is smallest for the vertical (90º) meridian. Table 2 shows the age-dependency of the k-value for each meridian of both surfaces.

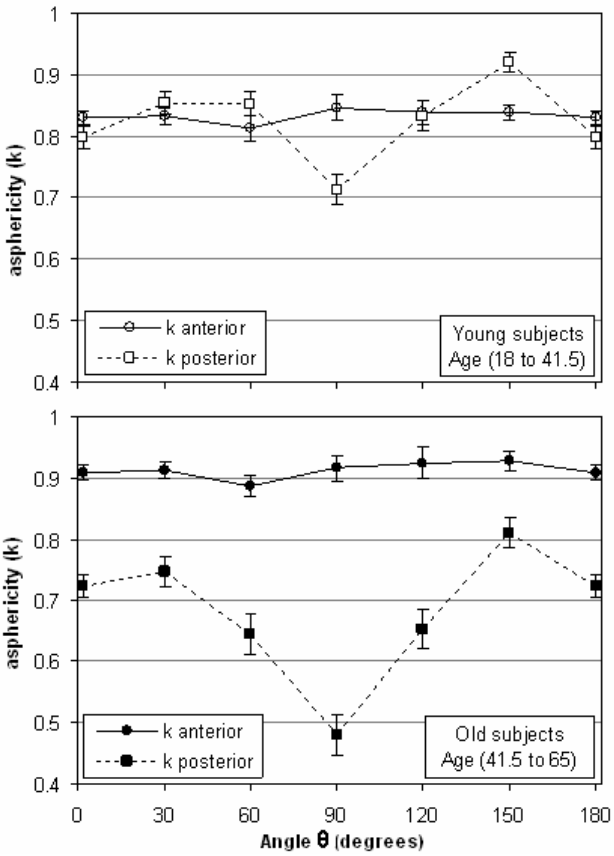

Figure 8 *Variation in asphericity as a function of meridian for both corneal surfaces for two age-groups (18 to 41.5 years and 41.5 to 65 years).*

Each meridian showed a significant change ($p<0.01$) with age. The change with age for the anterior corneal surface did not differ significantly between meridians. For the posterior surface, the change in k-value was greatest for the vertical meridian and smallest for the horizontal meridian.

Figure 9 shows that there is no correlation between the posterior asphericity (kp) as a function of the anterior asphericity (ka). As a result, it is not possible to make a reliable prediction of the asphericity of the

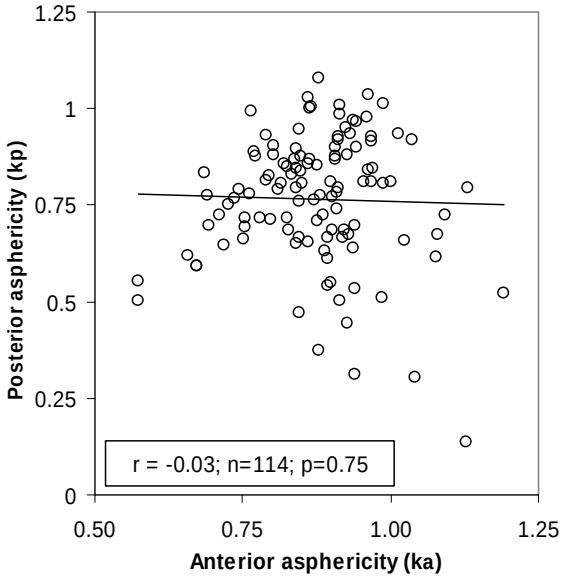

Figure 9 *The average posterior asphericity (kp) as a function of anterior asphericity (ka). There was no significant correlation.*

Table 2
The change in asphericity (k) as a function of age for all subjects (n = 114) and the linear correlation coefficient r

Asphericity (*k*)		
	Age-dependency	*r*
Anterior cornea		
Average *k*	0.76 (±0.027) + 0.0030 (±0.0007) x Age	0.39
0°	0.76 (±0.025) + 0.0026 (±0.0006) x Age	0.38
30°	0.77 (±0.027) + 0.0026 (±0.0007) x Age	0.36
60°	0.77 (±0.034) + 0.0022 (±0.0008) x Age	0.24
90°	0.78 (±0.04) + 0.0027 (±0.0007) x Age	0.24
120°	0.75 (±0.03) + 0.0037 (±0.0008) x Age	0.39
150°	0.76 (±0.027) + 0.0033 (±0.0007) x Age	0.43
Posterior cornea		
Average *k*	1.01 (±0.04) - 0.0062 (±0.0009) x Age	-0.53
0°	0.90 (±0.03) -0.0036 (±0.0009) x Age	-0.37
30°	1.00 (±0.04) - 0.0051 (±0.001) x Age	-0.45
60°	1.09 (±0.05) - 0.0085 (±0.001) x Age	-0.58
90°	0.95 (±0.05) - 0.0087 (±0.001) x Age	-0.55
120°	1.06 (±0.05) - 0.0076 (±0.001) x Age	-0.53
150°	1.06 (±0.04) - 0.0050 (±0.001) x Age	-0.43
Ratio average *k*-post / *k*-ant	1.26 (±0.04) - 0.0095 (±0.001) x Age	-0.66

All meridians of both the anterior and the posterior corneal surface showed a significant change with age ($p < 0.01$). *Also shown is the ratio of the mean value of the asphericity of The posterior* (*k* – post) *and the anterior corneal surface* (*k*-ant), *which also changed Significantly with age*.

posterior surface based on the asphericity of the anterior surface alone. Nevertheless, if the anterior k-value as well as the age is used, a reasonable assumption for the k-value of the posterior corneal surface can be made. The multiple regression was computed to be: kp = 0.76+0.325*ka-0.0072*age. Using this formula, the standard deviation of the difference between the predicted and measured posterior k-value was 0.14. This makes it clear that, based on the age and the anterior asphericity, the posterior k-value can be predicted with an accuracy of ±0.27 with a 95% confidence level.

4.4. DISCUSSION

The aim of the study was to measure the radius, astigmatism, asphericity and thickness of the whole cornea, and in particular the posterior cornea as a function of age.

4.4.1 Radius and astigmatism

Because the dioptric power of the anterior surface is positive while that of the posterior surface is negative, and because no significant difference was found between the cylinder axes of the two surfaces, the astigmatism of the anterior corneal surface (0.99 D) was compensated for 31% by that of the posterior corneal surface (-0.305 D). This reduction is greater than could be expected based on the astigmatism of the anterior surface, because the cylindrical component in mm of the posterior surface was almost twice the component of the anterior surface. The toricity of the posterior corneal surface thus does not simply reflect that of the anterior surface. This finding is supported by Dunne et al. (1991, 1992), who reported similar results with Purkinje imaging. The fact that the cylindrical component of the posterior corneal surface is larger than that of the anterior corneal surface would imply a difference in peripheral thickness between the various corneal meridians. This has also been shown in other studies. Hirji & Larke (1978), using topographic pachometry, and Rüfer,

Schröder, Arvani and Erb (2005), using Scheimpflug imaging, found that the peripheral cornea was thicker vertically than horizontally. Because of the larger cylindrical component of the posterior surface, the ratio between the radius of the posterior and the anterior corneal surface is not constant. Usually, based on Gullstrand's values of 7.7 mm for the anterior radius and 6.8 mm for the posterior radius of the cornea, a fixed ratio of 0.883 is assumed. For the Le Grand schematic eye the ratio is 0.833 (Le Grand & El Hage, 1980). In the present study, an average ratio (±sd) of 0.84 ± 0.014 was found. For the vertical meridian, this ratio (±sd) was 0.824 ± 0.017, and for the horizontal meridian, it was 0.85 ± 0.014. These ratios agree well with the finding of earlier studies in which Purkinje imaging was used. For the vertical meridian, Garner et al. (1997) and Lam & Douthwaite (2000) found a ratio of 0.827 ± 0.017 and 0.83 ± 0.02, respectively. For the horizontal meridian, Dunne et al. (1992) and Lam & Douthwaite (2000) found both a ratio of 0.84. A fixed ratio between the radius of the anterior and posterior corneal surface is assumed to calculate an effective refractive index of the cornea. This index that varies from 1.3315 to 1.3375 is used in keratometry and cornea topography in order to estimate the corneal power from the radius of the anterior corneal surface (Bennet & Rabbets, 2000; Olsen, 1986). Nevertheless, even an effective refractive index of 1.3315, which is based on the ratio of the Gullstrand schematic eye is too high. According to the results of the present study, the average index (±sd) is 1.329 ± 0.001. Because the ratio between the radius of the anterior and posterior corneal surface is dependent on meridian, the effective refractive index (±sd) is 1.328 ±0.001 for the vertical meridian and 1.330 ± 0.001 for the horizontal meridian. It must be noted that a change in the effective index of 0.001 gives a change in the calculated corneal power of approximately 0.13 D (Olsen, 1986).

The group was equally divided into males and females and it was found that the anterior and posterior corneal surface of the males was flatter than that of the females. For all other parameters, including asphericity and trends with age, no

gender difference was observed. Dunne et al. (1992) found significantly ($p<0.05$) more posterior corneal toricity in males (n=40) than in females (n=40), but in the present study, in which a larger group of subjects was measured, no significant difference was found.

4.4.2 Asphericity of the anterior corneal surface

In our earlier study, in which a smaller group of subjects and only the vertical meridian was measured, a significant change was only found in the asphericity of the posterior corneal surface. In the present study, in which the CCD-camera of the Scheimpflug camera had a higher resolution and a higher dynamic range, we also found an age-dependent change in asphericity of the anterior surface of the cornea. For all 6 meridians, the k-value of the anterior surface showed a significant increase. Not all earlier studies found such a change in the asphericity of the anterior surface. Kiely, Smith & Carney (1984), using photokeratoscopy, measured the shape of the anterior corneal surface of 54 males and 44 females ranging in age from 16 to 80 years of age, but found no significant change in asphericity with age. Using a videokeratoscope and an autokeratometer, Pardhan & Beesley (1999) measured the asphericity of the anterior surface of 20 young and 20 older subjects and found a significant shift to a more spherical surface, similar to that found in the present study. For both instruments, Pardhan & Beesley (1999) found an increase of 0.002 per year in the k-value for the horizontal meridian, which is close to our finding of 0.0026 per year.

In the present study, the average k-value of the anterior surface was 0.87, with a standard deviation of 0.11 and a range between 0.57 and 1.19, which indicates that the anterior surface appears to approximate an elliptical shape. The anterior surface of the cornea flattened in the periphery (k-value<1) in 97% of the subjects under the age of 40, but in only 84% of the subjects over 40 years of age. Thus, for 16% of the older subjects the k-value is more than 1, which

indicates that the cornea steepens toward the periphery. Figure 8 shows that, in contrast with that of the posterior surface, the asphericity of the anterior surface does not vary significantly between meridians, which is in agreement with Kiely et al. (1984) and Guillon, Lydon & Wilson (1986). Thus, there was no tendency for a different asphericity in any particular meridian. The average asphericity of 0.87 found in the present study, agrees well with the finding of earlier studies (ranging between 0.76 and 0.89) summarized in Eghbali, Yeung & Maloney (1995). Furthermore, the radius, astigmatism and cylindrical axis of the anterior corneal surface measured with the kerato-refractometer were also in agreement with those obtained using the Scheimpflug camera. This was especially the case if subjects with small astigmatism were excluded.

4.4.3 Asphericity of the posterior corneal surface

A significant average change in the k-value of –0.006 per year was found for the posterior surface, which indicates a shift to a more aspherical surface. The largest decrease was found around the vertical meridian (-0.0087 per year), while the smallest decrease was found in the horizontal meridian (-0.0036 per year). Nevertheless, all meridians showed a significant decrease with age. Because the k-value for the anterior surface increases, while that of the posterior surface decreases, there will be a thinning of the cornea in the periphery. Although the change in k-value of both corneal surfaces is highly significant, this peripheral thinning is only slight. At a distance of 3.75 mm from the apex, the thinning is approximately 20 micrometers between 18 and 65 years of age, which is on average 3% of the thickness of the cornea at that position. Rüfer et al. (2005) also found a peripheral thinning in the superior and nasal area with age. No significant change with age was found for the central corneal thickness, which is in agreement with the finding of other studies (Rüfer et al., 2005; Eysteinsson, Jonasson, Sasaki, Arnarsson, Sverrisson, Sasaki & Stefansson, 2002).

In contrast with that of the anterior surface, the asphericity of the posterior surface of the cornea varied significantly between meridians, and this variation became greater with age. The k-value was smallest for the vertical meridian. There was no correlation between the posterior asphericity and the anterior asphericity and therefore, it is not possible to measure the asphericity of the anterior surface and make a reliable prediction of the asphericity of the posterior surface. Nevertheless, using the formula presented in the results section, which also considers the age, the posterior k-value can be predicted with an accuracy of ±0.27 with a 95% confidence level. Finally, the asphericity of both corneal surfaces was independent of gender and radius. This makes it clear that a steep cornea is not likely to be more or less aspheric than a flat cornea.

ACKNOWLEDGMENTS

We would like to thank D. Koops for building the digital camera into the Scheimpflug camera

REFERENCES

Atchison, D.A., & Smith, G. (2000). *Optics of the human eye*. (pp.34-35, 166-167, 251-256). Oxford: Butterworth-Heinemann.

Bennet, A.G., & Rabbets, R.B. (1998). *Clinical Visual Optics (3 ed.).* (p.387). Oxford: Butterworth-Heinemann.

Brown, N. (1973). Slit-image photography and measurement of the eye. *Medical and Biological Illustration, 23*, 192-203.

Dragomirescu, V., Hockwin, O., & Koch, H. (1980). Photo-cell device for slit-beam adjustment to the optical axis of the eye in Scheimpflug photography. *Ophthalmic Research, 12*, 78-86.

Dubbelman, M., & Van der Heijde, G.L. (2001). The shape of the aging human lens: curvature, equivalent refractive index and the lens paradox. *Vision Research, 41*, 1867-1877.

Dubbelman, M., Van der Heijde, G.L., & Weeber, H.A. (2005). Change in shape of the aging human crystalline lens with accommodation. *Vision Research, 45*, 117-132.

Dubbelman, M., Weeber, H.A., Van der Heijde, G.L., & Völker-Dieben, H.J. (2002). Radius and asphericity of the posterior corneal surface determined by corrected Scheimpflug photography. *Acta Ophthalmologica*, 80, 379-383.
Dunne, M.C., Royston, J.M., & Barnes, D.A. (1992). Normal variations of the posterior corneal surface. *Acta Ophthalmologica, 70*, 255-261.
Eghbali, F., Yeung, K.K., Maloney, R.K. (1995). Topographic determination of corneal asphericity and its lack of effect on the refractive outcome of radial keratotomy. *American Journal of Ophthalmology, 119*, 275-280.
Eysteinsson, T., Jonasson, F., Sasaki, H., Arnarsson, A., Sverrisson, T., Sasaki, K., & Stefansson, E. (2002). Central corneal thickness, radius of the corneal curvature and intraocular pressure in normal subjects using non-contact techniques: Reykjavik Eye Study. *Acta Ophthalmologica, 80*, 11-15.
Garner, L.F., Owens, H., Yap, M.K., Frith, M.J., & Kinnear, R.F. (1997). Radius of curvature of the posterior surface of the cornea. *Optometry and Vision Science, 74*, 496-498.
Gimbel, H.V., Sun, R., & Kaye, G.B. (2000). Refractive error in cataract surgery after previous refractive surgery. *Journal of Cataract & Refractive Surgery, 26*, 142–144.
Guillon, M., Lydon, D.P., & Wilson C. (1986). Corneal topography: a clinical model. *Ophthalmic and Physiological Optics, 6*, 47-56.
Hirji, N.K., & Larke, J.R. (1978). Thickness of human cornea measured by topographic pachometry. *American Journal of Optometry and Physiological Optics, 55*, 97-100.
Kiely, P.M., Smith, G., & Carney, L.G. (1982). The mean shape of the human cornea. *Optica Acta, 29*, 1027-1040.
Kiely, P.M., Smith, G., & Carney, L.G. (1984). Meridional variations of corneal shape. *American Journal of Optometry and Physiological Optics, 61*, 619-626.
Kooijman, A.C. (1983). Light distribution on the retina of a wide-angle theoretical eye. *Journal of the Optical Society America*, *73*, 1544-1550.
Lam, A.K., & Douthwaite, W.A. (1997). Measurement of posterior corneal asphericity on Hong Kong Chinese: a pilot study. *Ophthalmic and Physiological Optics 17*, 348-356.
Lam, A.K., & Douthwaite, W.A. (2000). The ageing effect on the central posterior corneal radius. *Ophthalmic and Physiological Optics, 20*, 63-69.
Le Grand, Y., & El Hage, S.G. (1980). *Physiological Optics*. (pp. 65-67). Berlin: Springer-Verlag.
Liou, H.L., & Brennan, N.A. (1997). Anatomically accurate, finite model eye for optical modeling. *Journal of the Optical Society of America A-Optics & Image Science, 14*, 1684-1695.
Lotmar, W. (1971). Theoretical eye model with aspherics. *Journal of the Optical Society of America, 61*, 1522-1529.
Malacara, D. (1988). *Geometrical and instrumental optics*. (pp. 53-54). Boston: Academic Press.

Olsen, T. (1986). On the calculation of power from curvature of the cornea. *British Journal of Ophthalmology, 70,* 152-154.
Navarro, R., Santamaria, J., & Bescos, J. (1985). Accommodation-dependent model of the human eye with aspherics. *Journal of the Optical Society of America A, 2*, 1273-1281.
Patel, S., Marshall, J., & Fitzke, F.W. (1993). Shape and radius of posterior corneal surface. *Refractive and Corneal Surgery, 9*, 173-181.
Royston, J.M., Dunne, M.C., & Barnes, D.A. (1990). Measurement of the posterior corneal radius using slit lamp and Purkinje image techniques. *Ophthalmic and Physiological Optics, 10,* 385-388.
Rüfer, F., Schröder, A., Arvani, M.K., & Erb, C. (2005). Zentrale und periphere Hornhautpachymetrie, Normevaluation met dem Pentacam-system. *Klinische Monatsblätter für die Augenheilkunde, 222(2),* 117-122.

5

THE SPHERICAL ABERRATION OF THE ANTERIOR AND POSTERIOR SURFACE OF THE HUMAN CORNEA

VADP Sicam, M Dubbelman and RGL Van der Heijde

Journal of the Optical Society of America A 21, 1300-1306, 2004.

ABSTRACT

A ray-tracing procedure was applied to corrected Scheimpflug photography measurements to determine the spherical aberration of the anterior and posterior surface of the cornea. It was found that the total spherical aberration of the cornea increases slightly with age. The spherical aberration of the posterior corneal surface is negative at a young age, and becomes positive at an older age. In order to make an accurate description of the spherical aberration for the whole eye, the posterior surface must also be measured.

5.1 INTRODUCTION

The cornea and the lens are the main components of the eye that are responsible for focusing light at the retina, but the focusing is usually far from perfect. First, the location of the focused light does not always coincide with the location of the retina (defocus). Second, the size of the focused spot is determined by the aberrations of the eye of which astigmatism, (and to a lesser degree) coma and spherical aberration (SA) are the more dominant components.[1] With conventional spectacles or contact lenses, defocus and astigmatism can easily be corrected, but in standard practice no correction is applied for higher order aberrations.[2] Nevertheless, in the design of an intraocular lens (IOL) it appeared to be important to correct for the SA. [3]

Both surfaces of the cornea contribute to the SA of the eye. Because the anterior surface is easily accessible for standard ophthalmological measurement techniques the SA of this corneal surface has been extensively studied.[4,5,6,7] However, there is limited knowledge regarding the SA of the posterior corneal surface and, as a result, there is an uncertainty in determining the SA of the cornea and lens separately.[8] Barbero, Marcos and Merayo-Lloves (2002) measured an aphakic eye in order to determine the SA of the posterior corneal surface.[9] In an aphakic eye, this can easily be calculated by subtracting the contribution of the anterior surface from the aberrations of the whole eye.

In the present study the SA of both the anterior and the posterior surface of the cornea was investigated. Corrected Scheimpflug photography was used to determine the shape of both corneal surfaces. This technique has been validated, and produces shape parameters such as the radius of curvature and asphericity with reasonable accuracy.[10,11]

5.2 THEORY

5.2.1 Spherical Aberration of the anterior corneal surface

An anterior corneal surface will produce zero aberration for an incident light represented as a plane wave (Figure 1) if the optical path lengths from a reference plane to the focal plane are identical for all incident rays to the surface. This is a rotationally symmetric conic surface that can be described by the conic parameters *r* and *k*. The parameter *r* is the apex radius of curvature of the surface. The asphericity is represented by the parameter *k* (sometimes labeled as *p*), $k = 1$ for a sphere and $k = 0$ for a parabolic surface. It is related to the parameter Q, referred to by other authors as $k = Q+1$.[8,12] The asphericity of the anterior corneal surface that produces zero aberration can easily be determined using the three equations below:

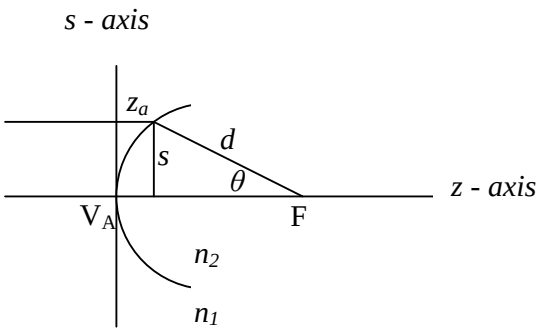

Figure 1 *Incident light on a corneal surface is refracted to a focus point, F.*

Equation of a rotationally symmetric conic surface:

$$s^2 - 2rz_a + kz_a^2 = 0 \qquad (1)$$

Equating optical path lengths:

$$n_1 z_a + n_2 d_1 = n_2 f \qquad (2)$$

Pythagorean Theorem:

$$d_1^2 = s^2 + (f - z_a)^2 \qquad (3)$$

The axis representing the surface is *z* and *s*, where *z* represents the optical axis. The *s*-axis is a generalization of the *x*-*y* plane since we are considering a rotationally symmetric surface. The anterior surface corneal height is labeled as z_a, f is the distance of the focus point (F) to the apex of the surface (V_A), and d is the distance of this focus point to an arbitrary point on the surface. The refractive indices, $n_1(1.0)$ and $n_2(1.376)$, are for air and cornea respectively. The

mean value for the corneal index of refraction of 1.376 is supported by anatomical and optical studies.[14,15,16]

Using equations (1), (2) and (3), one can find the k-value that gives zero SA:

$$k = 1 - \frac{{n_1}^2}{{n_2}^2} \approx 0.4718, \qquad (4)$$

$$f = \frac{n_2 r}{n_2 - n_1} \qquad (5)$$

Equation (5) is the same equation for locating the paraxial focal point of a spherical lens. Experimentally, it was found that the asphericity, *k*, of the anterior surface of the cornea is in most cases greater than the value of 0.4718.[10,12] Consequently, the anterior surface of the cornea produces a positive SA, which can be derived from the wave aberration generally defined as:

$$W_a = n_2 f - n_1 z_a - n_2 d_1 \qquad (6)$$

From this definition, one can perform a least squares fitting procedure to derive Zernike coefficients describing the wave aberration.[17] The value of the Zernike coefficient, C_4^0, expressed in μm is used to characterize the SA contribution.[18] Definition (6) is equivalent to another way of defining the wave aberration of the anterior surface in which the reference surface (*k*=0.4718) is used to calculate the wave aberration:[19]

$$W_a = n_2 (z_a - z_{ref}) \cos\theta - n_1 (z_a - z_{ref}) \qquad (7)$$

where z_{ref} are height values for the reference surface and the angle θ is illustrated in Figure 1. Definitions (6) and (7) are only approximations of actual optical path lengths. For example, in asymmetric surfaces the refracted ray does not necessarily lie in the meridial plane of the incident ray, but it has been found that wave aberration computation using either definition yields values that have a maximum deviation (for a 5.6 mm zone) of less than 0.06 μm (1.3%), compared to wave aberration values determined by exact ray-tracing.[19]

5.2.2 The SA of the posterior corneal surface

Smith, Cox, Calver and Garner (2000) have proposed a method to calculate the SA of the posterior surface.[8] In this method the same formula for calculating the SA of the anterior surface is applied to the posterior surface. However, this procedure will not reflect the correct SA of the posterior surface because the incident wave on the posterior surface is already an aberrated wave, in contrast to the unaberrated wave approaching the anterior surface. As a result, the method will only produce the correct SA for the posterior surface if the anterior surface has an asphericity of k = 0.4718, when the incident wave approaching the posterior surface will have zero aberration.

An alternative method that was used in the present study is to determine the SA of the whole cornea using ray-tracing principles (shown in Figure 2). The reference points, F_A and F_C is determined for each meridian. The location of the first reference point, F_A, which describes the focal point of the anterior surface of the cornea, is determined with equation (5). The location of the second reference point, $F_{c,}$ which describes the focal point of the whole cornea, is determined with an effective index of refraction for the cornea, n_{eff}. This refractive index can be found using the shape of the anterior and the posterior surface and the value was calculated for each individual subject in the present study.[20,21] Every point on the posterior surface (z_p,s_p) can now be traced back to a point on the anterior

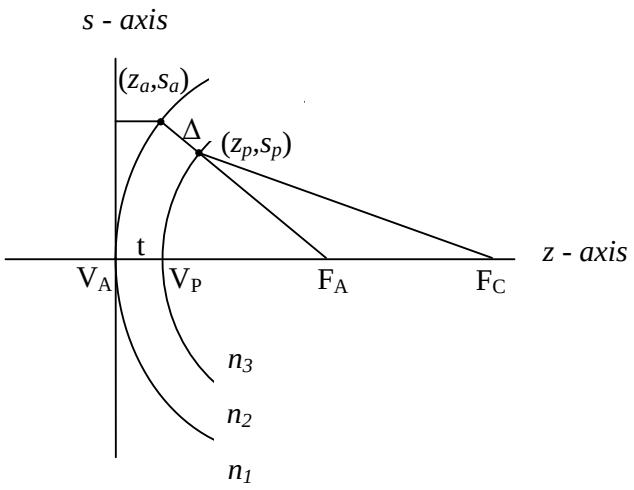

Figure 2 *Ray-tracing procedure to determine the SA of the cornea.*

surface (z_a,s_a) using F_A as a reference point. The wave aberration of the cornea is now represented as follows:

$$W_c = n_2 t + n_3 (f_c - t) - n_1 z_a - n_2 \Delta - n_3 d_2 \qquad (9)$$

where, $t = \overline{V_A V_P}$ is the thickness of the cornea measured at the optical axis; n_1,n_2,n_3 are the indices of refraction of air, cornea and anterior chamber, respectively; Δ is the distance between (z_p,s_p) and (z_a,s_a); and d_2 is the distance between (z_p,s_p) and F_C; and $f_c = \overline{V_A F_C}$ is the distance between the focal point F_C and the apex of the anterior surface. The SA of the whole cornea can now be determined by Zernike polynomial fitting of the wave aberration described in equation (9).[17] The SA contribution of the posterior surface is the difference between the SA of the whole cornea and the SA of the anterior surface.

5.3 METHOD

5.3.1 Subjects

Scheimpflug images were made of the anterior eye segment of the right eye of 114 subjects, ranging from 18 to 65 years of age, who had no corneal abnormalities. No exclusion criteria were applied for the equivalent refractive error (ERE): minimum ERE = -6.88 Diopters, maximum ERE = 3.50 Diopters. The ERE and age were not correlated.[20]

5.3.2 Measurement & Surface Modeling

Two series of Scheimpflug images were made in six meridians (90°, 60°, 30°, 0°, 150°,120°). Images were obtained with the Topcon SL-45 Scheimpflug camera, the film of which was replaced by a CCD-camera (St-9XE, SBIG astronomical instruments). [20] For each meridian, the radius of curvature (r) and asphericity (k) of both the anterior and the posterior surface of the cornea were determined for a 7.5 mm corneal zone. The equation used for the fitting is:[10]

$$z - z_0 = \frac{c(s - s_0)^2}{1 + \sqrt{1 - kc^2 (s - s_0)^2}} \qquad (11)$$

where, the curvature c is the reciprocal of r. The vertex for this curve is located at $(z,s) = (z_0,s_0)$.

The Scheimpflug apparatus was aligned to the geometric axis of the cornea during measurements. Hence, the meridian measurements are referenced with respect to the geometric axis of the cornea, and not with the line of sight axis. On average, the angle lambda, which is the angle between the line of sight and the geometrical axis of the cornea is less than 5 degrees.[22] Calculations made clear that the SA of the cornea is more sensitive to changes in the asphericity k than to changes in the radius of curvature r.[12] For a 5 degree angle lambda, calculation for the asphericity k at this reference angle will deviate from calculations made with the geometrical axis as reference at approximately Δk = 0.01. This change in the k-value will change the value of the SA by 2%. The effect is even less for a smaller angle lambda.[23] Therefore, the value of the SA calculated with the line of sight axis as a reference will not differ much from that calculated with the corneal geometric axis as reference. This consideration is appropriate if we compare this to the precision of the Scheimpflug apparatus in measuring the k-value. For a series of repeated measurements (10 trials) of the right eye of three subjects, the standard deviation in the k-value for both the anterior and the posterior surface of the cornea appeared to be approximately 0.035, and this value was independent of the meridian.

5.3.3 Calculation of Spherical Aberration

Three different methods were used to calculate the SA. The first method fits the k-value and the radius of curvature r from the six meridians to a cosine-squared function:[12]

$$r(\theta) = r_1 + r_2 \cos^2(\theta - \alpha) \qquad (12)$$

and

$$k(\theta) = k_1 + k_2 \cos^2(\theta - \beta) \qquad (13)$$

This fitting for the *r* and *k* will describe a surface representation of the cornea. It will describe defocus, astigmatism and the SA of the corneal surface, but not the higher order terms. With the reconstructed surface, the SA is calculated using a Zernike fitting of the corneal wave aberration (equation 9). The second method is based on the same fitting for the measured radius of curvature measurements for the six meridians (equation 12), but this time using the average *k*-value from the six meridian measurements to reconstruct the corneal surface, after which the SA is calculated. In the third method the SA is calculated separately for each meridian, and the average value for the six meridians is used to calculate the SA of the whole cornea. All three methods will yield almost identical results, with less than 1% difference. The results derived from the first method are presented in this paper.

5.4 RESULTS

The mean values for the apex radius of curvature and asphericity for both the anterior and the posterior surface are listed in Table 1. The age-trend for the asphericity values of both surfaces is also shown. Figure 3 shows the SA of both the anterior and the posterior surface of the cornea as a function of age. For both corneal surfaces a significant increase with age was found. The posterior corneal surface SA started with a negative value and increased to a positive value with age. The ratio $SA_{posterior}/SA_{anterior}$ varied between subjects from –10% to 26% (Figure 4). As a result, if the posterior surface is not taken into account, and a one surface model is used to calculate the SA of the whole cornea, the error will vary from –8% to 27% (Figure 5).

Table 1 *Mean Value* (±*s.d.*) *of the Radius and k Value of the Anterior and Posterior Surfaces of the Cornea*[a]

Parameter	Mean (±s.d.)	Linear Regression Age Trend (standard error specified)	*r*	*p*
Anterior *r* (mm)	7.79 ± 0.27			
Anterior *k*	0.87 ± 0.11	0.76 (± 0.027) + 0.0030 (± 0.0007) x age	0.39	< 0.001
Posterior *r* (mm)	6.53 ± 0.25			
Posterior *k*	0.77 ± 0.17	1.01 (± 0.040) + 0.0062 (± 0.0007) x age	-0.53	< 0.001

[a]Age trend for the *k* value is also shown.[20]

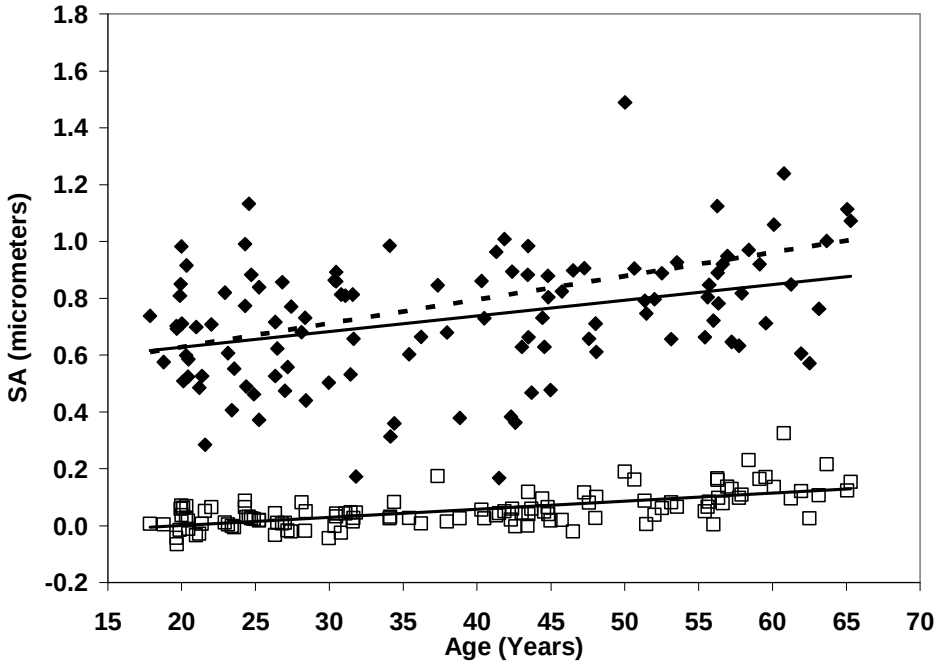

Figure 3 *SA for the anterior surface (solid diamonds, slope = 0.0055, r = 0.356, p < 0.001) and posterior surface (hollow squares, slope = 0.0028, r = 0.646, p < 0.001) of the cornea as a function of age for 7.5 mm zone. The age-trend for the whole cornea is shown in a line of dashes (slope = 0.0083, r = 0.464, p < 0.001).*

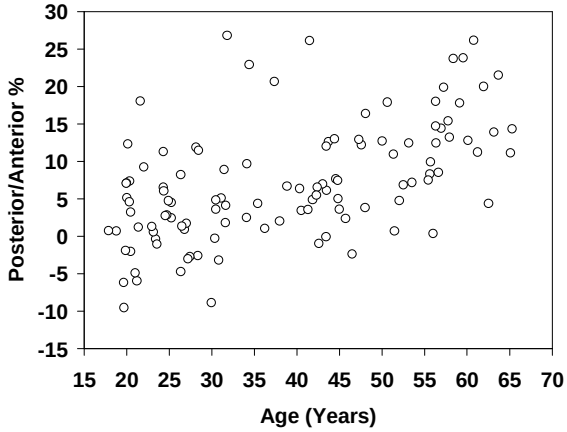

Figure 4 *% posterior SA contribution with respect to the anterior contribution*

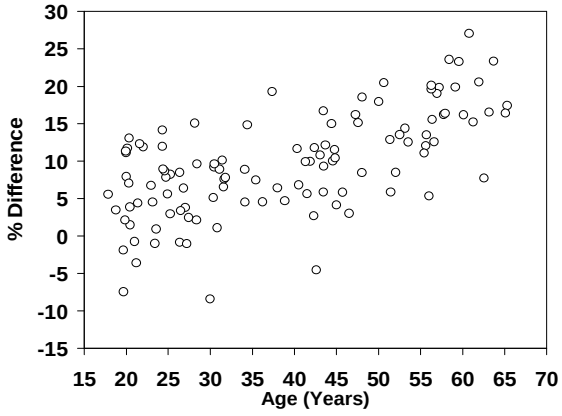

Figure 5 *% difference between SA calculated for one surface model compared to actual values.*

Table 2 *Mean value (±s.d.) (or range [..]) of calculated SA of the corneal anterior surface from different data sets.*

Investigators	Technique	Age Group (yr)	Number of eyes	Anterior Surface SA μm/mm^4	Increase with age?
Sicam *et al.* (this study)	Scheimpflug	[18,65]	114	0.049 ± 0.015	Yes
Amano *et al.*[24] (2004)	CT[a]	[18,69]	75	[0.033,0.050]	No
Wang *et al.*[25] (2003)	CT	[20,75]	228 (134 subjects)	0.046 ± 0.017	No
He *et al.*[26](2003)	CT	[9,29]	90 (45 subjects)	0.040 ± 0.013	—
Smith *et al.*[8] (2001)	keratometer	[20,31]	13	[0.018,0.062]	No
		[56,71]	13		
		[20,30]	27	0.032 ± 0.011	Yes
Guirao *et al.*[27] (2000)	CT	[40,50]	15	0.043 ± 0.010	
		[60,70]	17	0.044 ± 0.010	
Oshika *et al.*[28] (1999)	CT	[9,85]	102	~0.8 μm^2 [b]	No
Tomlinson *et al.*[6] (1993)	CT	[20,56]	20	0.048 ± 0.006	—

[a] Placido Ring Cornea Topographer
[b] (Maximum value for variance of coefficients for spherical-like aberration.

5.5 DISCUSSION

5.5.1 Spherical Aberration of the Anterior Surface

The SA of the anterior corneal surface found in this study is in good agreement with that found in other studies. Table 2 lists mean values for the SA of the anterior corneal surface reported by different investigators. In order to be able to compare the results of the different studies, the unit μm/mm^4 is used for the SA, details of which are given in the Appendix. The results of all the studies show that the SA of the anterior surface of the cornea is positive. The asphericity of the anterior corneal surface found in the present study is also in good agreement with the findings of those studies listed in Table 2 in which asphericity data was provided (Sicam, Dubbelman and Van der Heijde: k = 0.87 ± 0.11; Guirao, Redondo and Artal: k = [0.56,1.10]; Smith, Cox, Calver and Garner: k = 0.76 ± 0.11). As can be expected, a higher asphericity value produces higher SA.

5.5.2 Age Effect

The SA of both the anterior and the posterior surface of the cornea, evaluated at 7.5 mm corneal zone, increased with age. This increase with age was also found by Guirao, Redondo and Artal (2000)[27], but not in several other studies (see Table 2). All the other studies, except the Smith study,[8] used corneal topography, which might not be accurate in the peripheral region.[28,29] This may be a reason why different investigators reported different results with regard to the age-trend in the SA of the anterior surface of the cornea. However, in the present study the corneal periphery was measured accurately with the Scheimpflug technique.

Barbero, Marcos and Merayo-Lloves found a negligible contribution of the posterior corneal surface of a 30-year old aphakic eye to the SA of the cornea.[9] This agrees with the findings of the present study. As can be seen in Figure 3, the SA of the posterior corneal surface at 30 years of age is almost zero.

5.5.3 Is a one-surface model adequate?

There are three approaches to describe the SA of the cornea. One approach represents the aberration of the eye as composed of the aberration of the anterior corneal surface and the aberration of the internal optics.[4,8] However, in that approach, it is not possible to give a complete description of the SA of the whole cornea because the contribution of the posterior surface of the cornea is not quantified. A second approach is based on the use of an effective refractive index for the whole cornea to account for the contribution of the posterior surface.[30] Analysis of this concept, using data from the present study, shows that the SA of the cornea calculated with this model can differ from the actual value by as much as 27% (Figure 4b). The third approach estimates the SA of the posterior cornea by calculating a posterior radius of curvature derived from measured values of the corneal anterior radius of curvature, and combines this with a possible range of values for the asphericity of the posterior surface.[8] Nevertheless, the results of the present study show a large variation in the

asphericity of the posterior surface (the standard deviation: 0.17). A change in the *k*-value of 0.17 will result in a change of 20 % in the amount of SA of the cornea.

5.6 CONCLUSION

This study presents a method to determine the SA of both the anterior and the posterior surface of the cornea that was applied to corrected Scheimpflug photographs of human eyes. The results show that the SA of the cornea increases with age. The SA of the posterior corneal surface is negative at a young age and becomes positive at an older age. Consequently, a one-surface model is not sufficient to predict the SA of the cornea, so additional measurement of the posterior surface of the cornea is important. This approach, in which the SA of the whole cornea is determined, provides better understanding of the optics of the eye that is needed for further research on the SA of the human crystalline lens and for the construction of aspheric IOLs to make the optics of the whole eye aberration free.

APPENDIX A

Comparing different units used for describing SA

Comparison of SA of the anterior corneal surface measured by different researchers can present some difficulties. There are two reasons for this: first, the units that are used can differ and secondly, when the SA is derived from Zernike fitting, the value used to describe SA varies with size of the pupil.[31] Nevertheless, it is possible to reconcile these differences.

The SA is usually derived from a polynomial expansion of the wave aberration function. One such expansion expressed in rectangular coordinates *X,Y* is the following:

$$W(X,Y) = W_1X + W_2Y + W_3X^2 + W_4XY + W_5Y^2 + W_6X^3 + W_7X^2Y + W_8XY^2 + W_9Y^3 + W_{10}X^4 + W_{11}X^3Y + W_{12}X^2Y^2 + W_{12}X^2Y^2 + W_{13}XY^3 + W_{14}Y^4 + O(5) \quad \text{(A1)}$$

where *W(X,Y)* is the aberration function and the W_i 's are the assigned coefficients for each term in the expression. This form was suggested by Howland and Howland[32] (1977) and was later on adopted by Smith *et al.*[33] (1998) and also by Smith *et al.*[8] (2001). They applied this formula to eye aberration measurements obtained with a crossed-cylinder aberroscope. Based on the assumption that the cornea can be described by a conicoid,[7] the following expression for the SA can be expressed as follows:

$$W(X,Y) = W_{4,0}Y^4 \quad \text{(A2)}$$

which is analogous to the expression of the SA function in polar coordinates:

$$SA = CR^4 \quad \text{(A3)}$$

where[34]

$$C = W_{4,0} = \frac{(3W_{10} + W_{12} + 3W_{14})}{8} \quad \text{(A4)}$$

If the wave aberration function is expressed in μm (which means that *SA* is also in μm) and the pupil coordinates are expressed in mm, then the units of *C* in Equation (A3) are μm/mm^4. Because of the way in which *C* is derived, the value of *C* is independent of pupil size and therefore this expression is useful for reconciling calculations of SA derived from different pupil sizes (Table 2).

The SA component in Zernike fitting is:

$$SA = 6\sqrt{5}C_4^0\rho^4 \quad \text{(A5)}$$

where C_4^0 is the SA coefficient expressed in μm.[18] Equation (A5) can easily be compared with equation (A3) because the Zernike fitting is referred to a unit circle:

$$R = r_p\rho \quad \text{(A6)}$$

where r_p, is the pupil radius. Combining equations (A3), (A5) and (A6) results in the following conversion factor:

$$C = \frac{Seidel\_value}{r_p{}^4} \qquad \text{(A7)}$$

where *seidel value* is expressed in μm and the pupil radius, r_p, is expressed in mm. The *Seidel value*:

$$Seidel\_value = 6\sqrt{5}C_4^0 \qquad \text{(A8)}$$

is the SA component of the Seidel aberrations, which is another way in which to describe wave aberrations.[17,35]

If the SA coefficient is expressed in Diopters, then we can use the following conversion:[36]

$$Seidel\_value(\mu m) = \frac{r_p{}^2}{4} Seidel\_value(D) \qquad \text{(A9)}$$

D is the dioptric unit 1/m and, again, r_p is the pupil radius expressed in mm. One group listed in Table 2 uses the variance of the coefficients to describe spherical-like aberrations. To avoid confusion, no conversion was made in this case.

REFERENCES

1. J. Porter, A. Guirao, I.G. Cox and D.R. Williams, "Monochromatic aberrations of the human eye in a large population," J. Opt. Soc. Am. A 18(80, 1793-1803 (2001).
2. M. Millodot, "Effect of the Aberrations of the Eye on Visual Perception," In *Visual Psycophysics and Physiology*, (Academic Press, Inc., 1978) Ch. 35, pp. 441-452.
3. R. Belluci, S. Morselli and P. Piers, "Comparison of wavefront aberrations and optical quality of eyes implanted with five intraocular lenses," J. Ref. Surg. 20(4), 297-306 (2004).
4. S.G. El Hage and F. Berny, "Contribution of the crystalline lens to the spherical aberration of the eye," J. Opt. Soc. Am. 63(2), 205-211 (1973).
5. M. Millodot and J. Sivak, "Contribution of the cornea and the lens to the spherical aberration of the eye," Vis. Res. 19, 685-687 (1979).

6. A. Tomlinson, R. P. Hemenger and R. Garriot, ”Method for estimating the spherical aberration of the human crystalline lens in vivo.” Inv. Ophth. Vis. Sci. 34, 621-629 (1993).
7. P. Artal, A. Guirao, E. Berrio and D.R. Williams, “Compensation of aberrations by the internal optics in the human eye,” J. Vis. 1, 1-8 (2001).
8. G. Smith, M.J. Cox, R. Calver and L.F. Garner, “The spherical aberration of the crystalline lens of the human eye,” Vis. Res. 41, 253-243 (2000).
9. S. Barbero, S. Marcos and J. Merayo-Lloves, “Corneal and total optical aberrations in a unilateral aphakic patient,” J. Cat. Ref. Surg. 28 1595-1600 (2002).
10. M. Dubbelman, H.A. Weeber, R.G.L. van der Heijde and H.J. Völker-Dieben, “Radius and asphericity of the posterior corneal surface determined by corrected Scheimpflug photography,” Acta Ophth. Scand. 379-383 (2002).
11. M. Dubbelman and G.L. van der Heijde, “The shape of the aging human lens: curvature, equivalent refractive index and the lens paradox,” Vis. Res. 41, 1867-1877 (2001).
12. P.M. Kiely, G. Smith and G. Carney, “The mean shape of the human cornea,” Optica Acta, 29(8) 1027-1040 (1982).
13. D.A. Atchison and G. Smith, *Optics of the Human Eye*, (Butterworth-Heinemann, 2000) p. 251.
14. R.A. Moses, *Adler’s Physiology of the eye: Clinical application,* (The C.V. Mosby Company, 1981) p. 38.
15. S. Patel, J. Marshall and F.W. Fitzke 3rd, “Refractive index of the human corneal epithelium and stroma,” J. Ref. Surg. 11(2) 100-105 (1995).
16. H-L Liou and N.A. Brennan, “Anatomically accurate, finite model eye for optical modeling,” J. Opt. Soc. Am. A 14(8) 1684-1695 (1997).
17. A. Guirao and P. Artal, “Corneal wave aberration from videokeratography: accuracy and limitations of the procedure,” J. Opt. Soc. Am. A 17(6), 955-965 (2000).
18. L.N. Thibos, R.A. Applegate, J.T. Schwiegerling and R. Webb, “Standards for reporting the optical aberrations of eyes,” J. Ref. Surg. 18, 652-660 (2002).
19. T.O Salmon, “Corneal contribution to the wave aberration of the eye.” PhD Dissertation, December 1999 (revised: August 2002). http://arapaho.nsuok.edu/~salmonto/Dissertation/Dissertation.html
20. M. Dubbelman, V.A. Sicam and R.G.L. van der Heijde, Department of Physics and Medical Technology (FMT), VU University Medical Center, 1081 HV Amsterdam, The Netherlands are preparing a manuscript entitled “The shape of the anterior and posterior surface of the aging human cornea.”
21. T. Olsen, “On the calculation of power from curvature of the cornea,” B. J. Ophth. 70 152-154 (1986).

22. D.A. Atchison and G. Smith, *Optics of the Human Eye,* (Butterworth-Heinemann, 2000) p. 36.
23. T.O. Salmon and L.N. Thibos, "Videokeratoscope-line-of-sight misalignment and its effect on measurements of corneal and internal ocular aberrations," J. Opt. Soc. Am. A 19(4) 657-669 (2002).
24. S. Amano, Y. Amano, S. Yamagami, T. Miyai, K. Miyata, T. Samejima, C. Oshika and T. Oshika, "Age-related changes in corneal and ocular higher-order wavefront aberrations," Am. J. Ophthalmol. 137, 988-992 (2004).
25. L. Wang, E. Dai, D.D. Koch and A. Nathoo, "Optical aberrations of the human anterior cornea," J. Cat. Ref. Surg. 29(8), 1514-1521 (2003).
26. J. C. He, J. Gwiazda, F. Thorn and R. Held, "Wave-front aberrations in the anterior corneal surface and the whole eye," J. Opt. Soc. Am. A 20(7), 1155-1163 (2003).
27. A. Guirao, M. Redondo and P. Artal, "Optical aberrations of the human cornea as a function of age," J. Opt. Soc. Am. A 17(10), 1697-1702 (2000).
28. T. Oshika, S.D. Klyce, R.A. Applegate and H.C. Howland, "Changes in corneal wavefront aberrations with aging," Inv. Ophth. and Vis. Sci. 40 1351-1355 (1999).
29. R.A. Applegate, R. Nuñez, J. Buettner and H.C. Howland, "How accurately can videokeratographic systems measure surface elevation?", Opt. Vis. Sci. 72(11) 785-792 (1995).
30. R.P. Hemenger, A. Tomlinson and K. Oliver, "Corneal optics from videokeratographs," Ophth. Phys. Opt. 15(1), 63-68 (1995).
31. D.A. Atchison, "Recent advances in representation of monochromatic aberrations of human eyes," Clin. Exp. Opt. 87(3) 138-148 (2004).
32. H.C. Howland and B. Howland, "A subjective method for the measurement of monochromatic aberrations of the eye," J. Opt. Soc. Am. 67(11) 1508-1518 (1977).
33. G. Smith, R.A. Applegate and D.A. Atchison, "Assessment of the accuracy of the crossed-cylinder aberroscope technique," J. Opt. Soc. Am. A 15(9) 2477-2487 (1998).
34. D.A. Atchison and G. Smith, *Optics of the Human Eye,* (Butterworth-Heinemann, 2000) (eqn. 15.19) p. 145.
35. M. Born and E. Wolf, *Principles of Optics 7th ed.* (Cambridge University Press 1999) pp. 236-244
36. L.N. Thibos, *Handbook of Visual Optics v. 4/99*. http://research.opt.indiana.edu/default.html

6

THE CONTRIBUTION OF THE POSTERIOR SURFACE TO THE COMA ABERRATION OF THE HUMAN CORNEA

M Dubbelman, VADP Sicam and RGL Van der Heijde

Submitted

ABSTRACT

Scheimpflug imaging in 6 meridians was used to measure the shape of the anterior and posterior cornea of the right eye of 114 subjects, ranging in age from 18 to 65 years. Subsequently, a 3D model of the shape of the whole cornea was reconstructed, from which the coma aberration of the anterior corneal surface and the whole cornea could be calculated. This made it possible to investigate the role of the posterior corneal surface in compensating the coma aberration of the anterior corneal surface with age. Results show that, on average, the posterior surface compensates approximately 3.5% of the coma of the anterior surface. The compensation tends to be greater in young subjects (6%) than in older subjects (0%). This small effect of the posterior cornea on the coma aberration makes it clear that for the coma aberration of the whole eye only the anterior corneal surface and the crystalline lens play a role. Consequently, for the design of an intraocular lens that is able to correct for coma aberration, it would be sufficient to take only the anterior corneal surface into account.

6.1 INTRODUCTION

In general, corneal aberration is determined solely from measurements of the anterior corneal surface. Nevertheless, according to recent studies in which Scheimpflug imaging was used, the contribution of the posterior surface cannot be neglected. For example, the posterior corneal surface compensates for 31% of the anterior corneal surface astigmatism, which is more than could be expected based on the astigmatism of the anterior surface alone (Dubbelman, Sicam & Van der Heijde, 2006). Furthermore, the posterior corneal surface appears to have a significant effect on the spherical aberration of the cornea (Sicam, Dubbelman & Van der Heijde, 2006). This effect (10% reduction to 26% addition) is age-dependent, and is related to the asphericity of both the anterior and the posterior corneal surfaces.

Very little is yet known about the contribution of the posterior surface to corneal coma aberration. Barbero, Marcos & Merayo-Lloves (2002) measured the aberration in an aphakic eye. Their results show that the vertical coma aberration of the anterior corneal surface is compensated partially (aprox. 20%) by the posterior surface, whereas the lateral coma increased due to the contribution of the posterior surface.

More knowledge about the coma aberration of the posterior corneal surface is needed in order to be able to distinguish between the aberrations of the cornea and aberrations of the crystalline lens (Smith, Cox, Calver & Garner, 2001; He, Gwiazda, Thorn & Held, 2003). Currently, the aberrations of the anterior corneal surface and the aberrations of the whole eye are measured. Subtracting the aberrations of the anterior surface from those of the whole eye makes it possible to calculate the aberrations of the internal optics, i.e. lens and posterior corneal surface. More information about the coma of the posterior surface could make it possible to distinguish more accurately between the contribution of the posterior corneal surface and that of the lens. Furthermore, attempts have been

made to replace the crystalline lens by an intraocular lens (IOL), which also corrects for higher order aberrations. Traditionally, IOLs were only designed to correct spherical refractive error (Ridley, 1952). After that, toric IOLs were introduced in order to correct corneal astigmatism (Shimizu, Misawa & Suzuki, 1994). This was followed by the aspheric IOL, which made it possible to correct for spherical aberration (Marcos, S., Barbero, S., Llorente, L., Dorronsoro, C., Rosales, P., & Jiménez-Alfaro, I**.,** 2003; Padmanabhan, Rao, Jayasree, Chowdhry & Roy, 2006). Recently, initial attempts have been made to correct coma aberration (Tabernero, Piers & Artal, 2006).

In the present study, the compensatory role of the posterior surface to the coma aberration of the anterior corneal surface with age has been investigated. Using Scheimpflug imaging in six meridians, a 3D model of the shape of the whole cornea was reconstructed. From this model, the coma aberration of the anterior cornea and the whole cornea was calculated, and this made it possible to determine the contribution of the posterior corneal surface to the coma aberration of the whole cornea.
cornea.

6.2 METHODS

The sample population, the set-up of the Scheimpflug camera, and the necessary correction of the Scheimpflug images have all been described previously in detail (Dubbelman et al., 2006). Briefly, two series of Scheimpflug images were made in 6 meridians (90°, 60°, 30°, 0°, 150°, 120°) of the right eye of 114 subjects (57 males, 57 females) ranging in age from 18 to 65 years, who had not worn contact lenses in the previous 2 years. Images were obtained with the Topcon SL-45 Scheimpflug camera, the film of which was replaced by a CCD-camera (St-9XE, SBIG astronomical instruments) with a dynamic range of 16 bits of grey values (512 x 512 pixels, pixel size 20 x 20 micrometer,

magnification: 1x). The Scheimpflug images were corrected for distortion due to the geometry of the Scheimpflug imaging system and the refraction of the anterior corneal surface (Dubbelman et al., 2006). For each of the 6 meridians, the anterior and posterior surface of the cornea was fitted to the following function, which is used in various forms (Atchison & Smith, 2000):

$$y = \frac{c(x - x_0)^2}{1 + \sqrt{1 - kc(x - x_0)^2}} + y_0 \qquad (1)$$

where c is the curvature (inverse radius r) at the vertex (x0, y0) and k is the conic constant, which indicates the asphericity of the surface (e.g. hyperbola: k<0; parabola: k=0; circle: k=1). The y-axis is the axis of revolution of both the conic and the optical axis of the cornea. By combining the Scheimpflug images in 6 meridians, it is possible to determine the astigmatism (Dubbelman et al, 2006) and spherical aberration (Sicam et al., 2006) of the anterior and posterior cornea. Nevertheless, the coma aberration cannot be obtained using equation (1). It therefore has to be extended to:

$$y = \frac{c(x - x_0)^2}{1 + \sqrt{1 - kc(x - x_0)^2}} + t(x - x_0) + m(x - x_0)^3 + y_0 \qquad (2)$$

where *t* describes corneal tilt and *m* describes coma. The mathematical formulation is analogous to the primary Seidel aberrations (Atchison & Smith, 2000). For each of the 6 meridians, equation (2) was fitted to a 7.5 mm corneal zone as in Dubbelman et al. (2006). The 3D corneal profile is reconstructed by applying the following fit-functions to the measured values of the shape parameters from all 6 meridians:

$$r(\theta) = r_1 + \Delta r \cos^2(\theta - \alpha) \qquad (3)$$

$$k(\theta) = k_1 + \Delta k \cos^2(\theta - \beta) \qquad (4)$$

$$m(\theta) = m_1 + \Delta m \cos(\theta - \gamma) \qquad (5)$$

where α, β and γ are the angles of the meridian where the r, k and m are maximal. For the 3D modelling of the corneal surfaces, the measured tilt *t* of the

corneal shape appeared to have no influence on the coma aberration, and was therefore not taken into account.

After the 3D model of the anterior and posterior surface of the cornea had been reconstructed, meridian ray tracing was applied in order to find the coma aberration of the anterior and whole cornea. This procedure has been explained in detail in a previous article (Sicam, Dubbelman & Van der Heijde, 2006). Figure 1 illustrates the ray-tracing procedure for one ray. Firstly, a back focal point for the whole cornea (Fc) must be determined. This point was found by regarding the cornea as a single refractive surface with the radius of the anterior surface and an effective refractive index of approximately 1.329, which takes into account the influence of the posterior surface. This effective refractive index was calculated for each subject using the corneal thickness (t) and the anterior and posterior corneal radius (Bennet & Rabbets, 1998; Dubbelman et al., 2006). Because the corneal surface is not rotationally symmetric, Fc was calculated by taking the average for the 6 meridians. From the corneal focal point (Fc), for each meridian a bundle of 200 rays are traced to the posterior surface. From the intersection point on the posterior surface (x_p,y_p), the rays are traced to the anterior surface (x_a, y_a). This is done by using a second reference point F_A (the focal point of the anterior corneal surface) to guide the direction of the ray from the posterior surface to the anterior surface. Finally, the ray is traced from the anterior surface to the corneal apex plane. The corneal wave aberration is then defined as the difference in

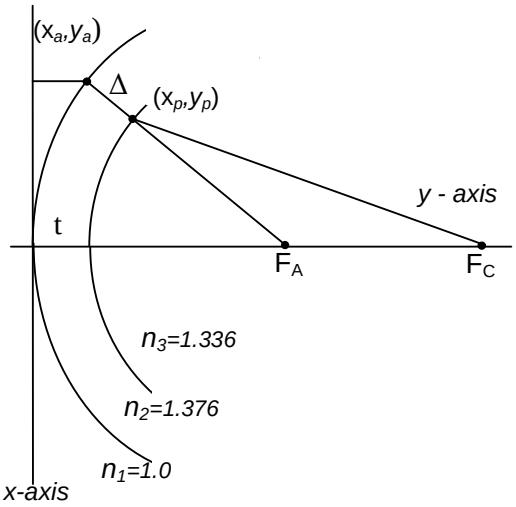

Figure 1 Ray-tracing procedure to determine the coma aberration of the cornea

optical path length of the traced rays, compared to the path along the principal ray, which is along the optical axis (Guirao & Artal, 2000).

The corneal wave aberration values are then fitted to a set of Zernike polynomials. The 3rd order coma aberration is indicated by Zernike coefficients Z_3^1(vertical coma) and Z_3^{-1}(horizontal coma) for this wave aberration (Thibos, Applegate, Schwiegerling & Webb 2002). In our study the corneal wave aberration was calculated for a 6.0 mm pupil size. Applying standard ray tracing principles (Guirao & Artal, 2000) to the shape of the anterior surface alone makes it possible to calculate the coma wave aberration of the anterior surface. Subtracting this aberration from that of the whole cornea (anterior and posterior) makes it possible to determine the contribution of the posterior corneal surface.

6.3 RESULTS

6.3.1 Coma and corneal shape

Figure 2 shows an example of the coma coefficient *m* of equation (2) of the anterior and posterior corneal surface as a function of meridian. The meridional variation of *m* of both corneal surfaces could be well fitted using the cosine function (5). The average r^2 was 0.66 and 0.61 for the anterior and posterior corneal surface, respectively. The m_1 of equation (5) is a DC offset term, and should be zero per definition due to the periodicity of the coma. It appeared that the average m_1 was around zero (-0.0001) for both the anterior and posterior surface, and did not differ significantly from zero for any individual subject. Because the goodness of fit varied among subjects, weighted linear regression was performed and the weighted mean, weighted standard deviation (sd) and weighted standard error of the mean (SEM) are presented (Bevington, 1969). The weight chosen was the inverse square of the error. Figure 3 shows the age-dependency of the meridional variation of *m* (Δm) of the anterior and posterior corneal surface. For clarity, the data are also grouped in 4 bins (±SEM) of equal age ranging between 18 and 65 years, which shows the trend more clearly. The

error bar is the weighted SEM of the average value of the subjects that fall within the bin width (11.8 years). The weighted linear regression was applied to the data of all subjects, but fitting only the data of the 4 bins did not produce significantly different results. The Δm of both the anterior and the posterior corneal surface changes significantly with age ($p<0.00001$), but in the opposite direction. The Δm of the anterior surface increases, while that of the posterior surface decreases with age. Figure 4 shows the ratio of the Δm of the posterior

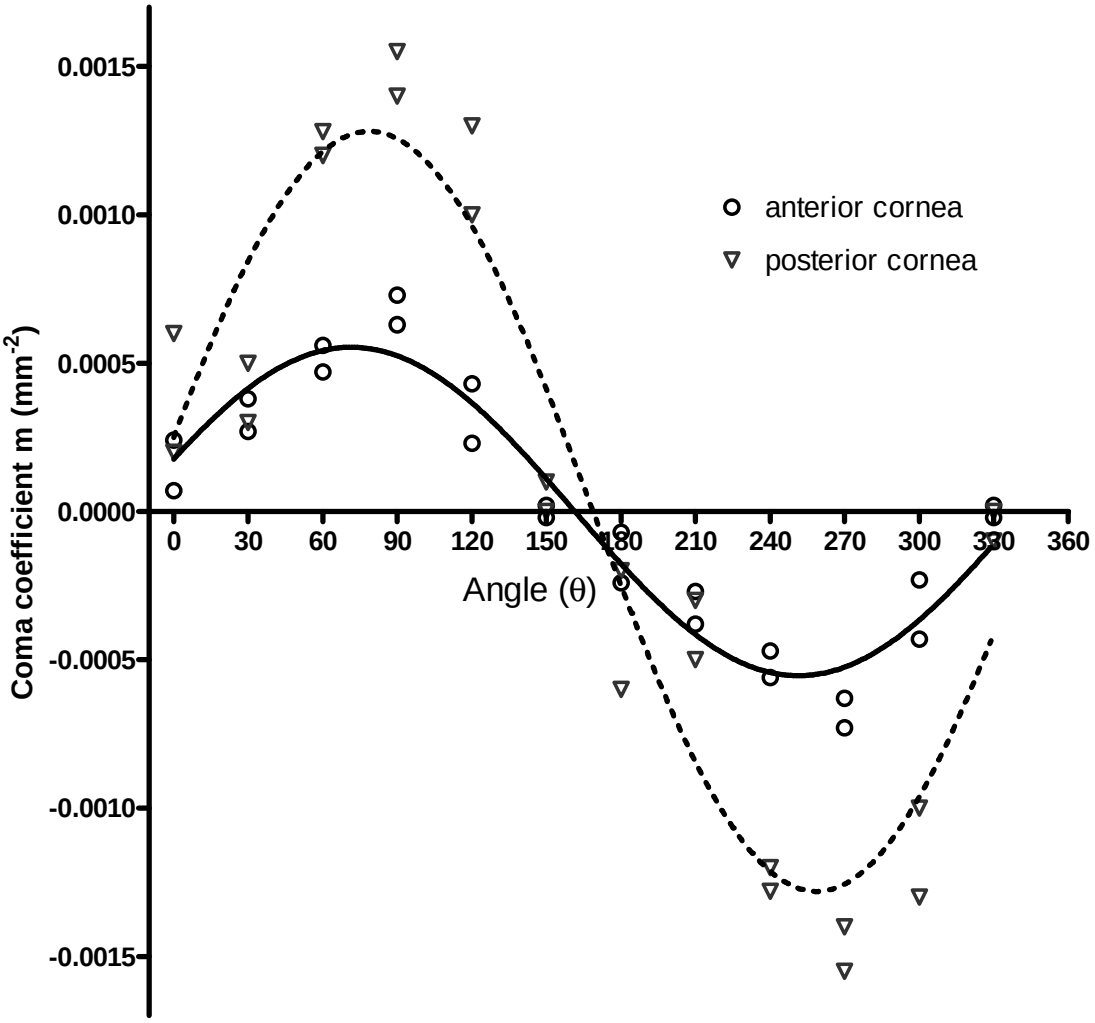

Figure 2 Typical example for a 44-year-old male of the coma of the anterior and posterior corneal surface as a function of meridian. The solid line represent equation (5) fitted through the 12 data-points of the anterior surface: $m= -1 (\pm 0.8) \times 10^{-4} + 7 (\pm 1) \times 10^{-4} * \cos(\theta-72(\pm 3.6))$, $r^2= 0.82$. The line of dashes was fitted to the data of the posterior surface: $m= -2 (\pm 2) \times 10^{-4} + 15 (\pm 3) \times 10^{-4} * \cos(\theta-78(\pm 5))$, $r^2= 0.73$. To illustrate the periodicity of function (5), the data-points after 150º have also been plotted, although they were not included in the fit.

corneal and the Δm of the anterior corneal surface, which significantly changes with age. At the age of 20, the Δm of the posterior corneal surface is almost twice that of the anterior surface, but with age the difference becomes smaller.

There was a small, but significant difference ($p<0.001$) between the axes of

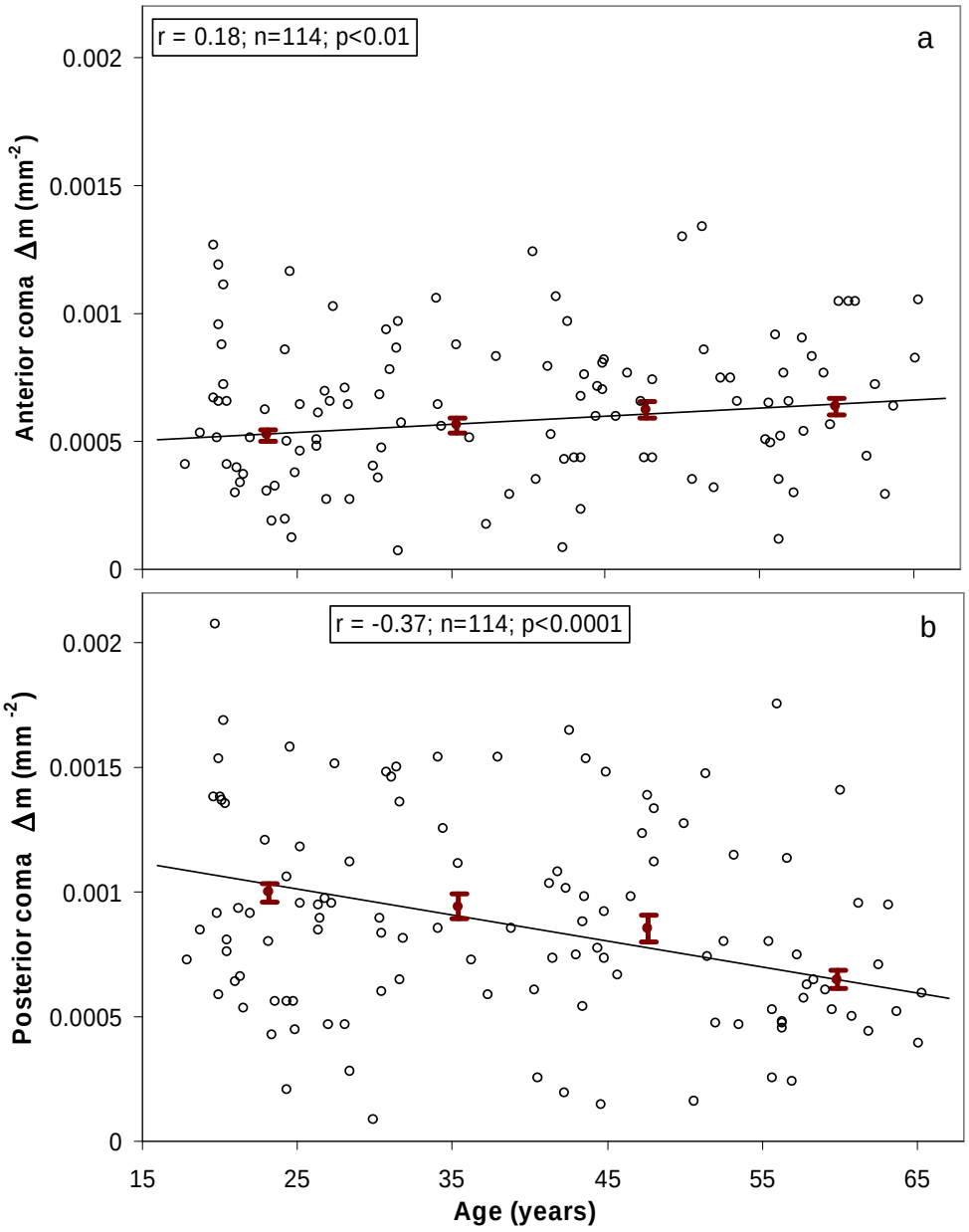

*Figure 3 The meridional variation of the m (Δm) of the anterior and posterior corneal surface as a function of age. The weighted linear regression showed for both surfaces a significant age-dependence. (a) Anterior surface: Δm= 4.5 (± 0.4) x 10^{-4} + 3.2 (±1.0) x 10^{-6} * Age; n=114; r=0.18; p<0.01. (b) Posterior surface: Δm= 1.3 (± 0.6) x 10^{-3} - 1.05 (±0.1) x 10^{-5} * Age; n=114; r= -0.37; p<0.00001. The error bars represent ± SEM for each age-group.*

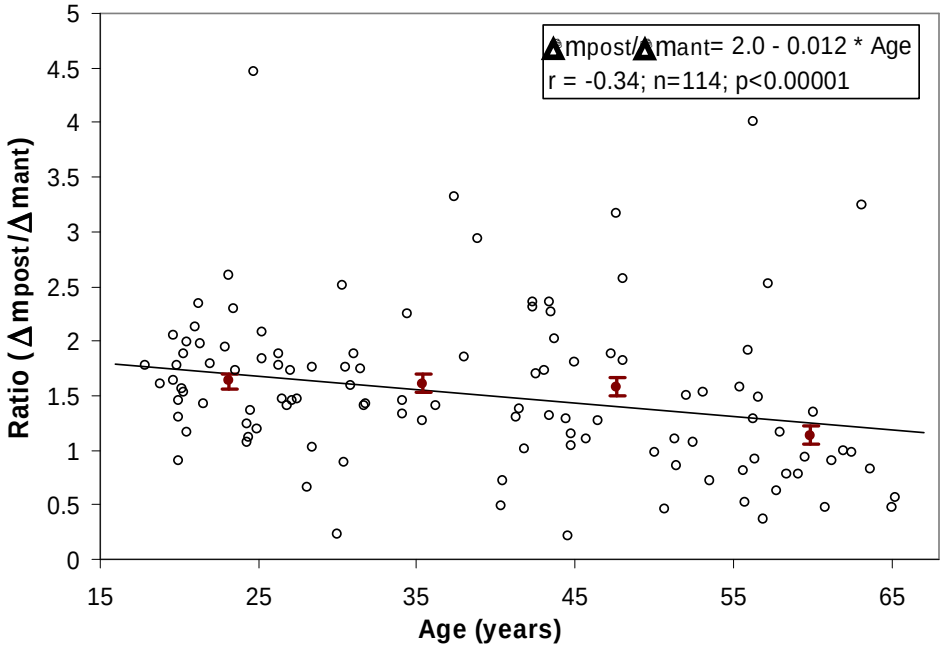

*Figure 4 Ratio of the coma (Δm) of the posterior corneal and that of the anterior corneal surface as a function of age. Weighted linear regression showed a significant age-dependence: Δmpost/ Δmant = 2.0 (±0.1) - 0.012 (±0.003) * Age; n=114; r= -0.34; p<0.00001.*

the coma of the two surfaces. The average axis γ (± sd) was 54 ± 21º for the anterior surface, while it was 64.5 ± 21º for the posterior surface. The mean of the paired difference in axis ± sd was 13º ± 16º, which makes it clear that the coma axes of the two surfaces are almost equal.

6.3.2 Coma aberration

Figure 5a shows the coma aberration of the anterior surface of the cornea alone as a function of age. There was a significant change with age ($p<0.01$). Figure 5b shows the age-dependency of the coma aberration of the whole cornea, i.e. both the anterior and posterior corneal surface. The difference between the aberration of the anterior cornea and the whole cornea is hardly visible, which indicates the limited effect of the posterior cornea on the coma aberration. Figure 6 shows the ratio between the coma of the whole cornea and that of the anterior surface as a function of age. A ratio smaller than 1 indicates that the posterior surface reduces the coma aberration of the anterior surface, a value of

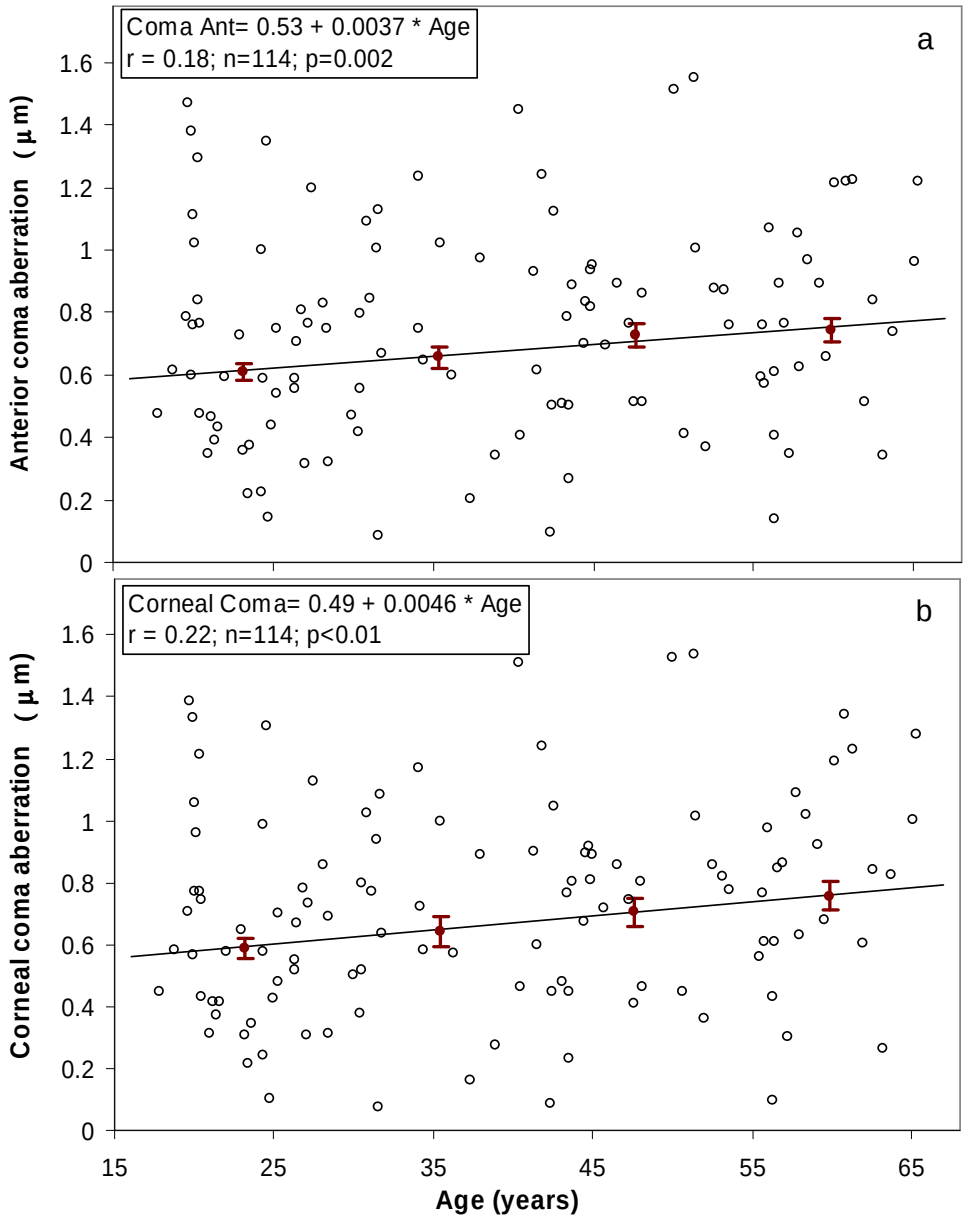

*Figure 5 Coma aberration of the anterior corneal surface (a) and the whole cornea (b) as a function of age. The weighted linear regression showed for both surfaces a significant change with age. (a) Anterior coma aberration= 0.53 (± 0.05) + 0.0037 (±0.001) * Age; n=114; r= 0.18; p<0.01. (b) Corneal coma aberration= 0.49 (± 0.06) + 0.0046 (±0.0015) * Age; n=114; r= 0.22; p<0.01.*

1 indicates no change, and a value above 1 indicates that the posterior surface increases the coma of the anterior corneal surface. It can be seen that the compensation of the posterior corneal surface is small (average compensation±sd is 3 ±3.5 %). Furthermore, because of the propagation of the uncertainties, the error in the ratio becomes large, and no significant change with age can be determined. Nevertheless, a trend can be seen. In young subjects the

posterior surface compensates approximately 6% of the coma of the anterior surface, but this compensation disappears completely with aging.

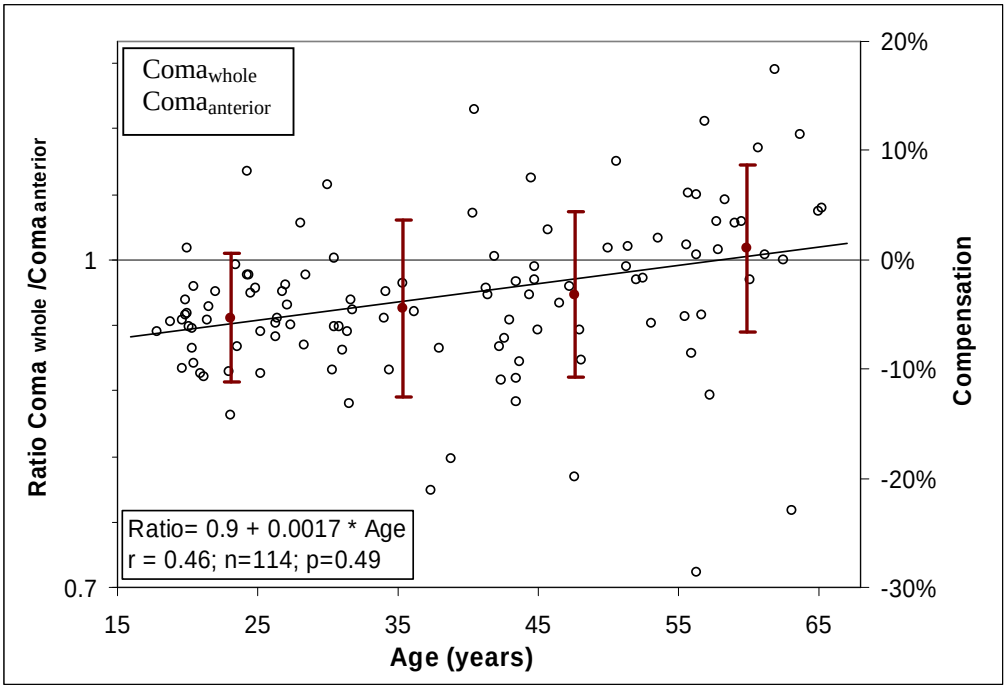

*Figure 6 Ratio of the coma aberration of the whole cornea and that of the anterior cornea as a function of age. The linear regression was not significant = 0.9 (± 0.1) + 0.0017 (±0.002) * Age; n=114; r= 0.46; p=0.49. The secondary right axis shows the percentage that the posterior surface compensates the coma aberration of the anterior surface ($Coma_{whole}/Coma_{anterior} - 1$).*

6.4 DISCUSSION

The aim of the study was to measure the relative contribution of the posterior corneal surface to the coma aberration of the cornea as a function of age. The refractive power of the whole cornea is due to the variation in the refractive indices of air (1.0), cornea (1.376) and the aqueous (1.336) (Atchison & Smith 2000). Because the difference in the indices of refraction at the anterior interface is 10 times greater than that at the posterior interface, it could be expected that the contribution of the posterior surface to the corneal aberration is small. However, from Dubbelman et al. (2006) and Sicam et al. (2006), it appeared that

the posterior surface does make a considerable contribution to the astigmatism and spherical aberration of the whole cornea. Nevertheless, the results of the present study show that this does not hold true for the coma aberration. Firstly, the shape of both corneal surfaces was measured, and it was found that the meridional variation of the coma coefficient (Δm) of both the anterior and posterior surface changes significantly with age. At the age of 20 the Δm is almost twice the size of that of the anterior surface, whereas it becomes almost equal to that of the anterior surface at the age of 65. Subsequently, the results concerning the shape of the corneal surfaces were used to calculate the coma aberration, and it was found that the contribution of the posterior surface was almost negligible. At the age of 20, the posterior surface compensates approximately 6% of the coma of the anterior surface, but this compensation decreases with age and is no longer present at the age of 60. This means that the dynamics of the refraction are different for coma aberration, compared to astigmatism and spherical aberration. Calculations show that when the Δm is almost the same for both the anterior and posterior surface, the posterior corneal surface does not contribute to the coma aberration of the whole cornea. This can be explained by the fact that after refraction of the anterior corneal surface, the coma component of the wave-front that approaches the posterior corneal surface has the same form as the coma shape feature of the posterior surface. As a result, there will be no change in the coma aberration at the posterior corneal surface. This is particularly true for older subjects: at the age of 60 the Δm of the posterior surface is equal to that of the anterior surface, which therefore results in minimal compensation of the corneal coma aberration by the posterior surface. This makes it clear that the contribution of the coma aberration of the posterior corneal surface is thus almost negligible, and that the coma aberration that remains when the coma aberration of the anterior corneal surface has been subtracted from that of the whole eye is due to the crystalline lens. For the

design of an intraocular lens that is able to correct for coma aberration, it is therefore sufficient to take only the anterior corneal surface into account.

The compensatory role of the posterior corneal surface has not yet been measured, but the coma aberration of the anterior corneal surface has been measured in previous studies, which allows comparison with the present study. The age-dependent increase in the coma aberration of the anterior surface is in agreement with the findings of Guirao, Redondo & Artal (2000), Oshika, Klyce, Applegate & Howland (1999), Wang, Dai, Koch, Nathoo (2003), Amano et.al (2004). Only Fujikado et al., 2004 found no significant increase in the corneal coma aberration with age, but this might be explained by the smaller size of their study population and the fact that they also included very young subjects (aged 4-9 years). We found a high inter-subject variability in the coma aberration of the anterior surface. This is also in agreement with the results of the studies mentioned above, which indicate that the coma aberration differs considerably between subjects, and that large groups are needed to determine age-related trends. In the present study, the anterior coma aberration was determined for a 6.0 mm pupil and an increase of 0.15 μm was found between 25 and 65 years of age. For the same pupil size and age-interval, Amano et al. (2004) and Wang, Dai, Koch, Nathoo (2003) found an increase of 0.12 μm and 0.09 μm, respectively, which does not differ significantly from our results. There was, however, a significant difference in the absolute value of the anterior coma aberration. For a pupil of 6 mm zone, the value for the coma aberration found in the present study was approximately twice the value found by Amano et al. (2004) and Wang et al (2003), who used a cornea topographer to measure the shape of the anterior corneal surface. However, the reason for this difference is not clear, and because the trend with age is similar, the difference in absolute value could indicate a systematic error in one or both methods. The results of the Scheimpflug imaging and corneatopography agreed well for the radius and asphericity of the anterior corneal surface (Dubbelman et al. 2006). This also

holds true for the absolute value of the spherical aberration (Sicam et al. 2006). In the present study, the shape of the 7.5 mm zone of the cornea was measured, and the aberrations were subsequently calculated for the 6 mm zone. It could be that Placido-based videokeratographs have a problem to capture data from the periphery of the cornea accurately (Oshika et al. 1999; Tripoli et al. 1996). It could also be that this error increases because the coma aberration is due to a non-rotation-symmetric feature of the corneal shape (Sicam & Van der Heijde, 2006). Furthermore, it must be noted that in the present study, Scheimpflug images were not made along the line of sight, but along the optical axis. On average, the fixation target was horizontally displaced 4.5° nasally from the slitbeam and vertically displaced 2° upwards (Dubbelman et al. 2006). Calculations have made it clear that this does not result in any significant change in radius or asphericity of either of the corneal surfaces. A calculation to determine the influence on the coma aberration is not straightforward, because the coma shape feature is non-rotational. It could be that this influences the absolute value of the coma aberration. Nevertheless, it will not change the ratio between the coma shape feature of the anterior and posterior corneal surface, the measurement of which was the primary aim of the present study.

ACKNOWLEDGMENTS:

Supported by the SenterNovem grant “Young eyes for elderly people” (ISO 43081) and Advanced Medical Optics (AMO Groningen B.V.)

REFERENCES

Amano S, Amano Y, Yamagami S, Miyai T, Miyata K, Samejima T, Oshika T (2004). Age-related changes in corneal and ocular higher-order wavefront aberrations. *American Journal of Ophthalmology* 137, 988-92.

Atchison, D.A., & Smith, G. (2000). *Optics of the human eye*. (pp.9, 12, 34-35, 166-167, 246-247). Oxford: Butterworth-Heinemann.

Barbero, S., Marcos, S., & Merayo-Lloves, J. (2002). Corneal and total optical aberrations in a unilateral aphakic patient. *Journal of Cataract & Refractive Surgery*, 28, 1595-1600.

Bevington, P.R. (1969). *Data reduction and error analysis for the physical sciences*. New York: McGraw-Hill, pp.77-80.

Dubbelman, M., Weeber, H.A., Van der Heijde, G.L., & Völker-Dieben, H.J. (2002). Radius and ashpericity of the posterior corneal surface determined by corrected Scheimpflug photography. *Acta Ophthalmologica*, 80, 379-383.

Dubbelman, M., Sicam, V.A., & Van der Heijde, G.L. (2006). The shape of the anterior and posterior surface of the aging human cornea. *Vision Research*. 46, 993-1001.

Fujikado T, Kuroda T, Ninomiya S, Maeda N, Tano Y, Oshika T, Hirohara Y, Mihashi T (2004). Age-related changes in ocular and corneal aberrations. *American Journal of Ophthalmology* 138,143-146.

He, J.C., Gwiazda, J., Thorn, F., Held, R. (2003). Wave-front aberrations in the anterior corneal surface and the whole eye. *Journal of the Optical Society of America A: Optics, Image Science and Vision*. 20, 1155-1163.

Guirao, A., & Artal, P. (2000). Corneal wave aberration from videokeratography: accuracy and limitations of the procedure. *Journal of the Optical Society of America A: Optics, Image Science and Vision*. 17, 955-965.

Guirao, A., Redondo, M., & Artal, P. (2000). Optical aberrations of the human cornea as a function of age. *Journal of the Optical Society of America A: Optics, Image Science and Vision*. 17, 1697-1702.

Marcos, S., Barbero, S., Llorente, L., Dorronsoro, C., Rosales, P., & Jiménez-Alfaro, I. (2003). Optical aberrations with aspheric intraocular lenses. *Journal of Vision*, 3, 39a.

Olsen, T. (1986). On the calculation of power from curvature of the cornea. *British Journal of Ophthalmology*. 70, 152-154.

Oshika, T., Klyce, S.D., Applegate, R.A., & Howland, H.C. (1999). Changes in corneal wavefront aberrations with aging. *Investigative Ophthalmology and Visual Science*. 40, 1351-1355.

Padmanabhan, P., Rao, S.K., Jayasree, R., Chowdhry, M., & Roy, J. (2006). Monochromatic aberrations in eyes with different intraocular lens optic designs. *Journal of Refractive Surgery*, 22. 172-177.

Ridley, H. (1952). Intra-ocular acrylic lenses after cataract extraction. *The Lancet*, 1, 118-29. Reproduced (2003) by *Bulletin of the World Health Organization*, 81, 758-761.

Shimizu, K., Misawa, A., & Suzuki, Y. (1994). Toric intraocular lenses: Correcting astigmatism while controlling axis shift. *Journal of Cataract and Refractive Surgery* 20, 523-526.

Sicam, V.A., Dubbelman, M., & Van der Heijde, R.G.L. (2006). Spherical aberration of the anterior and posterior surfaces of the human cornea. *Journal of the Optical Society of America A: Optics, Image Science and Vision*. 23, 544-549.

Sicam, V.A., & Van der Heijde, R.G.L. (2006). Topographer reconstruction of the non-rotation-symmetric anterior corneal surface features. (submitted).

Smith, G., Cox, M.J., Calver, R., & Garner, L.F. (2001). The spherical aberration of the crystalline lens of the human eye. *Vision Research* 41, 235-243.

Tabernero, J., Piers, P., & Artal, P. (2006). An intraocular lens correcting corneal coma. *Program Summary Book 2006 ARVO annual meeting*, P# 1503.

Thibos, L.N., Applegate, R.A., Schwiegerling, J.T., & Webb, R. (2002). Standards for reporting the optical aberrations of eyes. *Journal of Refractive Surgery*. 18, S652-S660.

Tripoli NK, Cohen KL, Obla P, Coggins JM, Holmgren DE. Height measurement of astigmatic test surfaces by a keratoscope that uses plane geometry surface reconstruction. Am J Ophthalmol. 1996 Jun;121(6):668-76.

Wang L, Dai E, Koch DD, Nathoo A. Optical aberrations of the human anterior cornea (2003). *Journal of Cataract and Refractive Surgery* 29, 1514-21.

7

SUMMARY AND DISCUSSION

7 SUMMARY AND DISCUSSION

Specifying the wave aberration of the eye is an important aspect in finding solutions to improve human vision. The classical approach is limited to correction of two basic refractive errors: defocus and astigmatism. These refractive errors, also known as lower order aberrations, can easily be corrected by spectacles and contact lenses. Nevertheless, higher order aberrations also play a role. Recent developments in corneal refractive surgery and intraocular lens (IOL) implantation show that spherical aberration and coma aberration are also important. Some studies have shown that mesopic vision is improved by placing an aspheric IOL that eliminates the spherical aberration of the eye. It is also known that coma aberration is induced by decentration of IOL's and thus reducing the quality of vision. Therefore, it is beneficial in these applications that pre-operation corneal measurements give the correct aberrations.

The technology for determining corneal aberrations needs development for at least two reasons. These involve measurements on both the anterior and posterior corneal surface. In ophthalmic practice, the aberration of the anterior surface is usually measured using Placido ring topographers. In these instruments, skew ray reflections are neglected in reconstructing the corneal shape. As a consequence, the non-rotation symmetric shape features of the anterior corneal surface are measured inaccurately. The instrument developed at the Vrije Universiteit (the VU topographer) was designed using a colored pattern instead of rings as stimulus for reflection. Thus, a one-to-one correspondence between source points and the captured reflected image points can be established. In principle, because of this property the skew ray error is eliminated. However, prior to this study, no experimental proof of this has been demonstrated. Thus, it is one of the objectives of this study to demonstrate by actual experiments that the VU topographer improves the accuracy of reconstructing the anterior corneal surface. Another important consideration

regarding corneal aberration is the contribution of the posterior surface. Little is known about this. Consequently, a second objective of this study was to determine the contribution of the posterior surface to corneal wave aberration. Both objectives will bring more certainty in determining the total corneal aberration.

To address the first objective, a surface reconstruction algorithm was developed for the VU topographer. This surface reconstruction algorithm uses Zernike polynomials to model the corneal shape. An advantage of using Zernike polynomials is that the individual components such as astigmatism, coma aberration and spherical aberration are used in ophthalmic practice. Also shape parameters such as radius of curvature and asphericity can be derived directly from the Zernike coefficients. The developed algorithm has sub-micrometer accuracy in determining corneal height. Thus this algorithm is suitable for use in numerical simulations as well as in processing experimental data. Results of measurements on various surfaces and sample eyes reveal that the VU topographer is superior in recovering the shape of the anterior corneal surface particularly the non-rotation symmetric features. It was demonstrated that because of skew ray ambiguity ring topographers give under-estimated value for the astigmatic power. The underestimation observed is small for regular toric surfaces (about 4%: 0.25 D for a surface with 6.25 astigmatic power), but the results of this study suggest that the error increases with the degree of complexity of the surface. The under-estimation of the astigmatic power was measured to be 13% for an eye that had undergone radial keratotomy. The under-estimation was also observed for other non-rotation symmetric surface features. On the other hand, the VU topographer is able to give the correct astigmatism and the correct non-rotation surface feature of the anterior corneal surface.

To address the second objective of the study measurements using Scheimpflug photography were employed. By combining different meridian

measurements, the 3D surface properties of the posterior surface can be reconstructed. This shape information was used to determine the contribution of the posterior surface to the total corneal aberration. The results show that on average the total corneal astigmatism is lower than the anterior surface by 31% due to the contribution of the posterior surface. Also the posterior corneal surface contributes to the total corneal spherical aberration. This contribution increases with age. The addition to the corneal spherical aberration is 15% at age 65. In order to specify the correct corneal astigmatism and corneal spherical aberration the contribution of the posterior surface must be measured. On the other hand, the contribution of the posterior surface to corneal coma aberration is negligible. This means that accurate measurement of the coma aberration of the anterior surface will be sufficient to provide information for the total corneal coma aberration.

Apart from achieving the objectives of the study, there are some insights gained in the process. The measurement technique employed for the VU topographer also has the advantage that it is a non-invasive technique to measure the anterior corneal surface. This has at least four implications. First, in the clinical set-up a non-invasive procedure is convenient for patients. Second, being a non-invasive procedure, the surface measurements would reveal the actual state of the cornea in contrast with invasive techniques such as those that use fluorescein solvents. Adding solvents to the eye would produce additional uncertainty in reconstructing the actual surface shape. Third, with modifications in some aspects of the apparatus, this technique could also be extended beyond ophthalmology to industrial applications such as surface diagnostics. Surfaces to be measured could be mirrors, lenses and other basic components of optical devices. Fourth, the technique uses only one camera to recover the 3D shape properties of the cornea. Thus, the process is straightforward and simple as opposed to procedures that use multi-camera systems. It is anticipated that these

multi-camera systems would require more complex mathematical algorithms to arrive at the same accuracy in reconstructing the 3D shape features of objects.

The results from this thesis are helpful in finding ways to measure *in vivo* the gradient refractive index profile of the lens. This information could prove useful in studies on presbyopia and also investigations involving the chromatic aberration of the eye. Because the human lens is an internal component of the eye, direct measurements are not possible. An indirect way of approaching this predicament is to combine information from wave-front aberration measurements for the whole eye and combine it with corresponding information for the corneal contribution. Applying tomography principles, algorithms can be developed to calculate the refractive index profile of the lens from in vivo measurements. The needed information for the corneal contribution will be provided for by the VU topographer and Scheimpflug photography. This is an interesting research activity for the future.

NEDERLANDSE SAMENVATTING

Optische eigenschappen van het hoornvlies van de mens

Het vastleggen van de golfaberraties van het oog is een belangrijk aspect bij het vinden van oplossingen om het menselijke zien te verbeteren. De klassieke aanpak is veelal beperkt tot de correctie van twee basis refractiefouten: onscherpte en astigmatisme. Deze refractiefouten, bekend als lagere orde aberraties, kunnen goed gecorrigeerd worden door een bril of een contactlens. Desalniettemin spelen hogere orde aberraties ook een rol. Recente ontwikkelingen in refractieve corneachirurgie en intra-oculaire (IOL) lens implantaties laten zien dat sferische aberratie en coma aberratie ook erg belangrijk zijn. Sommige studies hebben aangetoond dat het mesopisch zien (zien in schemering) verbeterd wordt door het plaatsen van een a-sferische intra-oculaire lens. Deze lens minimaliseert de sferische aberratie van het oog. Verder is bekend dat coma aberratie geïnduceerd kan worden door een decentratie van de (intra-oculaire) lens. Hierdoor wordt de kwaliteit van het zien sterk gereduceerd. Daarom is het wenselijk voor de operatie cornea aberraties te bepalen.

De technologie voor het vastleggen van cornea aberraties moet tenminste op twee punten verbeterd worden. Dit houdt in dat er metingen van zowel het voorste als het achterste oppervlak van de cornea gedaan zullen moeten worden. In de praktijk wordt de aberratie van het voorste oppervlak normaal gesproken gemeten door gebruik te maken van Placido ringtopografen. Bij deze

ringtopografen worden de scheef invallende (zogenaamde ‘skew ray’) reflecties genegeerd bij de reconstructie van de vorm van de cornea. Dit heeft tot gevolg dat de niet-rotatie symmetrische vormeigenschappen van het voorste corneale oppervlak niet nauwkeurig gemeten worden.

Op de Vrije Universiteit is een instrument ontwikkeld, de VU topograaf, die gebruik maakt van een kleurenpatroon als stimulus voor reflectie in plaats van een ringenpatroon. Hierdoor is het mogelijk om een 1 op 1 overeenkomst tussen stimuluspunten en gereflecteerde beeldpunten te verkrijgen. De “skew ray error” kan door deze eigenschap worden geëlimineerd. Voorafgaand aan deze studie is dit echter niet experimenteel aangetoond. Een van de doelen van deze studie is om met behulp van experimenten aan te tonen dat met behulp van de VU topograaf de nauwkeurigheid van de reconstructie van het voorste corneale oppervlak kan worden verbeterd. Een andere belangrijke overweging met betrekking tot de cornea aberraties is de bijdrage van het achterste oppervlak. Over deze bijdrage is weinig bekend. Het tweede doel van deze studie is derhalve om de bijdrage van dit oppervlak aan de corneale golfaberraties vast te stellen. Beide doelen zullen meer zekerheid geven over het vaststellen van de totale cornea aberratie.

Om het eerste doel te bereiken is een oppervlak reconstructie algoritme ontwikkeld voor de VU topograaf. Dit oppervlak reconstructie algoritme maakt gebruik van Zernike polynomen om de vorm van de cornea te modelleren. Het gebruik van Zernike polynomen heeft als voordeel dat de individuele componenten zoals astigmatisme, coma aberratie en sferische aberratie gebruikt worden in de oogheelkunde. Ook kunnen direct uit de Zernike coëfficiënten vormparameters zoals straal en a-sfericiteit afgeleid worden. Het ontwikkelde algoritme heeft een sub-micrometer nauwkeurigheid bij het vaststellen van de hoogte van de cornea. Dit maakt het algoritme geschikt voor zowel het gebruik in numerieke simulaties als ook bij het verwerken van experimentele data. Resultaten van metingen aan diverse oppervlakken en humane ogen laten zien

dat de VU topograaf superieur is bij het reconstrueren van het voorste oppervlak van de cornea, met name de niet-rotatie symmetrische kenmerken. Het is in de literatuur aangetoond dat ten gevolge van de skew ray ambiguiteit de ringtopografen een onderschatting geven van de astigmatische power. Deze waargenomen onderschatting is klein voor reguliere torische oppervlakken (circa 4% ≡ 0.25 D voor een oppervlak met een astigmatische power van 6.25D), maar de resulaten van deze studie suggereren dat de fout toeneemt met de mate van complexiteit van het oppervlak. De onderschatting van astigmatische power is 13% voor een oog na een radiële keratotomie. Deze zelfde onderschatting is ook waargenomen bij andere niet-rotatie symmetrische oppervlakte eigenschappen. De VU topograaf is daarentegen in staat om het juiste astigmatisme en de juiste niet-rotatie symmetrische eigenschappen van het voorste oppervlak van de cornea weer te geven.

Voor het tweede doel van deze studie zijn metingen gedaan door middel van Scheimpflug fotografie. 3D oppervlak eigenschappen van het achterste oppervlak kunnen gereconstrueerd worden door het combineren van metingen in verschillende meridionale richtingen. Deze informatie over de vorm is gebruikt om de bijdrage van het achterste oppervlak aan de totale aberratie van de cornea vast te stellen. De resultaten laten zien dat het totale astigmatisme van de cornea gemiddeld 31% lager is dan van het voorste oppervlak ten gevolge van de bijdrage van het achterste oppervlak. Verder draagt het posterieure oppervlak van de cornea bij aan de totale sferische aberratie van de cornea. Deze bijdrage neemt toe met de leeftijd. De toename in sferische aberratie van de cornea is ongeveer gelijk aan 15% van die van een 65-jarige. De bijdrage van het achterste oppervlak moet gemeten worden om het correcte astigmatisme en de sferische aberratie van de cornea te kunnen specificeren. De bijdrage van het posterieure oppervlak aan de coma aberratie van de cornea is daarentegen verwaarloosbaar. Dit houdt in dat nauwkeurige metingen van de coma aberratie

aan het voorste oppervlak voldoende informatie geven over de totale coma aberratie van de cornea.

Naast het bereiken van de doelen van deze studie is er ook dieper inzicht verkregen in het proces van oppervlakte reconstrueren. De meettechniek gebruikt in de VU topograaf heeft mede als voordeel dat het een niet-invasieve techniek is om het voorste oppervlak van de cornea te bepalen. Dit heeft tenminste 4 implicaties. Ten eerste is het toepassen van een niet-invasieve procedure in een klinische set-up gunstig voor patiënten. Ten tweede, omdat het een niet-invasieve procedure is, zullen de metingen van het oppervlak de actuele staat van de cornea weergeven. Dit in tegenstelling tot invasieve technieken die bijvoorbeeld gebruik maken van fluorescine oplossingen. Toevoeging van oplossingen aan het oog zullen bij de reconstructie van de vorm van het actuele oppervlak additionele onzekerheid met zich meebrengen. Ten derde zou, bij modificaties van sommige aspecten van het apparaat, deze techniek naast de oogheelkunde toegepast kunnen worden in de industrie zoals bijvoorbeeld bij oppervlakte metingen. Voorbeelden van mogelijk oppervlakken zijn spiegels, lenzen en andere basis componenten van optische apparaten. Ten vierde, de techniek maakt gebruik van één camera om de 3D vormeigenschappen van de cornea vast te stellen. Dit houdt in dat het proces duidelijk en simpel is, in tegenstelling tot methodes die gebruik maken van multi-camera systemen, die complexere mathematische algoritmes nodig zullen hebben om tot dezelfde nauwkeurigheid bij de reconstructie van 3D vorm eigenschappen van een object te kunnen komen.

De resultaten van deze studie zijn nuttig bij vinden van manieren om *in vivo* het gradient refractie index profiel van de lens te meten. Deze informatie zou nuttig kunnen zijn bij studies naar presbyopie (veroudering van de ooglens) en bij onderzoeken waarbij de chromatische aberratie van het oog een rol speelt. Directe metingen aan de lens zijn niet mogelijk, omdat de humane lens een intern deel van het oog is. Een indirecte manier om dit te benaderen is door

informatie van de golffront aberratie metingen van het hele oog te combineren met overeenkomstige informatie van de cornea. Door tomografische technieken toe te passen, kunnen algoritmes worden ontwikkeld om het refractie index profiel van de lens te berekenen uit in vivo metingen. De benodigde informatie voor de corneale bijdrage zal door de VU topograaf en Scheimpflug fotografie verschaft worden. Dit is een uitdagend onderzoek voor de toekomst.

WORD OF THANKS

This project would not have been possible without the contribution of many people. I would like to express gratitude by way of narrating my journey to complete my PhD studies.

The period prior to my PhD studies was an exciting time at the Department of Physics, University of San Carlos (USC), Talamban, Cebu City, Philippines. Two ongoing projects sponsored by the Netherlands organization for International Cooperation in Higher Education (NUFFIC) provided the impetus for this excitement at the USC: the Physics Development Project (PDP:1999-2004) and Science Teacher Education Project (STEPS: 1995-2004). The teamwork for the project was very good mainly because of the contribution of key persons: 1) Helena delos Reyes – chairperson of the USC Physics Department. She is a very dynamic leader and thinks of the welfare of her constituents. I am grateful for her efforts to support me in my career, during difficult times she was there to find ways to help. 2) PDP Dutch consultants:
i) Gerrit Kuik, along with his wife Mae Ann, created a family atmosphere in the Physics Department. ii) Ben Zuidberg was very relatable and has a good sense of humour iii) Kees Karremans was very helpful especially in helping the junior faculty develop their skills in experimental physics. 3) STEPS - Ed and Daday Van den Berg, both very good physics educators. From them, I learned a lot of teaching skills.

I thank Gerard Thijs and Rob Merkus for overseeing the PDP. Along with STEPS, the PDP created a conducive atmosphere that made us dream big about our careers. I remember seven years ago, Rommel Bacabac and I express our aspirations of pursuing higher studies in Physics. It is so amazing to experience the realization of our dreams, Rommel finished his studies almost a year ago. To

date, some of our colleagues are now here in Holland pursuing their own PhD studies: Edcel Salumbides, Renante and Marites Violanda. The times spent with them make our stay here in the Netherlands more pleasant, a second family away from home.

Through PDP, I was introduced to Professor Rob Heethaar., which led to the organization of this PhD project . The project was organized as a collaborative effort between two laboratories: The Physics Research in Ophthalmology (PRO) group at the Department of Physics and Medical Technology (FMT) of the VU University Medical Center (VUMC) and the Physics group of the Netherlands Ophthalmic Research Institute (IOI). It was at the IOI where I spent the first two years of my study. I learned the basics of wavefront analysis, especially the use of Zernike polynomials. I enjoyed the group discussions with Tom Van den Berg, Luuk Franssen, Gerard de Wit, Linda Müller, Liesbeth Pels and Joris Coppens, from whom I learned programming skills in MATLAB. It was also nice to have interacted with Spanish visiting researchers both at the IOI and VUMC: Juan Tabernero, Guillermo Perez and Patricia Rosales. The group at the VUMC combined with the linkage from the Physics department of the Vrije Universiteit Amsterdam provided a very good dynamic research environment. It was in this group where I did research work about the VU topographer and the Scheimpflug apparatus. I am grateful for the times working together with Rob Van der Heijde and Michiel Dubbelman. Both closely and regularly supervised my work. It was also a pleasure working with other colleagues: Nanouk Wiemer, Anne Vrijling, Ivo van Stokkum, Evgeni Markine; and Erik Hermans and Joris Snellenburg, who both helped in the development of the software for the VU topographer.

There were people who helped my family with some practical aspects. Bart Visser's assistance for our housing made a big difference. I am grateful to Bart Takkenberg for organizing an excellent health management. During some vacation periods my family spent time with Roel, Jerly, Sarah and Tyrah van

Bergen-Henegouwen. Their house holds special memories, it was there where I wrote two of my papers.

All through this journey, four wonderful ladies were with me all the way: Mama, thank you for all those long distance conversations full of wisdom, love and encouragement; Beryl, thank you for all your prayers to God that I would succeed in my thesis; Chrys, I'm touched by those special moments you approached me and gave me words of encouragement during late nights of work; and Eloise, I can't imagine my life without you, you gave me strength to weather all the difficult challenges I went through.

For those friends who, in one way or another, have supported me, thank you very much.

CURRICULUM VITAE

Victor Arni de Paz Sicam was born in Davao City, Philippines, on September 21, 1968. In 1985 he finished his secondary education at the Philippine Science High School in Diliman, Quezon City, Philippines. He did his Bachelors (1985-1990) and Masters (1990-1994) study in Physics at the University of the Philippines, Diliman where he received the recognition of cum laude and outstanding graduate, respectively. During his masters study, he worked as part time instructor in the University and was involved in teaching Fundamental Physics, Mathematical Methods and Computational Physics. He was also the coordinator of the Nonlinear Dynamics Cluster of the Laser Physics Group at the National Institue of Physics, University of the Philippines. In this same period, he was an associate member of the National Research Council of the Philippines – an organization that evaluates research project proposals for eventual government funding. In 1997, he was employed by the University of San Carlos, Cebu City, Philippines. He held the position of Assistant Professor and was involved in teaching Mathematical Methods, Computational Physics, Optics/Laser Physics, Semiconductor Devices and Thermodynamics. While he was at the University of San Carlos he came into contact with Dutch physicists who were involved in the Physics Development Project sponsored by the NUFFIC, Netherlands. Through this contact he was introduced to the Medical Physics program of the VU University Medical Centre and eventually was employed starting January 2002 as an Assistant Researcher at the Physics and Medical Technology Department. It was in this department where he performed the research described in this thesis. Apart from his academic career, the author likes singing. For a brief period, he had singing performances with the University of the Philippines Madrigal Singers. Currently, he is married to a beautiful Filipina and has two lovely daughters.